Soft gluons and hard scales in QCD

—

Heavy quarks at finite and all orders

Tim Oliver Eynck

Soft gluons and hard scales in QCD

—

Heavy quarks at finite and all orders

Zachte gluonen en harde schalen in QCD

–

Zware quarks in eindige en oneindige orde berekeningen

(met een samenvatting in het Nederlands)

PROEFSCHRIFT

ter verkrijging van de graad van Doctor
aan de Universiteit Utrecht op gezag
van de Rector Magnificus, Prof. Dr. W.H. Gispen,
ingevolge het besluit van het College voor Promoties
in het openbaar te verdedigen op
donderdag 20 november 2003 des middags te 12.45 uur

door

Tim Oliver Eynck

geboren op 18 october 1971, te Düsseldorf, Duitsland

promotor: **Prof. Dr. E.L.M.P. Laenen**
Faculteit Natuur- & Sterrenkunde
Universiteit Utrecht

ISBN 90 6464 729 1

The work described in this thesis is part of the research programme of the *Nationaal Instituut voor Kernfysica en Hoge-Energie Fysika* (NIKHEF). The author was financially supported by the *Stichting Fundamenteel Onderzoek der Materie* (FOM).

I feel your attraction
It's a strong interaction
(Les Horribles Cernettes)

Contents

Chapter 1

Introduction

Quantum Chromodynamics (QCD) *is* the theory of the strong interaction. Nevertheless, its study still creates a lot of excitement and constitutes a prerequisite for current and future particle physics.

The previous short paragraph may sound more like the concluding remarks to a dissertation than its opening. One expects here some words about the quest for understanding the fundamental laws governing the dynamics of the elementary constituents of matter, and a condensed historicizing tour, departing perhaps in ancient Greece and arriving eventually at the celebrated Standard Model (SM). The present introduction attempts none of this, neither a chronology of physics nor an exposition accessible to the layman. It merely offers some remarks on how its initial sentence is supposed to be understood and sets the stage for subsequent core chapters.

As a quantum field theory, QCD is a relativistic quantum theory of the continuum. As such it combines some of the key ideas of 20^{th} century physics. QCD is consistent with the special theory of relativity, its expressions are Lorentz covariant. QCD is based on the gauge principle, deriving the coupling of gauge bosons to spinors and to each other from an $SU(3)$ gauge invariance. QCD is a quantum theory, individual amplitudes contributing to observables are first added and the resultant sums then squared to yield probabilities. Quantum theories have originally been formulated, and by the majority of the scientific community are also today still seen, loosely speaking, as not pertaining to the world as it is but as expressing what the educated observer can possibly know about the world. This introduction is not intended to defend a particular point of view in this interpretational discourse on the foundations of modern science. Instead, it seems worthwhile here to draw attention to the practical importance of invariance arguments. They often constitute powerful tools of undisputed phenomenological importance, and will feature prominently also in this work. Pursuing a quantitative description of scattering experiments theoretical physicists may introduce unobservable intermediaries, but the freedom in choosing these auxiliary constructs (gauges, renormalization and factorization scales etc.) must by no means affect the values predicted for experimentally accessible quantities.

Comprising except gravitation all the fundamental interactions known today the SM is a collection of gauge theories. As the only non-abelian unbroken theory of these, QCD

describes the strong force between fermionic quarks and bosonic gluons. But these fundamental degrees of freedom are not accessible directly; they form strongly bound states, the hadrons. The strong coupling constant α_s does only partly deserve its name, since in fact it runs, i.e. depends on the energy scale of the process under consideration. One and the same Lagrangian can thus describe rather dissimilar physical phenomena in two different coupling regimes, characterized by large and small α_s, respectively. Whereas regions of small α_s are accessible to perturbative methods based on Taylor expansions in the coupling constant, non-perturbative techniques are required in the large α_s domain. This is a feature displayed not only by QCD, but shared by other field theories and also by some more speculative and allegedly more fundamental approaches, some of which aspire to transcend the quantum field theoretic framework altogether. With no intention of derogating competing endeavours, it seems justified to insist that currently QCD constitutes the only theory of undisputed empirical relevance presenting itself in two surprisingly dissimilar coupling regimes. This interplay of perturbative versus non-perturbative physics makes QCD exciting from a more formal field theoretic point of view, but at the same time calls for a concerted effort of conceptual progress with often lengthy technical calculations to keep it on a par with experimental accuracy. In comparison to for instance models with broken symmetries the QCD Lagrangian may look rather compact and perhaps deceivingly simple, nevertheless computations can become very involved, especially of the higher order corrections phenomenologically relevant for present and future experiments. These facts make it important to keep devising powerful methods, conceptual as well as computational. Also researchers not interested in QCD *per se*, but in whatever type of new physics might be hiding beyond it, would probably agree on this point, since in view of the ample precision data supporting the Standard Model successful new discoveries seem almost impossible without accurate knowledge of their inevitable backgrounds. The absence of serious contestants to QCD therefore does not obviate the need for continuing research and improved descriptions of the dynamics inside the hadrons. As an example consider the nucleon spin. Spin, besides mass the second invariant under action of the Lorentz group, plays a central role in any relativistic field theory. It is quantized and occurs in units of $\hbar/2$ at the partonic as well as at the hadronic level, i.e. in *both* regimes of QCD. But how the nucleon spin emerges dynamically from the many spin-quantized constituent partons still requires further investigation.

This thesis constitutes to a large extent a study of methods and tools, and their quality as applied in QCD. These include factorization, resummation (both of large threshold logarithms and constants), and numerical phase space integrations. Chapter 2 collects and summarizes results unfortunately somewhat scattered throughout the literature but required for understanding subsequent chapters. Chapter 3 contains a resummation calculation for polarized charm production through photon gluon fusion, the results of which are then utilized to estimate higher order contributions to this process in chapter 4. Instead of finite order re-expansions the full resummed exponent as derived in chapter 3 is numerically investigated in chapter 5. Chapter 6 presents a calculation resumming not only large logarithms but also constants in the Drell Yan process. Chapter 7 investigates and compares two methods of phase space generation which can be used in the numerical computation of (differential) scattering cross sections. Finally, chapter 8 contains some concluding remarks. A more extensive tour of the thesis embedding its core chapters in a general context can be found at the end of this chapter. Chapters 3 through 7 are based on publications [1, 2, 3, 4].

1.1 Perturbative aspects of QCD

This and the following sections of this chapter introduce some aspects and concepts of perturbative QCD. They serve mainly to fix notation, mostly considering as an example the process of (inclusive) deep inelastic scattering (DIS). However, they also provide motivation for the investigations of subsequent chapters. The ubiquitous factorization property of hadronic cross sections for example, introduced here and usually taken for granted by experimentalist and phenomenologists alike, can actually be given a solid field theoretic justitification as in chapter 2. As a field theory containing massless partons QCD exhibits in individual higher order diagrammes besides ultraviolet also infrared divergences. These must either cancel among themselves or be dealt with in a consistent manner in order for the theory to be of any empirical use. In a nutshell, the cancellation of infrared divergences and their residual effects on (imperatively) finite observables can be regarded as the focal points of this thesis.

Quarks and gluons are the fundamental dynamical entities of QCD. However, they are not observed as free particles but confined inside the observed hadrons. This interplay complicates the phenomenological application of QCD and requires the introduction of non-perturbative parton densities following the concept of factorization. Since the coupling constant of the strong interaction decreases with increasing energy, perturbative QCD calculations with expansion parameter α_s can provide very accurate descriptions of high energy scattering processes, but they cannot explain the properties of low energy bound states, i.e. the parton densities inside hadrons. As discussed already in the previous section, this constitutes no fundamental flaw of the theory but points to the limitations of perturbation theory and the importance of the non-perturbative regime.

Section 1.2 covers inclusive deep inelastic scattering at lowest order, introducing in particular the hadronic tensor and (spin-averaged) structure functions. Section 1.3 ascends to one higher order in the strong coupling, where divergences first occur. Both sections 1.2 and 1.3 follow mostly the presentation in [5, 6]. Section 1.4 expands on the complications encountered in section 1.3 and explains why and how they constitute starting points for the investigations of subsequent chapters.

1.2 Deep inelastic scattering and the parton model

This section deals with the inclusive scattering of electrons off nucleons, through the exchange of a gauge boson, in the following always assumed to be a photon. Fig.1.1 illustrates this process for the particular case of a proton. The electron-photon vertex follows from the electon current $\bar{\psi}\gamma_\mu\psi$ of Quantum Electrodynamics (QED). Unfortunately, no corresponding expression for the proton-photon vertex, the oval blob in Fig.1.1, can be derived from first principles. However, symmetry arguments severely constrain the possible form of this coupling. It is customary to separate the less exciting leptonic $L^{\mu\nu}(l,l') = e^2/(8\pi^2)\mathrm{Tr}\left(\not{l}\Gamma^\mu\not{l}'\Gamma^\nu\right)$ from the hadronic part $W^{\mathrm{P}}_{\mu\nu}(p,q)$ of a spin-averaged (differential) deep inelastic cross section

$$d\sigma = \frac{d^3\vec{l}'}{l'}\frac{L^{\mu\nu}(l,l')\,W^{\mathrm{P}}_{\mu\nu}(p,q)}{2sQ^4}\ , \tag{1.1}$$

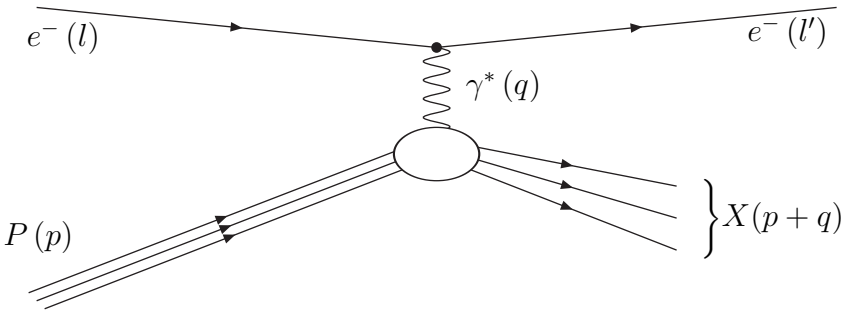

Figure 1.1: *Deep inelastic scattering of an electron off a proton via the exchange of a space-like photon.*

with p the proton momentum, l, l' the electron momentum before and after the scattering, respectively, and $s = (l+p)^2$. The photon momentum is given by $q = l - l'$ and the usual convention $-q^2 = Q^2 > 0$ will be adopted. The hadronic final state is denoted by X. Spin-dependent contributions to the hadronic tensor can be discussed in complete analogy, but to avoid lengthy formulae in this introductory chapter will only be introduced in chapter 3. The superscript on $W_{\mu\nu}$ will allow to distinguish hadronic quantities from the partonic ones to be introduced later. Throughout this discussion, lower case superscripts will denote partonic quantities, upper case superscripts refer to hadronic quantities (P for proton in this case). Imposing parity and current conservation the hadronic tensor can be parametrized as

$$\begin{aligned} W^{\mathrm{P}}_{\mu\nu}(p,q) &= -\left(g_{\mu\nu} - q_\mu q_\nu/q^2\right) W^{\mathrm{P}}_1(x,Q^2) \\ &\quad + \left[p_\mu - q_\mu\left(p\cdot q/q^2\right)\right]\left[p_\nu - q_\nu\left(p\cdot q/q^2\right)\right] W^{\mathrm{P}}_2(x,Q^2)\ , \end{aligned} \tag{1.2}$$

with the Bjorken scaling variable

$$x = -q^2/2p\cdot q = Q^2/2p\cdot q\ . \tag{1.3}$$

As indicated by their arguments, the structure functions W^{P}_1 and W^{P}_2 depend not on p and q directly, but only on the scalar variables Q^2 and x. For convenience one introduces the dimensionless structure functions

$$F^{\mathrm{P}}_1\left(x,Q^2\right) = W^{\mathrm{P}}_1\left(x,Q^2\right)\ ,\quad F^{\mathrm{P}}_2\left(x,Q^2\right) = \nu W^{\mathrm{P}}_2\left(x,Q^2\right)\ ,$$

where $\nu = p\cdot q$.

One could now simply measure for various scattering processes these structure functions $F^{\mathrm{P}}_1(x,Q^2)$ and $F^{\mathrm{P}}_2(x,Q^2)$. However, such a proliferation of data alone is truly not enough to gain insight into the structure of matter, but requires a connecting field theoretic framework. According to the quark model the proton is at a more fundamental level composed of quarks and gluons, so one can look at the underlying partonic process and compute this in perturbation theory - an approach justified if the high energy photon encounters an asymptotically free parton. This situation is depicted in Fig.1.2. Naturally, one now asks in which way this result is related to the (experimentally measurable) nucleon structure functions. From now on only the structure function F_2 will be treated explicitly, since this will be the function of interest in later chapters and in any case sufficiently illustrates the concepts involved.

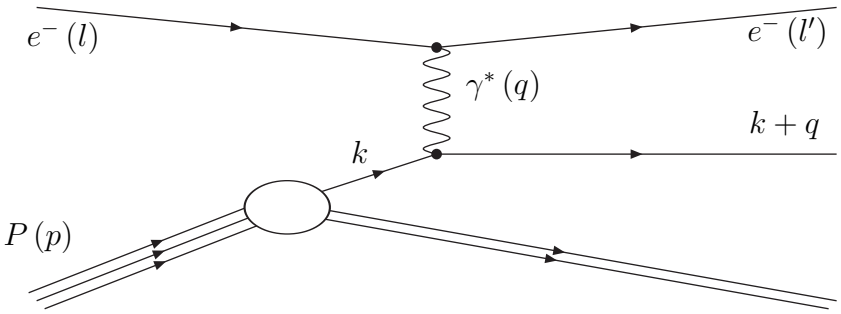

Figure 1.2: *Deep inelastic scattering of an electron off a quark carrying a fraction $k = \xi p$ of its parent proton's momentum.*

Zooming in on the photon-quark vertex of Fig.1.2 one can work out at lowest, i.e. zeroth order in the strong coupling, the structure functions for a free quark of charge e_q. This gives the result

$$F_2^{(\mathrm{q},0)}\left(x, Q^2\right) = e_q^2\, \delta\left(1-x\right) \ . \tag{1.4}$$

The superscripts on this function indicate that it is a lowest order partonic quantity. The parton model allows to relate it to its hadronic counterpart as

$$F_2^{(\mathrm{P},0)}\left(x\right) = \sum_i \int_0^1 d\xi F_2^{(i,0)}\left(\frac{x}{\xi}\right) \phi_{i/\mathrm{P}}\left(\xi\right) \ , \tag{1.5}$$

where the lowest order distributions $\phi_{i/\mathrm{P}}\left(\xi\right)$ of parton i (for a quark $i = q$ or gluon $i = g$) in the proton have been introduced. Combining equations (1.4) and (1.5) gives

$$F_2^{(\mathrm{P},0)}\left(x\right) = \sum_{\mathrm{q}} e_{\mathrm{q}}^2 x \phi_{\mathrm{q/P}}^{(0)}\left(x\right) \ , \tag{1.6}$$

expressing the intuitive idea that at lowest order the constituent quarks, weighted according to their charge and probability distributions, simply contribute incoherently to overall hadronic observables. Since gluons do not carry electric charge, the electromagnetic current does not couple to them directly. Note also that the mass shell conditions for the initial and final state partons of momenta p and $k+q$, respectively, lead to $\xi = x$ and thus at lowest order allow the interpretation of the Bjorken variable as a measure of the momentum fraction of the proton carried into the hard scattering by the quark.

1.3 DIS at next-to-leading order

Is the rather simple and intuitive picture of the previous section altered at going to higher orders in perturbation theory? One expects to encounter the usual ultraviolet divergences resulting from unconstrained loop momentum integrations. There is no need to review at this point the framework of renormalization which allows these divergences to be consistently taken care of. It suffices to recall that they manifest themselves as $1/\epsilon$ poles in $d = 4 - 2\epsilon$ dimensions, the regularization scheme to be applied throughout this thesis. Besides these ultraviolet also soft and collinear singularities are encountered in the absence

of regulating partonic masses. Such divergences result from internal propagators going on-shell, because massless partons are of very low energy (they become soft) or because they split into two collinear particles. To illustrate this consider the subprocess of a massless quark of momentum $p+k$ radiating a gluon of momentum k. The scattering amplitude of the overall process with both final state partons on mass shell will be proportional to

$$\frac{1}{(p+k)^2} = \frac{1}{2pk} = \frac{1}{2E_q E_g \left(1-\cos\theta\right)} \,, \tag{1.7}$$

where E_q, E_g denote the energies of the quark and gluon, respectively, and θ the angle subtended by the spatial momenta of the two resultant partons. Clearly, in four dimensions this expression diverges if either the energy of the emitted gluon (soft singularity) or the angle of emission (collinear or mass singularity) vanish. In dimensional regularization one obtains for these kinematic regions $1/\epsilon$ poles. Of course, nothing prevents a gluon from being both soft and collinear, a configuration producing double poles in the regulator.

These features can be illustrated for one-loop free quark DIS [5, 6, 7, 8, 9, 10]. At this order in the strong coupling the quark can either emit a gluon and later reabsorb it (virtual correction) or the emitted gluon can be radiated into the final state (real emission). With the arguments given above in mind, one expects to find divergences in at least some of the diagrammes to be computed. Cancellations of some of these divergences happen, but not yet at the level of integrands. They occur instead only after the integration over phase spaces, since the numbers of final state particles differ for virtual and real diagrammes. Consider now for simplicity a contraction of the hadronic with the metric tensor. The virtual corrections to this quantity are given by

$$\frac{\alpha_s}{\pi} g^{\mu\nu} W_{\mu\nu}^{(\mathrm{v},1)} = \frac{\alpha_s}{\pi} e_q^2 C_F \left(\frac{4\pi\mu^2}{Q^2}\right)^{\epsilon} (1-\epsilon) \frac{\Gamma\left(1+\epsilon\right)\Gamma^2\left(1-\epsilon\right)}{\Gamma\left(1-2\epsilon\right)} \left(\epsilon^{-2} + \frac{3}{2}\epsilon^{-1} + 4\right) \delta\left(1-x\right), \tag{1.8}$$

with $C_F = 4/3$ the contribution from the quark colour structure. The variable μ denotes both factorization and renormalization scales throughout this thesis, since the two are usually kept equal. Although some choice for this auxiliary scales has to be made, physical observables should in principle not depend on it. The real emission correction reads

$$\begin{aligned} \frac{\alpha_s}{\pi} g^{\mu\nu} W_{\mu\nu}^{(\mathrm{r},1)} = & -\frac{\alpha_s}{\pi} e_q^2 C_F \left(\frac{4\pi\mu^2}{s}\right)^{\epsilon} (1-\epsilon) \frac{\Gamma\left(1-\epsilon\right)}{\Gamma\left(1-2\epsilon\right)} \\ & \left[-\frac{1-\epsilon}{\epsilon}\left(1-x+\left(\frac{2x}{1-x}\right)\left(\frac{1}{1-2\epsilon}\right)\right) + \frac{1-\epsilon}{2\left(1-2\epsilon\right)\left(1-x\right)} + \frac{2\epsilon}{1-2\epsilon}\right]. \end{aligned} \tag{1.9}$$

So far these expressions still contain the anticipated soft, collinear and double poles in the dimensional regulator. Defining +-distributions $\left[\ln^n(1-x)/(1-x)\right]_+$ via their integrals against an arbitrary smooth test function $f(x)$ according to

$$\int_z^1 dx f(x) \left[\frac{\ln^n\left(1-x\right)}{1-x}\right]_+ = \int_z^1 dx \left(f(x)-f(1)\right)\left(\frac{\ln^n\left(1-x\right)}{1-x}\right) + f(1)\frac{\ln^{n+1}(z)}{n+1} \,, \tag{1.10}$$

one can expand

$$(-\epsilon)^{-1}(1-x)^{-1-\epsilon} = \epsilon^{-2}\delta(1-x) - \epsilon^{-1}\left[\frac{1}{1-x}\right]_+ + \left[\frac{\ln(1-x)}{1-x}\right]_+ + O(\epsilon) \ . \tag{1.11}$$

With $s = Q^2(1-x)/x$ this effects a cancellation of the double poles and allows the sum of (1.8) and (1.9) to be written as

$$\begin{aligned}\frac{\alpha_s}{\pi} g^{\mu\nu} W^{(1)}_{\mu\nu} &= -\frac{\alpha_s}{2\pi} e_q^2 (1-\epsilon)\left(\frac{4\pi\mu^2}{Q^2}\right)^{\epsilon}\Bigg[-\epsilon^{-1} P_{qq}(x)\frac{\Gamma(1-\epsilon)}{\Gamma(1-2\epsilon)} \\ &\quad + C_F\Bigg(\left(1+x^2\right)\left[\frac{\ln(1-x)}{1-x}\right]_+ - \frac{3}{2}\left[\frac{1}{1-x}\right]_+ \\ &\quad - \left(1+x^2\right)\frac{\ln(x)}{1-x} + 3 - x - \left(\frac{9}{2}+\frac{\pi^2}{3}\right)\delta(1-x)\Bigg)\Bigg] .\end{aligned} \tag{1.12}$$

The quark-quark splitting function $P_{qq}(x)$ occurring in (1.12) is given by

$$P_{qq}(x) = C_F\left((1+x^2)\left[\frac{1}{1-x}\right]_+ + \frac{3}{2}\delta(1-x)\right) \ . \tag{1.13}$$

It expresses the probability for a quark to emit a parton before entering the hard scattering as a quark carrying a fraction x of the original momentum. In section 3.3 similar expressions will be derived for gluons.

It should be noted at this point that the double and soft poles (proportional to $\delta(1-x)$) have cancelled but a collinear pole remains in (1.12). It complicates the interpretation of this result as well as that for the structure function $F_2^{(q,1)}$, which upon computation of the contraction $p^\mu p^\nu W^{(1)}_{\mu\nu}$ can be given as

$$\begin{aligned}\frac{\alpha_s}{\pi} F_2^{(q,1)}\left(x,Q^2\right) &= \frac{\alpha_s}{2\pi} e_q^2 x\Bigg[-\epsilon^{-1}\left(\frac{4\pi\mu^2}{Q^2}\right)^{\epsilon}\frac{\Gamma(1-\epsilon)}{\Gamma(1-2\epsilon)} P_{qq}(x) \\ &\quad + C_F\Bigg(\left(1+x^2\right)\left[\frac{\ln(1-x)}{1-x}\right]_+ - \frac{3}{2}\left[\frac{1}{1-x}\right]_+ \\ &\quad - \left(1+x^2\right)\frac{\ln(x)}{1-x} + 3 + 2x - \left(\frac{9}{2}+\frac{\pi^2}{3}\right)\delta(1-x)\Bigg)\Bigg].\end{aligned} \tag{1.14}$$

Provided the collinear pole can be taken care of, one might still be worried about the +-distributions in expressions (1.12) and (1.14), which consequently are meaningful only as integrands, not as stand-alone functions. However, this does not pose any problems, since partonic quantities are always integrated against some kind of parton distribution to form hadronic observables. The relation of (1.14) to the corresponding hadronic and thus empirically accessible quantity is provided by the factorization theorem

$$F_2^{(h)}\left(x,Q^2\right) = \sum_i \int_0^1 d\xi C_2^{(i)}\left(x/\xi, Q^2/\mu^2, \alpha_s\left(\mu^2\right)\right)\phi_{i/h}\left(\xi,\epsilon,\alpha_s\left(\mu^2\right)\right) + O\left(m^2/Q^2\right) \ . \tag{1.15}$$

The two functions in the convolution (1.15) are of a very different field-theoretic character. Whereas the perturbative coefficient C_2 is characteristic for the particular hard-scattering process under investigation and should thus be infrared finite as indicated by the absence of ϵ in its list of arguments, the universal parton distributions $\phi_{i,h}$ of parton i in hadron h are not perturbatively calculable and thus have to be fixed by measurement. However, once determined through some scattering process they can be used to make reliable predictions for other experiments by folding them with appropriate, calculable, i.e. finite partonic coefficient functions. Since the factorization theorem is not restricted to partons in hadrons, but could equally well be applied to partons in partons, one requires for consistency for partons i, j

$$\phi_{i/j}\left(\xi,\epsilon,\alpha_s\left(\mu^2\right)\right) = \delta_{ij}\delta(1-x) + O(\alpha_s)\ , \tag{1.16}$$

which at Born level leads to

$$C_2^{(i,0)}\left(x/\xi, Q^2/\mu^2, \alpha_s\left(\mu^2\right)\right) = e_q^2\delta(1-x/\xi)\ . \tag{1.17}$$

Chapter 2 will expand on the justification of the factorization theorem. This section is limited to exploring its role and consequences for DIS. Expanding the factorization theorem in its version for partons in partons to first order in the strong coupling gives

$$F_2^{(j)}\left(x,Q^2\right) = e_j^2\delta(1-x) + \frac{\alpha_s}{\pi}\left[\sum_i e_i^2 x\phi_{i/j}^{(1)}(x,\epsilon) + C_2^{(j,1)}\left(x,Q^2/\mu^2\right)\right] + O\left(\alpha_s^2\right)\ . \tag{1.18}$$

To render the coefficient function C_2 finite one must absorb at least the collinear divergence found in (1.14) into the parton distributions by defining

$$\phi_{q/q}(x,\epsilon) = \delta(1-x) - \frac{\alpha_s}{2\pi}\epsilon^{-1}P_{qq}(x) + \mathcal{O}(\alpha_s^2)\ . \tag{1.19}$$

But there exists some freedom or arbitrariness at this point in allotting the finite terms, requiring for consistency a choice of scheme. In the minimal subtraction (MS) scheme as defined by (1.19) only the pole is absorbed by the parton distributions. In the modified minimal subtraction ($\overline{\rm MS}$) scheme to be applied from now on the same is done with the finite contributions $(\gamma_E - 4\pi)\,P_{qq}(x)$, with γ_E the Euler constant. The coefficient function can then be read off from (1.15) and (1.18) as

$$\begin{aligned}\frac{\alpha_s}{\pi}C_2^{(q,1)}\left(x,Q^2\right) &= \frac{\alpha_s}{2\pi}e_q^2 x\Bigg[\ln\left(\frac{Q^2}{\mu^2}\right)P_{qq}(x) + C_F\Bigg(\left(1+x^2\right)\left[\frac{\ln(1-x)}{1-x}\right]_+ - \frac{3}{2}\left[\frac{1}{1-x}\right]_+ \\ &\quad -(1+x^2)\frac{\ln(x)}{1-x} + 3 + 2x - \left(\frac{9}{2}+\frac{\pi^2}{3}\right)\delta(1-x)\Bigg)\Bigg]. \end{aligned}\tag{1.20}$$

In a similar manner different hard partonic scattering processes can be computed. Hadronic observables are obtained upon convolution of the partonic results with parton distributions. The latter can formally be expressed as operator matrix elements

$$\begin{aligned}\phi_{q/h}(\xi) &= (2\pi)^{-1}\int_{-\infty}^{\infty} dy^-\exp(-i\xi p^+ y^-) \\ &\quad \frac{1}{2}\sum_\sigma \langle h(p,\sigma)\mid \bar{q}(0,y^-,\vec{0}_\perp)\frac{1}{2}\gamma^+ q(0)\mid h(p,\sigma)\rangle_{A^+=0}\end{aligned}\tag{1.21}$$

of quark creation and annihilation operators evaluated on the lightcone sandwiched between hadronic states of momentum p and helicity σ. Lightcone coordinates $(x^+, x^-, \vec{x}_\perp)$ with $x^\pm = (x^0 \pm x^3)/\sqrt{2})$ and $\vec{x}_\perp = (x^1, x^2)$ have been introduced here. The subscript $A^+ = 0$ contains information on the gauge. Expressions like (1.21) cannot be computed in perturbation theory. The parton distributions are instead fitted to world data by a number of independent groups and usually made available also in electronic form to be used as subroutines in numerical evaluations, cf. e.g. [11, 12]. However, if not hadronic but partonic external states are considered, equation (1.21) is modified to

$$\begin{aligned} \phi_{q/q}(\xi) &= (2\pi)^{-1} \int\limits_{-\infty}^{\infty} dy^- \exp(-i\xi p^+ y^-) \\ &\quad \frac{1}{2} \sum_\sigma \langle q(p,\sigma) \mid \bar{q}(0, y^-, \vec{0}_\perp) \frac{1}{2} \gamma^+ q(0) \mid q(p,\sigma) \rangle_{A^+=0} \; . \end{aligned} \tag{1.22}$$

The calculation of such an expression is possible and at order α_s yields a single ϵ pole multiplying the splitting function (1.13). A similar calculation will be described in detail in section 3.3 for the case of (polarized) gluons.

1.4 From problems towards solutions

The concepts of perturbative QCD sketched so far constitute starting points for the core chapters of this thesis. The first is to be found in equation (1.20) for the next-to-leading order partonic coefficient function in DIS. After the cancellation of soft and double poles and the absorption of collinear divergences into non-perturbative parton distributions there remain +-distributions of the argument $(1-x)$. The divergences proper may have been taken care of, but their remnants still take the form of distributions rather than continuous functions. The +-distributions are therefore viewed as originating from an *imperfect cancellation* of virtual and real emission contributions. As a slight abuse of language, the partonic configurations with propagators either exactly or almost on-shell are often collectively referred to as leading regions. The terms soft and collinear are used in much the same fashion, with the context preventing confusion. Very close to partonic threshold, i.e. in the limit $x \longrightarrow 1$ where both the term in the denominator and the argument of the logarithm become very small, the +-distributions clearly dominate numerically. At higher orders this picture persists, with every power in the strong coupling accompanied by two extra powers in the potentially large leading logarithm

$$\alpha_s^n \left[\frac{\ln^{2n-1}(1-x)}{1-x} \right]_+ \; , \tag{1.23}$$

and the next-to-leading logarithm

$$\alpha_s^n \left[\frac{\ln^{2n-2}(1-x)}{1-x} \right]_+ \; . \tag{1.24}$$

The list can of course be continued down to $[1/(1-x)]_+$. The reliability of perturbation theory requires that the parameter of expansion be small. For QCD this parameter is

the strong coupling, with $\alpha_s \simeq 0.1$ for most energy regions of interest. But close to $x = 1$ one is effectively expanding not in the strong coupling alone but in the combination given by equations (1.23) and (1.24). The reliability of the perturbative expansion is thus put at stake. Note that these boundary or threshold regions of partonic phase space are phenomenologically relevant unlike hadronic phase space edges. There may be for principal regions (e.g. finite detector sensitivity and angular resolution) no measurements at hadronic $x = 1$. But the convolution with parton densities allows the partonic $x \longrightarrow 1$ region to sizably influence hadronic quantities also well away from their phase space boundaries. To retain control over the theory and confidence in its phenomenological predictions for such situations it thus seems desirable to assess the numerical importance of these dominant logarithmic contributions and reorder the perturbation series to reexpand in a suitably small parameter. It turns out that as a result of certain approximations to the dynamics and kinematics near partonic threshold this can indeed be accomplished in the framework of resummation. Such resummation calculations are conveniently carried out in Laplace or Mellin moments, defined by

$$\tilde{f}(N) = \int_0^\infty dx e^{-Nx} f(x) \tag{1.25}$$

and

$$\tilde{f}(N) = \int_0^1 dx x^{N-1} f(x) \ , \tag{1.26}$$

respectively. A list of moments of +-distributions can be found in appendix A, with differences between Laplace and Mellin moments being of order $1/N$. Characteristically, threshold limits in x correspond to large N limits in moment space. The leading terms in the moment space expression resulting from $[\ln^n(1-x)/1-x]_+$ are given by $\ln^{n+1} N$, often abbreviated L^{n+1}. The subleading differences between Laplace and Mellin moments can be neglected close to threshold. Resummation allows the soft gluon effects $1 + \alpha_s(L^2 + L + \ldots) + \alpha_s^2(L^4 + L^3 + \ldots) + \mathcal{O}(\alpha_s^3)$ to be factored out off the hard scattering and shown to exponentiate in the form $\exp(\alpha_s L^2 + \ldots)$, where all coefficients of α_s except for the L terms have been suppressed. Albeit of perturbative nature, such exponents nevertheless contain information about the theory beyond finite orders. Not only does this formalism provide valuable insights into the near-threshold structure of (just about perturbative) all-order field theory, the exponent can also be considered as a generating functional. From this often good estimates for higher order corrections can be generated via reexpansion, at relatively low computational cost.

The threshold behaviour just described is generic not only to fully inclusive DIS considered in this introductory chapter. Similar enhancements occur in the semi-inclusive deep inelastic production of heavy final state quark pairs, and in the Drell-Yan process (DY), the hadronic production of a final state lepton pair. The major part of this thesis deals with resummation calculations for these two processes. These calculations rest on extra factorizations of partonic cross sections, in addition but similar to those expressed in (1.15). Therefore, chapter 2 reviews these factorization proofs in quite some detail. Chapter 3 describes how the resummation calculation is carried out for the case of (polarized) deep inelastic charm production, a process of much phenomenological interest since it is employed to measure the polarized gluon density inside the nucleon. The result

of chapter 3 is utilized in chapter 4 as a generating functional to estimate finite order corrections so far unknown exactly. These finite order results could be of interest in particular to experimentalists and phenomenologists investigating polarized photon gluon fusion near the charm production threshold. But also a numerical evaluation of the full resummed exponent seems desirable, first results of which are presented in chapter 5. The resummation calculation for DY in chapter 6 supplies estimates not only for the leading large logarithms, but extends the formalism to include also constant terms.

In the derivation of partonic coefficient functions infrared divergences cancelled between virtual and real boson emission contributions, equations (1.8) and (1.9), respectively, with different numbers of final state particles for virtual gluon loops and real gluon radiation. This cancellation takes place only after phase space integrations have been performed. For many phenomenological applications it is convenient or even crucial to compute such phase space integrals not analytically but numerically (for lack of analytical solutions or to allow for the easy implementation of detector-specific acceptance cuts). In order to do this the number of final state particles has to be fixed prior to the random generation of their momenta. But final states with differing numbers of particles produce intermediate results containing infrared divergences. Clearly, such infinities are neither easily handled by numerical routines, nor simple to subtract from each other to yield finite predictions. In order to apply numerical phase space generation techniques beyond lowest order, methods to avoid intermediate divergences have to be devised. Two such methods, a dipole subtraction and a phase space slicing method will, with emphasis on the latter, be presented in chapter 7. The dipole method is for the first time employed to study heavy final state quarks. In the phase space slicing method, cut-off independence can be achieved by including correction terms. The numerical performance of the two methods is then compared both at integrated and differential levels, for the latter with binning in either transverse momentum or rapidity.

Chapter 2

Factorization and resummation

The importance of the QCD factorization theorem has been amply emphasized in the previous chapter. It guarantees the predictability of hadronic cross sections as convolutions of universal parton distributions with process specific partonic cross sections. The factorization property of hadronic cross sections is under threat by soft gluons which could be interchanged by the interacting particles or jets of particles long before or long after the spatiotemporally localized hard scattering. Hence soft gluons must be shown to play no role in sufficiently inclusive hard scattering processes. The ideas presented here are thus rather general and constitute the backbone for all the factorization theorems guaranteeing the predictive power of QCD. But in the form of an extra partonic refactorization they also form the basis upon which rest the (threshold) resummation techniques applied throughout a major part of this thesis. This last fact constitutes the main motivation for the inclusion of this chapter. The treatment will usually follow examples given in the literature, some of which play no role in the rest of the thesis. However, it should be clear that the emphasis here is not on particular processes, but on the general structure of the arguments.

In view of the length of this chapter a short overview of its structure seems in place. Section 2.1 shows that leading regions have to satisfy the Landau equations, solutions to which can conveniently be found employing the method of Coleman and Norton as explained in section 2.2. The necessary criteria for leading regions are supplemented by sufficient ones in section 2.3, which deals with infrared power counting. These results are generalized to all orders in the strong coupling in section 2.4. The factorized expressions derived from this still display complicated Lorentz index structures, which are simplified to scalar multiplications in section 2.5. Section 2.6 modifies the arguments leading to factorization to imply also near threshold, which finally leads to the exponentiation of the constituent factors in section 2.7.

2.1 Infrared divergences and the Landau equations

The large logarithmic corrections endangering the perturbative expansion of QCD result from soft and collinear singularities in Feynman diagrammes. Their behaviour must be controlled to all orders in the strong coupling. To an L-loop Feynman diagramme with

external momenta p_s and loop momenta l_r there corresponds a multi-dimensional complex (indicated by the $i\epsilon$) integral

$$G = \prod_{i=1}^{L} \int d^d l_i N\left(k_i, p_s\right) \prod_{j=1}^{I} \frac{1}{k_j^2 - m_j^2 + i\epsilon} \ , \tag{2.1}$$

where N is some numerator factor. Overall normalization constants are of no importance in the following discussion and will often be suppressed. The line momenta k_i of the I internal lines are linear combinations of the loop and external momenta. To make more obvious the singularity structure of (2.1) it is useful to combine all of its denominator into a single one employing Feynman parameters α_i. This manipulations yields

$$G = (I-1)! \prod_{j=1}^{I} \int_0^1 d\alpha_j \delta(1 - \alpha_1 - \ldots - \alpha_I) \prod_{i=1}^{L} d^d l_i N\left(k_i, p_s\right) D^{-I} \ . \tag{2.2}$$

Singularities result from the denominator

$$D = \sum_{j=1}^{I} \alpha_j \left(k_j^2\left(l_i, p_s\right) - m^2\right) + i\epsilon \tag{2.3}$$

going to zero. However, not all zero points of D necessarily produce singularities. By Cauchy's theorem the contour of integration can be deformed to stay clear of isolated singularities in the complex plane. There remains no room to manoeuvre only if $D = 0$ results from a fixed endpoint of an α_j contour or from two almost coalescing poles in l_i, one just above and the other below the real axis, respectively, pinching the contour between them. This leads to the necessary conditions

$$D = 0, \qquad \frac{\partial D}{\partial l_i^\mu} = 0 \qquad\qquad \forall i, \mu \ \ , \tag{2.4}$$

for a singular point to be developed by the momentum integrals. These conditions can be fulfilled in either of two ways. Either D does not depend on α_j, i.e. $k_j^2 - m^2 = 0$, or the singular point is at the end of the α_j integral and thus cannot be moved, i.e. $\alpha_j = 0$. The Landau equations [13] summarize this result as

$$\begin{aligned} & k_j^2 = m^2 \quad \text{or} \quad \alpha_j = 0 \\ & \sum_{j \ \in \ \text{loop} \ r} \alpha_j k_j \epsilon_{jr} = 0 \qquad\qquad \forall j, r \end{aligned} \tag{2.5}$$

where the incidence matrix

$$\epsilon_{jr} = \begin{cases} +1 & : \ k_j \text{ in same direction as } l_r \\ -1 & : \ k_j \text{ in opposite direction to } l_r \\ \ \ 0 & : \ \text{otherwise} \end{cases} \tag{2.6}$$

ensures that momenta are added vectorially in the sum over all loop lines.

The Landau equations hold at any order for any diagramme. To give a simple example without initial state partons, they can be studied for the decay of a virtual photon into a massless final state quark-antiquark pair as shown at lowest order in Fig. 2.1a. To be

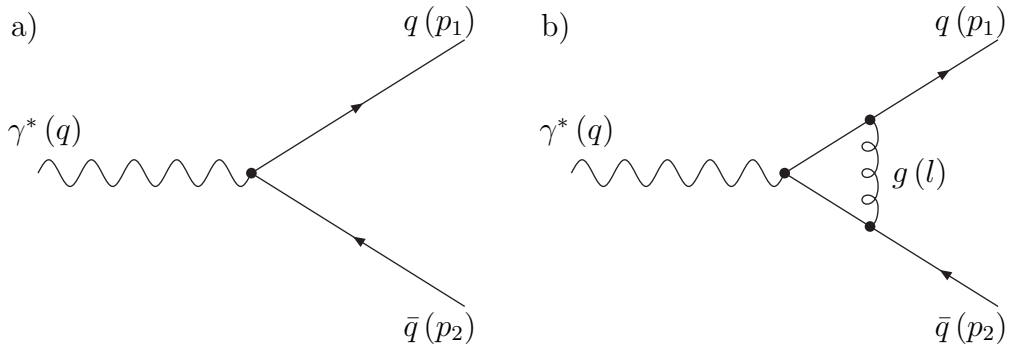

Figure 2.1: *a) Decay of a virtual photon into two quarks. b) QCD correction to this process.*

more precise, one should really think of this as a decay to two partonic jets. No observer could identify exclusively a single parton. It might be accompanied by soft or collinear gluons, degenerate states leaving identical signatures in a (hypothetical) detector. The one-loop correction as shown in Fig. 2.1b is proportional to

$$G = \int d^d l \frac{1}{\left(l^2 + i\epsilon\right)\left(\left(p_1 + l\right)^2 + i\epsilon\right)\left(\left(p_2 - l\right)^2 + i\epsilon\right)} \ , \tag{2.7}$$

or, using Feynman parameters,

$$G = \int d^d l \int \prod_i d\alpha_i \frac{1}{D^3\left(\alpha_i, l, p_j\right)} \delta(1 - \alpha_1 - \alpha_2 - \alpha_3) \ , \tag{2.8}$$

where $D = \left(\alpha_1 l^2 + \alpha_2 \left(p_1 + l\right)^2 + \alpha_3 \left(p_2 - l\right)^2 + i\epsilon\right)$. This denominator has to vanish, and from the derivative condition it follows that

$$\alpha_1 l^\mu + \alpha_2 \left(p_1 + l\right)^\mu - \alpha_3 \left(p_2 - l\right)^\mu = 0 \ . \tag{2.9}$$

To these conditions there exist two collinear solutions, namely

$$l^\mu = -z p_1^\mu, \quad \alpha_1 z = \alpha_2 \left(1 - z\right), \quad \alpha_3 = 0 \ , \tag{2.10}$$

and

$$l^\mu = z' p_2^\mu, \quad \alpha_1 z' = \alpha_3 \left(1 - z'\right), \quad \alpha_2 = 0 \ ,$$

as well as one soft solution

$$l^\mu = 0, \quad \alpha_2/\alpha_1 = \alpha_3/\alpha_1 = 0 \ .$$

Double soft and collinear singularities are possible for either $z \longrightarrow 0$ or $z' \longrightarrow 0$.

2.2 The Coleman-Norton picture

Although solving the Landau equations is not too difficult for the simple case as discussed in the previous section, it seems desirable to have at hand a general method of finding

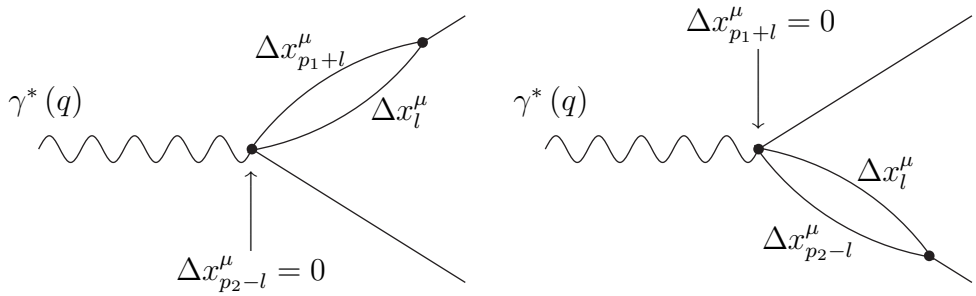

Figure 2.2: *Reduced diagrammes for collinear singularities in the QCD correction to the decay of a virtual photon into two massless quarks. Note that, by the Landau equation, the distances travelled are equal for collinear partons, i.e.* $\Delta x^\mu_l = \Delta x^\mu_{p_1+l}$ *for the first and* $\Delta x^\mu_l = \Delta x^\mu_{p_2-l}$ *for the second configuration.*

solutions to more complicated diagrammes. This is offered by the graphical interpretation of the Landau equations due to Coleman and Norton [14, 5]. They define

$$\Delta x^\mu_j = \alpha_j k^\mu_j \tag{2.11}$$

and interpret the Feynman parameter as the Lorentz invariant ratio

$$\alpha_j = \frac{\Delta x^0_j}{k^0_j} \ . \tag{2.12}$$

It follows from (2.11) and (2.12) that $\Delta x^\mu_j = \Delta x^0_j v^\mu_j$, with the four-velocity of an on-shell particle of momentum k^μ given by $v^\mu_j = (1, \vec{k}_j/k^0_j)$. In this picture on-shell particles can be viewed as propagating freely along classical trajectories prescribed by the lines of the Feynman diagramme. Its vertices interpreted as spacetime points are separated by distances Δx^μ_j. The condition in (2.5) on the sum over all propagators making up a loop is thus expressed in the Coleman-Norton picture as the requirement that physical distances be independent of which lines are used to compute them, provided the intermediate contributions are added vectorially. Since it follows from $k^2_j \neq m^2$ that $\alpha_j = 0$, such off-shell lines are to be contracted to points in the Coleman-Norton analysis. In this way there corresponds to every singularity a so called reduced diagramme. In such reduced diagrammes the particle character (quark, gluon) is often suppressed since one is more interested in the topological features of a particular configuration.

The example of virtual photon decay discussed above can also be used to illustrate the Coleman-Norton method. The two collinear solutions correspond to the reduced diagramme shown in Fig.2.2, where vertices containing contracted lines have been indicated. In Fig.2.3, depicting the soft solution, the labelling of lines in the by now familiar process has been suppressed. Since this already exhausts the list of divergences found algebraically other reduced diagrammes should be excluded. Two such examples are given in Fig.2.3b and 2.3c. The first of these graphs is excluded because the two particles created at the photon vertex cannot rejoin at the second vertex if in between the two they propagate freely. If they were travelling collinearly in the original photon direction they would have to be off-shell and thus not possess uncontracted lines, as in the graph they clearly do. Hence the configuration is unphysical. In the second graph a particle is created at the

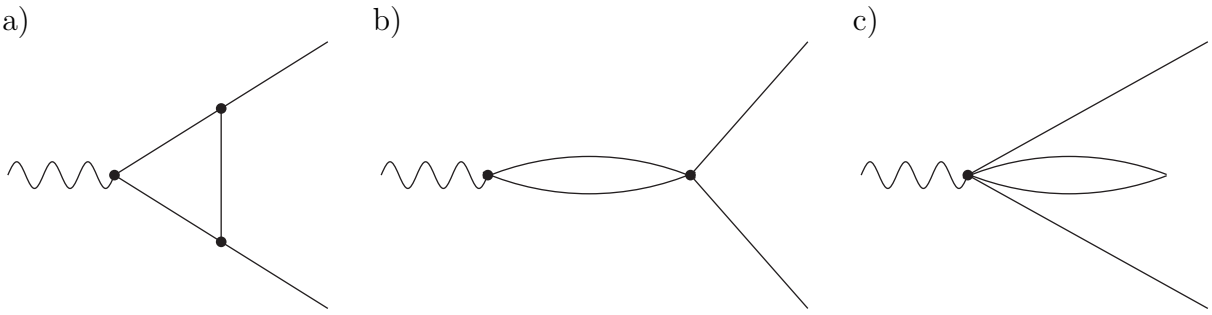

Figure 2.3: *a) Trivial reduced diagramme for soft singularity in the QCD correction to the decay of a virtual photon into two quarks. b) Reduced diagramme for the same process not corresponding to allowed physical processes since freely propagating non-collinear particles cannot rejoin. c) Reduced diagramme disallowed because physical particles cannot follow spacelike trajectories.*

photon vertex and after prescribing a curve returns to the same spacetime point. Since physical particles cannot follow space-like trajectories this configuration is also excluded. These observations generalize to higher orders and more complicated diagrammes. In particular, also for multi-particle, or really multi-jet production all jets have to be created already at the hard vertex and cannot recombine later.

2.3 Infrared power counting

The Coleman-Norton method described above is very useful in providing necessary conditions for the occurrence of singular regions in Feynman diagrammes. It does not supply sufficient criteria to decide whether a pinch singular point of the denominator really leads to a divergence and is not perhaps balanced by a numerator factor, due to e.g. the measure of integration or a vertex factor. To this end a power counting procedure for pinch surfaces is needed [5, 15]. Since the task resembles the analysis of ultraviolet divergences in renormalization it should hardly come as a surprise that the power counting techniques applied in the two regimes will display similarities. At each point of a pinch surface the integration variables in (2.2) are divided up in such a way that the coordinates fall into two disjunct sets, comprising intrinsic and extrinsic variables, respectively. Of these the integral is singular only in the normal variables, whereas the intrinsic coordinates serve merely to parameterize the pinch surface. All information on the divergence will be contained in the homogeneous integral to be introduced below.

The normal variables κ_j are by no means restricted to be linear in momentum components. Their choice depends very much on the nature of the divergence as will become clear below. To study the integral in the vicinity of the pinch surface it is convenient to introduce a scaling variable λ according to $\kappa_j = \lambda^{a_j}\kappa'_j$. Keeping the ratios κ_j/κ'_j fixed, approach to the surface is controlled by $\lambda \to 0$. In (2.1) the line momenta now become functions of λ and κ_i so that the denominators can be expressed as

$$\frac{1}{k_j^2\left(\kappa'_i, \lambda\right) - m_i^2} \,.$$

They will in general be polynomials in λ. Near the pinch surface only the lowest order monomial in λ contributes a power of a_j from the denominator, so all higher powers can be, and for the homogeneous integral are, discarded. Also, the l_i loop integrations are reexpressed in terms of the new coordinates, but to estimate the degree of divergence only the normal variables are relevant and kept in the homogeneous integral, contributing b_j powers of λ. Since the numerator depends on k_i there could also be an extra factor c from $N\left(\kappa'_j, p_s\right)$. This construction leads to the homogeneous integral

$$\left(\int \prod_j d\kappa'_j \frac{N\left(\kappa'_j, p_s, m_j\right)}{D\left(\kappa'_j, m_j\right)}\right) \lambda^{\sum_j b_j - \sum_j a_j + c} \quad , \tag{2.13}$$

from which the degree of divergence $n_s = \sum_j b_j - \sum_j a_j + c$ can then be read off as

$$n_s \begin{cases} = 0 & : \quad \text{logarithmic divergence} \\ > 0 & : \quad \text{finite} \\ < 0 & : \quad \text{power divergence} \; . \end{cases}$$

Again this method is best illustrated by means of the simple photon decay example. To investigate the collinear singularity $(p_1 + l)^2 \to 0$ first fix the quark momenta in lightcone coordinates as

$$p_1^\mu = \delta^{\mu +} \frac{Q}{\sqrt{2}}, \qquad p_2^\mu = \delta^{\mu -} \frac{Q}{\sqrt{2}} \; . \tag{2.14}$$

Since $(p_2 - l)^2$ remains finite the three denominators

$$\begin{aligned} l^2 &= 2l^+l^- - l_\perp^2 \\ (p_1 + l)^2 &= 2p_1^+ l^- + 2l^+l^- - l_\perp^2 \\ (p_2 - l)^2 &= -2p_2^- l^+ + 2l^+l^- - l_\perp^2 \end{aligned} \tag{2.15}$$

suggest the choice l^-, $l_\perp^2$ as normal and l^+ as well as the azimuthal angle ϕ as intrinsic coordinates. Hence scaling $l^- = \lambda l'^-$ and $l_t^2 = \lambda l'^2_\perp$ the denominators exhibit proportionalities

$$l^2 \sim \lambda, \qquad (p_1 + l)^2 \sim \lambda, \qquad (p_1 - l)^2 \sim \lambda^0 = 1 \; . \tag{2.16}$$

Together with the volume element $d^d l = dl^+ dl^- d\,|l_t|\,|l_t|^{d-3}\, d\Omega \sim \lambda^{\frac{d}{2}}$ one counts in four dimensions a logarithmic divergence $G \sim \lambda^{\frac{d-4}{2}}$ or, equivalently, $n_s = 0$. The treatment of the soft divergence is even simpler. Here the choice $l^\mu = \lambda l'^\mu$ yields

$$l^2 \sim \lambda^2, \qquad (p_1 + l)^2 \sim \lambda, \qquad (p_1 - l)^2 \sim \lambda \; . \tag{2.17}$$

Together with the volume element $d^d l \sim \lambda^d$ this leads to again a logarithmic divergence $n_s = 0$.

2.4 All-order analysis of soft and collinear regions

The power counting techniques introduced in the previous section can also be applied at higher orders and to an arbitrary number of jets [16]. This involves some careful

bookkeeping of powers of the scaling variable λ as contributed by propagators, vertices and measures of integration. From such an analysis conclusions can be drawn e.g. about the type (scalar, fermionic, vector) of soft particles attaching to the jets. Many restrictions on the allowed topology of reduced diagrammes are already derived from the Coleman-Norton picture. As mentioned at the end of section 2.2 it can be applied in all-order analyses not only of the photon decay example but also to other processes, involving e.g. initial state hadrons. It was argued in reference to Fig. 2.3b that two jets created at the hard photon vertex cannot rejoin later. This statement holds process-independently, i.e. in particular for an arbitrary number of jets J, and at all orders in perturbation theory. Hence any final state jet must be formed already at the hard vertex H. Such a hard vertex could result from the contraction of a complicated diagramme consisting only of off-shell lines. Inside jets massless particles can split and recombine. Also, the jets can interact, but only through the exchange of soft lines collectively denoted by S. Although the generalization of the power counting procedure to arbitrary orders will in this section be illustrated by means of again virtual photon decay, it should become clear that the arguments supplied are general enough to apply also to other processes.

Besides the generalization of power counting to more than two jets, also the concept of cut diagrammes can conveniently be introduced at this point. In the description of scattering processes as considered in this work, and indeed quite in general in quantum field theory, physical observables depend not on individual amplitudes G, but rather on the product $\sum_i G_i \sum_j G_j^*$ of some diagramme (or sum of diagrammes) and its complex conjugate. A cut diagramme provides first of all a graphical visualization of this algebraic manipulation. It contains besides the diagramme proper also a complex conjugate (not necessarily a *mirror image* of the first, but certainly with the same final state), and a final state cut separating the two. Thus a cut diagramme could, but does not have to be the square of an uncut graph. An example is provided by Fig. 2.4, according to the Coleman-Norton picture the most general allowed reduced cut diagramme for the decay of a virtual photon to n jets, where the soft function S, the jets J_1, J_2 up to J_n, as well as the hard scattering function H and its complex conjugate H^* have been represented graphically. Both the jets and the soft function extend across the final state cut, seemingly blurring the distinction between contributions to the amplitude on the one hand and its complex conjugate on the other. Of course, such worries pertain only to cut diagrammes as general as Fig. 2.4 which, illustrating a particular set of kinematic configurations, depicts no details internal to the functions J_i and S. Given any element of this set, i.e. any individual cut diagramme with all on-shell jet and soft lines drawn in, the assignment of its subdiagrammes to either G or G^* is uniquely defined by the final state cut. Shifting only the final state cut (and thus reallocating vertices from G to G^* and/or vice versa) but otherwise leaving the topology of the diagramme unaltered allows one to sift through the contributions to a particular physical process in a specific way. [1] This powerful bookkeeping strategy can be employed in field theoretic unitarity proofs and will play a key role in the discussion of factorization as presented here.

Note that to avoid graphical clutter in Fig. 2.4 the (longitudinal) couplings of collinear gluons to the hard function has been exemplified for the top and bottom jets only, although

[1] A graphical representation of this method will be given in Fig. 2.7b of section 2.5. The cut graphs there look less symmetrical than Fig. 2.4 and are therefore perhaps more illustrative of the general concept.

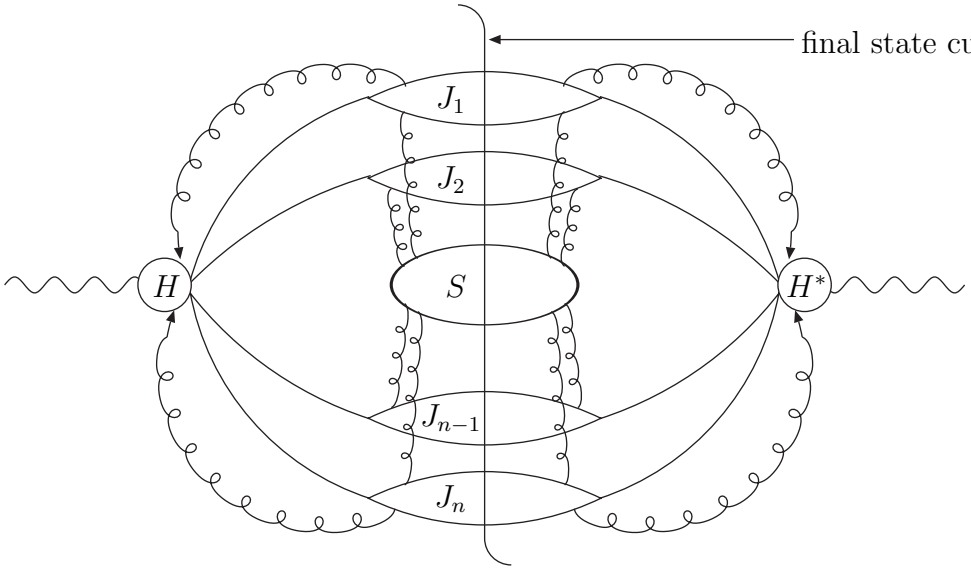

Figure 2.4: *Most general allowed reduced cut diagramme for the decay of a virtual photon into n jets; single gluons stand for multiple attachments.*

these are in no way distinct from the others. For the same reason, single soft gluons symbolize multiple attachments. As a matter of fact, in Feynman gauge $\partial \cdot A = 0$ collinear gluons couple to the hard function only with their longitudinal degrees of freedom, as indicated by the arrows in Fig.2.4, and are even completely absent in the axial gauge $n \cdot A = 0$. These results follow from power counting arguments applied to the gluon propagators vertices [16, 5].

In section 2.3 the degree of divergence n_s was introduced and shown to equal zero for the one-loop two-jets case. The generalization of this result to an arbitrary number of jets at all-orders is again based on power counting the contributions of soft and collinear vertices, propagators, integration measures and numerator factors. In the notation of [16] one finds

$$n_s \geq \left(4L^{(s)} + 2L^{(j)} + K\right) - (2S + J) + N \ , \tag{2.18}$$

where $L^{(s)}$ and $L^{(j)}$ denote the number of soft and jet loops, respectively, K counts the number of jets, J and S are the numbers of finite- and zero-momentum lines and N contains all numerator contributions. [2] This result can be expressed making explicit the contributions from individual jets and soft line attachments to these. Required in this derivation is the topological Euler identity

$$l = j - v + 1 \ , \tag{2.19}$$

relating the number of internal loops l of a jet to its numbers of lines and vertices, j and v, respectively. Clearly, as they rely only on the QCD Feynman rules and topological features shared by arbitrary graphs, the arguments employed here are not limited to the particular example considered.

Furthermore, one needs some combinatorial relations between the different types of vertices in a jet and the lines emanating from it. The reasoning in [16] allows besides soft vector also soft scalar particles, and is in this sense even more general than required here.

[2] Jet loops contain exclusively collinear lines, soft loops contain at least one soft line.

Finally, a lower bound on the contribution from the numerator is provided by a careful examination of the two-fermion-vector coupling $(\not{p}+\not{k})\gamma_\mu\not{p}$, which contributes at least a power of $\lambda^{1/2}$. After some algebra this leads to

$$\begin{aligned} n_s \;\geq\; & \frac{1}{2}\sum_{i=1}^{K}\left[\sum_{\alpha\geq 4}(\alpha-4)\,x_{i,\alpha}+\sum_{\beta\geq 4}(\beta-4)\,y_{i,\beta}+\gamma_i+\delta_i-2\right] \\ & +\frac{1}{2}\sum_{i=1}^{K}\left[b_i^{(0)}+\left(b_i^{(1)}-z_i^{(1)}\right)\right]+\frac{1}{2}f\ . \end{aligned} \tag{2.20}$$

Here $x_{i,\alpha}$ stands for the number of soft vertices in jet i with α jet lines and no soft lines attached; $y_{i,\beta}$ denotes the number of soft vertices with β jet lines and in addition one or more soft lines attached. Furthermore, γ_i and δ_i are the numbers of jet lines of jet i attached to the left and right hand hard vertices, respectively. Moreover, $b_i^{(0)}$, $b_i^{(1)}$, and f refer to soft scalar, vector, and fermion lines attached to jet lines. It should be noted that a soft scalar, vector or fermion line is counted double if at both its ends it attaches to jet lines. Finally, $z_i^{(1)}$ stands for the number of soft vector lines emitted by jet lines of jet i at three-point vertices.

After the somewhat lengthy nomenclature of the previous paragraph the physics implications of (2.20) can be discussed. First of all, one can at worst have logarithmic divergences, $n_s \geq 0$. The bound is saturated at

$$b_i^{(1)}=z_i^{(1)}\ ,\quad b_i^{(0)}=f=0\ ,\quad \gamma_i=\delta_i=1\ ,\quad \forall\alpha>4:\ x_{i,\alpha}=y_{i,\alpha}=0\ . \tag{2.21}$$

This means that in leading regions the jets and the soft function are connected not by soft fermions, but only by soft vector particles. These emerge from the jets exclusively at three-point vertices. Note that this does not exclude soft fermions internal to the soft function. There are no direct connections of the soft and the hard functions (cf. Fig.2.4); not an unexpected result since by construction the hard function contains only off-shell lines, coupling to which would increase the number of internal off-shell propagators by one and thus render the diagramme sub-leading. All jets must be created at the hard vertex (or otherwise be present already in the initial state), a conclusion which had been reached already in section 2.2 on the basis of the Coleman-Norton analysis alone. Finally, there are no vertices in the jets with more than four jet lines attached. Such non-fundamental vertices could be introduced upon contracting off-shell lines to points in passing from the original to the reduced diagramme.

It has thus been possible to represent a general leading region in the form of a reduced diagramme involving soft and jet functions and to derive severe restrictions on the diagrammatic topology. However, in their couplings the different functions still exhibit a complicated index structure of the form

$$J_1^{\mu_1\ldots\mu_l}J_2^{\nu_1\ldots\nu_m}\ldots J_i^{\rho_1\ldots\rho_n}S_{\mu_1\ldots\mu_l\nu_1\ldots\nu_m\rho_1\ldots\rho_n}\ , \tag{2.22}$$

where arguments, integrations, colours and spin sums etc. have been suppressed. For sufficiently inclusive cross sections this can in fact be reduced to a simple scalar multiplication. Only then can one fully exploit the universality of the theory in inclusive processes and almost as a by-product achieve resummation through a separate exponentiation of jets and soft functions, e.g. near production thresholds. This, at points rather technical, programme will be sketched in the next section.

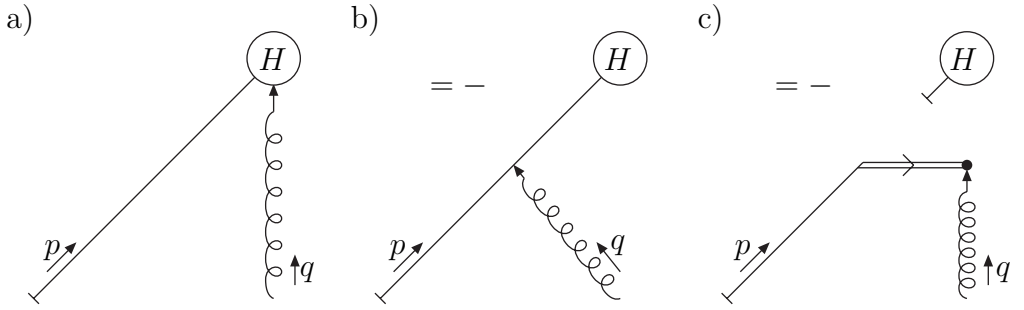

Figure 2.5: *Application of the non-abelian Ward identities in showing that a single longitudinal collinear gluon decouples from the hard function.*

2.5 Simplification of the Lorentz structure

So far the couplings of the constituent hard, soft and jet functions even for leading regions still depend on the full Lorentz structure of the collinear and soft gluons attached, as well as on spin and colour sums. In this section it will be sketched how to achieve the desired full factorization covering also initial state hadrons (i.e. for a class of processes even more general than depicted in Fig.2.4, where the initial state consisted of a virtual photon only) as presented in [17, 18, 15], and reiterated recently in [19]. Although the following discussion focusses on inclusive scattering, the arguments can later be modified slightly to apply also near (partonic) production thresholds.

The decoupling of the soft function from the hard part follows already from equations (2.20) and (2.21). Shortly, collinear gluons will be shown to also decouple from H. This will be followed by a section on time-ordered perturbation theory and unitarity. These tools will feature prominently in the final step towards full factorization, the decoupling of soft gluons from jets.

2.5.1 Decoupling of J from H

It has been remarked in section 2.4 that the coupling of the jets to the hard function depends on the gauge chosen. In the axial gauge only one parton connects each J_i to H, but in Feynman gauge it is accompanied by longitudinal collinear gluons. Clearly, one would like to retain the freedom of gauge choice, in particular in view of the practical prevalence of the Feynman gauge. This requires proving that longitudinal gluons decouple from the hard part. The proof proceeds through an application of the non-abelian QCD Ward identities to carefully defined sets of diagrammes. It will be illustrated for a single gluon and the generalization to all-orders briefly sketched.

Consider the coupling of a single collinear gluon to the hard function as shown in Fig.2.5a, where the quark has been chosen to move in the + direction. By the non-abelian Ward identities (cf. for instance [20, 21, 5, 6]), the sum over all attachments of the longitudinal gluon must vanish. But the only other attachment possible is depicted in Fig. 2.5b, hence this graph must equal the negative of the first. Now applying the usual

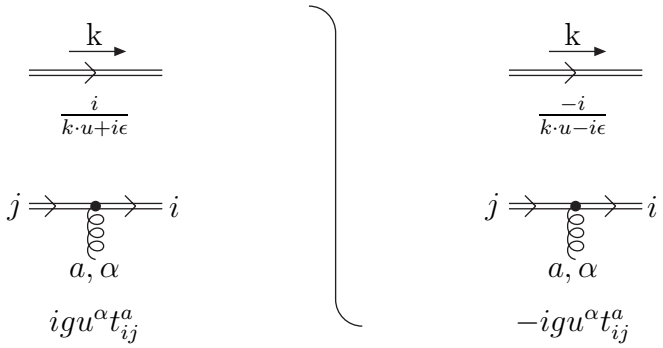

Figure 2.6: *Feynman rules for eikonal lines in the u^μ direction and their vertices, for both left and right of the final state cut.*

Feynman rules to Fig.2.5b yields

$$gH\frac{\not p+\not q}{(p+q)^2}\gamma^\alpha\ u\left(p\right)\epsilon^\beta\left(q\right)g_{\alpha\beta}\ ,$$

where the gluon is longitudinally polarized, $\epsilon^\beta=(\epsilon^+,0^-,0_\perp)$. Now multiply and divide by q^+ to find

$$gH\frac{\not p+\not q}{(p+q)^2}\gamma^-\ u\left(p\right)\epsilon^+\frac{q^+}{q^+}=gH\frac{\not p+\not q}{(p+q)^2}\not q\ u\left(p\right)\frac{\epsilon\cdot v}{q\cdot v}\ ,$$

where the vector $v^\alpha=(0^+,1^-,0_\perp)$ points in the direction opposite to the quark momentum. The replacement $\not q=\not p+\not q-\not p$ allows a further simplification, since by the massless Dirac equation $\not p u(p)=0$, upon which one obtains

$$gH\ u\left(p\right)\frac{\epsilon\cdot v}{q\cdot v}\ . \tag{2.23}$$

But this corresponds to Fig.2.5c if one applies the eikonal Feynman rules as summarized in Fig.2.6. Note the extra minus sign in Fig.2.5c due to the gluon momentum flowing opposite to the eikonal arrow as opposed to the definition in Fig.2.6.

At higher orders, i.e. with two or more soft gluons attaching, the number of diagrammes in the Ward identity increases considerably. However, the same algebraic techniques are applicable, and a pattern emerges which to all orders can be compactly summarized [22, 18, 15] as a Wilson line

$$1+\mathrm{P}\sum_{n=1}^{\infty}\prod_{i=1}^{n}\int\frac{d^4q_i}{(2\pi)^4}gu\cdot\tilde{A}\left(q_i^\mu\right)\frac{1}{u\cdot\sum_{j=1}^{i}q_j+i\epsilon}=\mathrm{P}\exp\left[ig\int_0^\infty d\lambda u\cdot A\left(\lambda u^\mu\right)\right]\ , \tag{2.24}$$

an exponential of integrals over the Lie-algebra valued gluon, multiplying the freely propagating quark. The non-abelian gauge group requires a path-ordering P with respect to group multiplication, with lower values of η ordered to the right. Graphically, possibly many collinear gluons are usually represented by just one attachment to the jet as in Fig.2.11 at the end of this section.

2.5.2 Time-ordered perturbation theory and unitarity

The decoupling of the soft function from the jets will rely heavily on the use of time-ordered (or light-cone-ordered) perturbation theory and summations over sets of cut diagrammes.

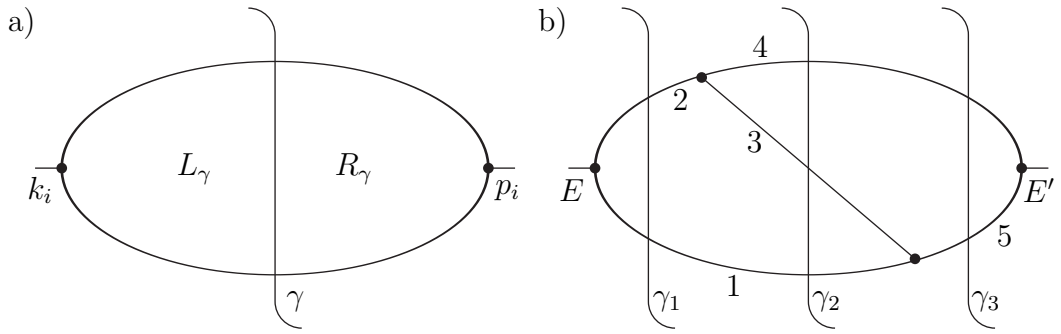

Figure 2.7: *Cut diagrammes illustrating the unitarity arguments, a) General case b) Concrete example with its three possible final state cuts (the numbering of the internal lines corresponds to the notation in (2.27) and (2.28)).*

The physics concepts are all too easily lost amid digressions necessary to explain the tools required for the proof. It therefore seems justified to introduce them in a separate section. For more details consult [5].

Time-ordered perturbation theory (TOPT), sometimes also called old-fashioned perturbation theory, can be derived from the usual Feynman integrals by integrating over the energy components of internal loop momenta. These integrations set the lines internal to the considered diagramme on shell. In this respect, TOPT is closer to the version of perturbation theory familiar from ordinary quantum mechanics. It thus makes explicit the transitions of the system through unperturbed intermediate states. Propagators depend on on-shell energies, but intermediate states do not have to respect energy conservation. The price to be paid for this is the introduction of a sum over time-orderings and the loss of Lorentz covariance at the level of the individual time-ordering (although covariance is restored upon summation). Instead of repeating the derivation of time-ordered from the usual perturbation theory as presented e.g. in [5], it should suffice here to show its application in unitarity proofs by means of an explicit example.

Consider some diagramme G as shown in Fig. 2.7a, with left and right parts L_γ and R_γ, respectively, whose dependence on the location of the final state cut is reflected in the subscript. The external momenta are denoted collectively by k_i and p_i. In TOPT one needs to sum over all time-orderings. Given a particular time-ordering τ, one can still cut G in various ways consistent with τ, effecting an allocation of the lines in G to L_γ, R_γ, or the final state. Intermediate states contribute propagators whose imaginary parts depend on whether they form part of L_γ or R_γ. Lines crossing the final state cut supply no propagators but final state delta functions in energy, which are reexpressed according to the delta function identity

$$-2\pi i\delta\left(x\right) = \frac{1}{x+i\epsilon} - \frac{1}{x-i\epsilon}\ . \tag{2.25}$$

Taking the sum over all cuts then yields

$$\begin{aligned}\sum_\gamma G_\gamma \;=\; & \sum_{\tau\in G}\int\prod_{a\in G}\frac{d^3q_a}{\left(2\pi\right)^3}\;\prod_{b\in G}\frac{N_G}{2\omega_b}\;\sum_{\gamma\in\tau}\;\prod_{s\in R_\gamma}\frac{1}{E_s-\sum\limits_{c\in s}\omega_c-i\epsilon}\\ & (-i)\left(\frac{1}{E_\gamma-\sum\limits_{m\in\gamma}\omega_m-i\epsilon}-\frac{1}{E_\gamma-\sum\limits_{m\in\gamma}\omega_m+i\epsilon}\right)\end{aligned}$$

$$\prod_{s\in L_\gamma} \frac{1}{E_s - \sum\limits_{c\in s}\omega_c + i\epsilon} \ . \tag{2.26}$$

Here a counts the internal loops of the diagramme G and b are its internal lines. The notation $\gamma \in \tau$ refers to all cuts consistent with the time-ordering τ. Intermediate states s are either part of the left or the right hand parts of the diagramme and themselves composed in turn of possibly many lines; ω_c denotes the on-shell energy of line c. N_G is some numerator factor depending on external and loop momenta, but will play no central role in the argument to follow.

For any fixed time-order τ the contributions of the different possible cuts to (2.26) cancel pairwise at the integrand level, except for γ at either the extreme right or left. One can see this happening in the concrete example of Fig.2.7b. Suppressing overall factors and integrations the three possible cuts contribute denominators

$$\begin{aligned}
\gamma_1 \ &: \ \left(\frac{1}{E-\omega_1-\omega_2-i\epsilon} - \frac{1}{E-\omega_1-\omega_2+i\epsilon}\right) \frac{1}{\omega_2-\omega_3-\omega_4+i\epsilon} \ \frac{1}{\omega_1+\omega_3-\omega_5+i\epsilon} \\
\gamma_2 \ &: \ \frac{1}{E-\omega_2-\omega_1-i\epsilon} \left(\frac{1}{\omega_2-\omega_3-\omega_4-i\epsilon} - \frac{1}{\omega_2-\omega_3-\omega_4+i\epsilon}\right) \frac{1}{\omega_1+\omega_3-\omega_5+i\epsilon} \\
\gamma_3 \ &: \ \frac{1}{E-\omega_2-\omega_1-i\epsilon} \ \frac{1}{\omega_2-\omega_3-\omega_4-i\epsilon} \left(\frac{1}{\omega_1+\omega_3-\omega_5-i\epsilon} - \frac{1}{\omega_1+\omega_3-\omega_5+i\epsilon}\right) \ .
\end{aligned} \tag{2.27}$$

Adding all these leads to mutual cancellations and leaves only the difference of

$$\frac{1}{E-\omega_2-\omega_1-i\epsilon} \ \frac{1}{\omega_2-\omega_3-\omega_4-i\epsilon} \ \frac{1}{\omega_1+\omega_3-\omega_5-i\epsilon} \tag{2.28}$$

and its complex conjugate. This observation generalizes and the only terms left in (2.26) are

$$\begin{aligned}
\sum_\gamma G_\gamma \ &= \ i \sum_{\tau\in G} \int \prod_{a\in G} \frac{d^3q_a}{(2\pi)^3} \ \prod_{b\in G} \frac{N_G}{2\omega_b} \\
&\left(\prod_{s\in G} \frac{1}{E_s - \sum\limits_{c\in s}\omega_c + i\epsilon} - \prod_{s\in G} \frac{1}{E_s - \sum\limits_{c\in s}\omega_c - i\epsilon}\right) \ .
\end{aligned} \tag{2.29}$$

This result can compactly be expressed as

$$\sum_\gamma G_\gamma = 2 \ \mathrm{Im} \ G \ , \tag{2.30}$$

and visualized diagrammatically as in Fig.2.8. Since G constitutes a contribution to the transition amplitude T, (2.30) is equivalent to $i\left(T - T^\dagger\right) = -T^\dagger T$ and implies $S^\dagger S = \mathcal{I}$ for the perturbative S-matrix $S = \mathcal{I} + iT$. [3] In this way TOPT and sums over cut diagrammes can be employed to prove unitarity of the field theory under consideration. The methods just described will now be applied in only slightly modified form (light-cone- instead of time-ordered perturbation theory) to achieve the decoupling of the soft function from the jets.

[3] The S-matrix will not feature again in the following sections, so no confusion with the soft function otherwise denoted by S can occur.

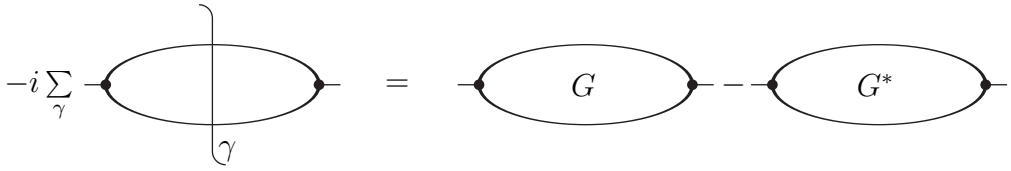

Figure 2.8: *Illustration of the identity in (2.30).*

2.5.3 Decoupling of S from J

The decoupling of the soft function from the jets [17, 18] constitutes the last, and most difficult, step towards the proof of full factorization of hadronic cross sections. One first shows that the jet function depends only on the q_l^--components of the soft momenta. This implies that the soft gluons become longitudinal and their coupling to the jets can consequently be simplified employing the Ward identities, a method very similar to that applied in the decoupling of collinear gluons from the hard part.

To begin, choose the jet to be moving in the +-direction. Since the jet carries energy of the order of the large invariant characterizing the process, clearly q_l^+ can be neglected with respect to the +-components of the collinear particles in the jet. It thus remains to be shown that $q_l^\perp$ can be neglected relative to q_l^-. Typically, this is the case and the decoupling follows almost immediately, but there are exceptions. In their initial definitions, internal loop integrations over −-components of momenta can pass through regions where $q_l^- \simeq 0$, and thus $q_l^- \ll q_l^\perp$, so that $q_l^\perp$ cannot be neglected with respect to q_l^-. Such regions are referred to as either Coulomb or, more frequently, as Glauber regions [23, 18]. However, as complex integrations, the q_l^- contours can be deformed away from the origin without affecting the result, provided no singularities obstruct this manipulation. Indeed, in the absence of initial state hadrons such obstructions do not exist since all poles lie in the same q_l^- half plane. However, because in later sections and chapters processes with initial state hadrons will be considered, it seems worthwhile to discuss the more general case at this point.

Consider thus an initial state hadron of momentum P_A. Most of its +-momentum, in fact precisely the fraction x_A, is carried into the hard scattering by some parton of momentum k_A, whereas another parton splits off with $l_A^+ = (1-x_A)\,P_A$ and escapes into the final (partonic) state. [4] Such partons are commonly referred to as spectators. If soft gluon momenta attach to such spectator lines and flow into the hard interaction from there as shown in the simple example of Fig.2.9 they contribute to the amplitude q^- integrals of the form

$$G \sim \int dq^- \frac{1}{2q^+q^- - q_\perp^2 + i\epsilon}\,\frac{1}{2x_AP_A^+\left(k_A^- + q^-\right) - \xi + i\epsilon}\,\frac{1}{2\,(1-x_A)\,P_A^+\left(l_A^- - q^-\right) - \xi + i\epsilon}\,. \tag{2.31}$$

Here k_A is the momentum flowing into the hard interaction, with $k_A^+ = x_AP_A$. The q^--contour is thus pinched between the poles

$$q_1^- = -k_A^- + \frac{\xi}{2x_AP_A^+} - \frac{i\epsilon}{2x_AP_A^+}\,, \qquad q_2^- = l_A^- - \frac{\xi}{2\,(1-x_A)\,P_A^+} + \frac{i\epsilon}{2\,(1-x_A)\,P_A^+}\,. \tag{2.32}$$

[4] As any parton crossing the final state cut of the partonic diagramme it will later undergo hadronization.

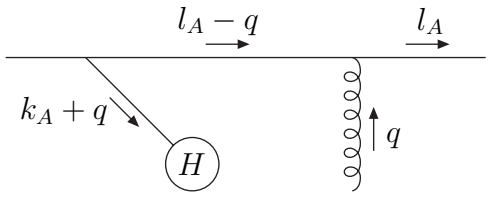

Figure 2.9: *Gluon coupling to a spectator line in a (rather simple) jet; this configuration leads to a pinch of the q^--contour.*

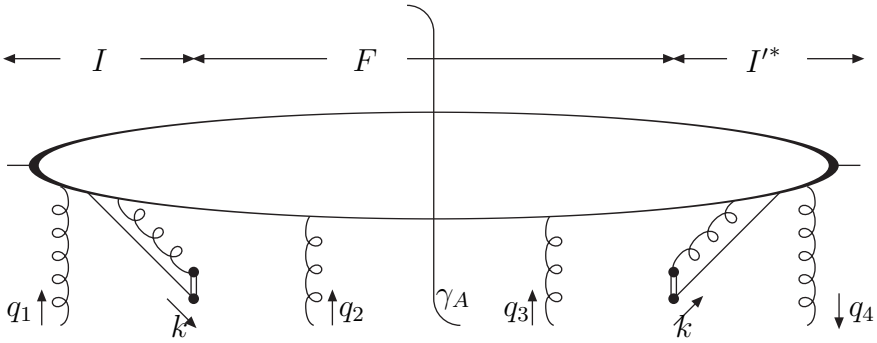

Figure 2.10: *A jet in x^+ ordered perturbation theory subdivided into initial and final state contributions I and F, respectively. Soft momenta q_j^- flow into the jet from the soft function. The subscripts on the q_j in the graphs are supposed to denote an ordering rather than a limitation to exactly four attachments.*

The two solutions are close together since they differ only by small components of k_A and l_A. Also, ξ is of the same order as $k_\perp^2$.

This observation generalizes to higher orders; the poles due to spectator attachments prevent one from deforming the q_l^--contours into the upper half planes away from the dangerous Glauber regions, into regions where the $\vec{q}_\perp$ components could be safely neglected with respect to q^+, q^-. However, it turns out that all such poles cancel upon summing over final state cuts of the jet, thus allowing the desired deformation. To achieve this result, one first splits the rest of the diagramme from the jet and carries out all x^+ loop integrations for the jet only. This procedure differs from the derivation of time-ordered perturbation theory only in the choice of space-time coordinates (x^+ instead of $t = x^0$). Consequently, this light-cone perturbation theory (LCPT) leads to results very similar to those of the previous section, albeit with energy replaced by *minus* components of momenta in propagators. LCPT introduces not a time- but a light-cone-ordering of vertices. Since the hard interaction involves exclusively large +-momenta, its location on the light-cone is precisely determined. [5] It can therefore serve as a reference point with soft gluons attaching either *before* or *after* the hard interaction as measured in *light-cone time*, justifying the separation into initial and final state attachments I and F, respectively, as shown graphically in Fig. 2.10. In Fig.2.10 the four soft gluons connecting to the jet each signify multiple attachments. Note also that according to the results of previous sections the factorization of collinear gluons from the hard function and their absorption by eikonal lines have been indicated for both the amplitude and its complex conjugate.

[5] Just as short wavelengths can resolve small spatiotemporal scales.

The observations justifying Fig.2.10 can be expressed algebraically as

$$J_A^{(\gamma_A)} = \sum_T I'^*_T \otimes F_T^{(\gamma_A)} \otimes I_T \ , \tag{2.33}$$

where the tensor product $\otimes$ serves to abbreviate vector indices and internal loop momentum integrals. The sum is over x^+-orderings T. The imaginary parts resulting from the $i\epsilon$ prescriptions in final state gluon attachments as well as the contributions to the mass-shell delta functions depend on the location of the cut γ_A, indicated by the superscripts on $F_T^{(\gamma_A)}$ and $J_A^{(\gamma_A)}$. In constructing the cross section all such cuts need to be summed over according to

$$\sum_{\gamma_A=1}^{N} \left[\prod_{n=\gamma_A+1}^{N} \frac{1}{-k_A^- - D_n - i\epsilon} 2\pi\delta\left(-k_A^- - D_{\gamma_A}\right) \prod_{n=1}^{\gamma_A-1} \frac{1}{-k_A^- - D_n + i\epsilon} \right] \ . \tag{2.34}$$

Here the possible locations of the cut as well as the intermediate states are numbered from left to right. Any state left or right of the cut contributes a denominator with imaginary part as indicated. The D_n and D_{γ_A} are functions of the soft momenta. The sum over cuts is unweighted as in (2.34) provided the rest of the diagramme is independent of whether a particular soft gluon attaches to the jet before or after the cut. This independence can be proven for the general case applying x^--ordered perturbation theory [18]. An explicit and instructive low order example is presented in [19].

Similar to the unitarity arguments of the previous section, carrying out the sum in (2.34) gives

$$i \prod_{n=1}^{N} \frac{1}{-k_A^- - D_n + i\epsilon} - i \prod_{n=1}^{N} \frac{1}{-k_A^- - D_n - i\epsilon} \ . \tag{2.35}$$

This result constitutes the integrand for $(2\pi)^{-1} \int dk_A^-$. If there are no soft gluon attachments at all to F only a single term each remains of the two products in (2.35). The two remaining terms can be combined and integrate to 1. If, on the other hand, there is at least one soft gluon attaching to F, then $N > 1$ and (2.35) can be shown to integrate to zero by closing the contour at infinity and avoiding the poles. All soft final state interactions thus cancel after summing over cuts. The q_l^--contours are unpinched and can be deformed into the upper half plane away from the Glauber region. Along the deformed contours the $q_l^\perp$ are negligible. After deleting these terms the contours can be returned to their original positions.

Hence the soft gluons coupling S to J have become longitudinal. To decouple them one can now utilize the Ward identities, as in the decoupling of collinear gluons from H. The soft function is then seen to couple to eikonal lines moving in the jet direction. In Fig.2.11 this is shown along with two hadronic jets and a hard scattering function. Note that due to the complete factorization from the rest of the diagramme, the sum over final state cuts can be carried out independently for the soft function. Applying once again the unitarity arguments introduced in the previous section one can now show [24] that for inclusive scattering $S = 1$. This concludes the proof of factorization for inclusive processes. Observables can thus be expressed in the form

$$\tilde{\sigma}\left(N\right) = \tilde{H}\left(N\right) \tilde{J}_A\left(N\right) \tilde{J}_B\left(N\right) \tag{2.36}$$

in moment space or, equivalently, as convolutions

$$\sigma\left(x_A, x_B\right) = \int_0^1 \frac{d\xi_A}{\xi_A} \frac{d\xi_B}{\xi_B} H\left(x_A/\xi_A, x_B/\xi_B\right) J_A\left(\xi_A\right) J_B\left(\xi_B\right) \tag{2.37}$$

in momentum space, where all arguments except the Bjorken variables have been suppressed. Note the generality of this result; the jets J_A and J_B could be either of the two parton distributions $\phi_{i/j}$ or $\phi_{i/H}$ familiar from chapter 1. No soft, long-wavelength gluons upset the separation into short distance (partonic) hard scattering and jet functions (absorbing non-perturbative effects); this provides the field-theoretic justifications for equations like (1.15). In this sense Fig.2.11 summarizes in graphical form the ultimate result of this section, namely the full factorization of both collinear and soft gluons, allowing even initial state hadronic particles. Concrete examples for such initial state jets are provided by the matrix elements introduced in (1.21) and (1.22) for quarks in hadrons and quarks in quarks, respectively.

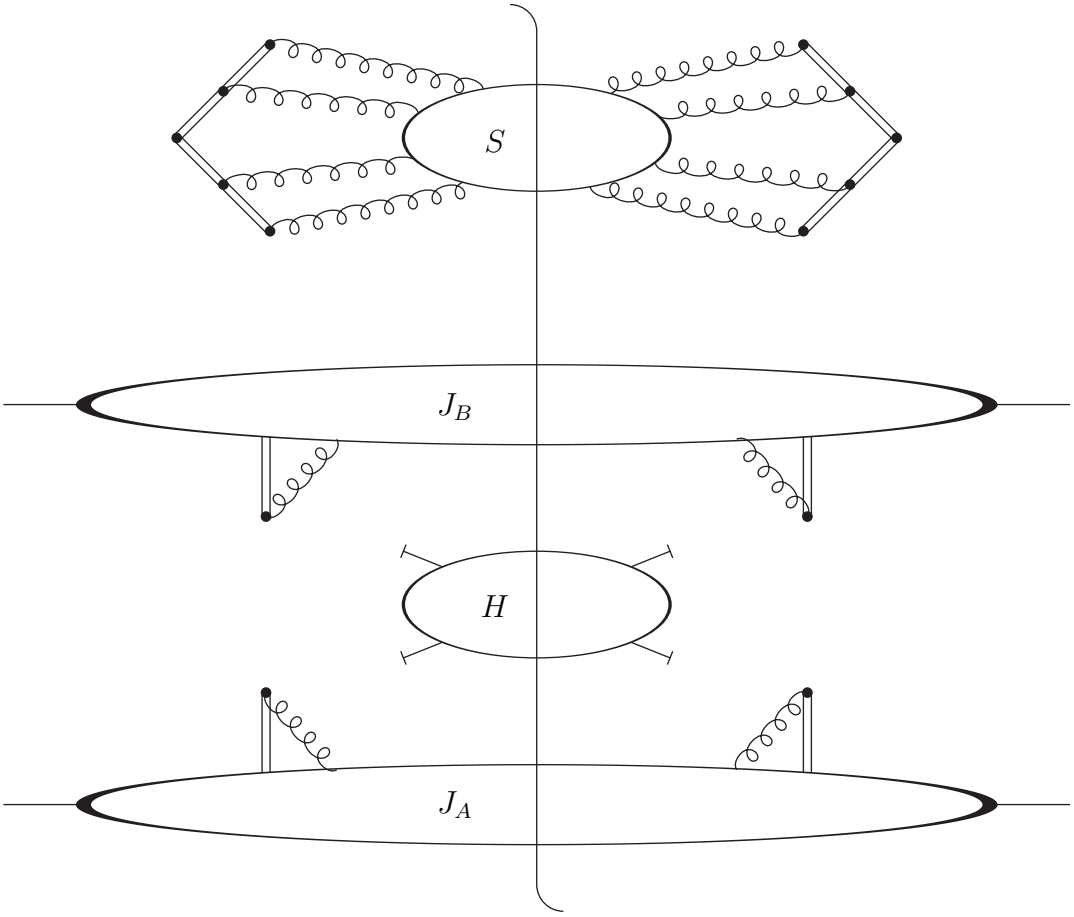

Figure 2.11: *General leading region for hadron-hadron scattering after complete factorization of collinear and soft gluons.*

2.6 Factorization near threshold

The discussion of factorization theorems up to this point has focussed on inclusive processes [25]. Its aim has been to provide a solid basis for expressing hadronic scattering cross sections (and related quantities such as structure functions) as convolutions of the corresponding partonic quantities with (non-perturbative) parton distributions. The importance of these results cannot be overstated, since they constitute (tacit) presuppositions for most experimental or phenomenological investigations of observables in hadronic collisions. Besides, many of the arguments presented can also be applied in only slightly modified form to achieve in certain regions of phase space re-factorizations of partonic cross sections, which in turn allows resummation calculations. The aim of the latter is to control large logarithmic terms of the type introduced at the end of section 1 in (1.23) and (1.24), and even some of the constants occurring in partonic cross sections. All these finite but potentially large terms are still present in the partonic hard function after the factorization as expressed in (2.36) and (2.37). In the factorization near production thresholds new parton distributions ψ different from the ϕ densities will play a key role. Since near threshold the overall energy of the partonic process is severely restricted, in ψ partonic energies instead of light-cone momenta will be fixed. In section 3.3 an explicit example for the computation of both a ϕ and a ψ density will be given, but already at this point it should be clear that this fixing of a different momentum component does not affect the decoupling of the jets from the hard scattering function as presented in section 2.5. However, the energy restrictions on S could upset the decoupling of the soft function from the jets. Recall that this result followed only upon taking an unweighted sum over radiated soft gluons. In contrast to this, final states are not freely summed over now, since the energy condition restricts also the +-momenta in the leading region. But any extra terms resulting from this incomplete cancellation of final state interactions can be absorbed into the soft function. This will be reflected by the presence of soft gluon interactions with final state particles in the concrete examples to be computed in section 3.4. The soft function is no longer unity but still infrared finite (collinear divergences have been absorbed by the jets) and contains only single logarithms. The absence of double logarithms follows from arguments identical to those for the complete cancellation of S in the inclusive case, for such collinear and soft configurations would require an even softer scale, integration over which is unrestricted by the threshold condition. As in Fig.2.11 the soft function thus decouples from the rest of the diagramme, but unlike in the inclusive case not all positions of the final state cut contribute with the same weight.

2.7 Exponentiation and resummation

This section constitutes the last step in the derivation of resummation [26, 27, 28, 29, 30, 31, 32, 33, 34, 35, 36]. It is even more sketchy than previous sections where factorization proofs for QCD cross sections have been discussed and particularized to kinematic regions dominated by soft radiation. The large higher order corrections resulting from this are completely accounted for by soft and jet functions. These ingredient factors of the partonic refactorization can now all be shown to exponentiate. Whereas the soft functions S are particular to the partonic process under consideration, the partonic jets ψ are universal in the sense that they only depend on the types of partons involved (in this sections always

assumed to be quarks, so the subscripts q/q can be suppressed on $\psi_{q/q}$ and $\phi_{q/q}$), but not on the final state produced in the hard scattering. It is therefore sufficient to derive the exponentiated forms of the latter in whichever process lends itself best to this purpose. For reasons of simplicity the DY process has become the standard choice and will also be considered in the present treatment. Near threshold, i.e. for large N (cf. the discussions of (1.25) and (1.26) in section 1.4), its moment space unsubtracted cross section factorizes according to

$$\tilde{\sigma}(N) = \tilde{\psi}(N)\,\tilde{\psi}(N)\,\tilde{U}(N)\,H_{\mathrm{DY}}(N) + \mathcal{O}(1/N) \ , \tag{2.38}$$

with two initial state quarks jets ψ and a soft function, for historical reasons denoted U. ψ contains double and single, but U has only single threshold logarithms and is furthermore free of collinear divergences. Functions of the type U and ψ will be computed explicitly in chapter 3. To render (2.38) finite collinear singularities have to be factorized according to

$$\tilde{\sigma}_{\mathrm{fin}}(N) = \tilde{\sigma}(N)/\tilde{\phi}^2(N) \ . \tag{2.39}$$

Rewriting the mass shell delta function for the DY pair near threshold[26] ensures that all factors contribute with the correct weight in

$$\begin{aligned}\sigma\left(z,Q^2\right) &= H_{\mathrm{DY}}\left(Q^2\right)\int\frac{d\xi_1}{\xi_1}\frac{d\xi_2}{\xi_2}\psi(\xi_1,Q)\,\psi(\xi_2,Q)\int\frac{dw}{w}U(wQ)\,\delta\left(z-(1-w)\,\xi_1\xi_2\right)\\ &\quad +\mathcal{O}\left((1-z)^0\right) \ ,\end{aligned} \tag{2.40}$$

the moment space counterpart of equation (2.38). In (2.40) leading terms due to soft radiation are generated by the lower limit on the w integration and by the upper limits on ξ_1, ξ_2.

Since, as remarked earlier, U has only single logarithmic enhancements near threshold, its exponentiation follows quite simply from renormalization group techniques. The soft function depends on the renormalization scale μ directly and through the running coupling α_s. Under scale variations it behaves as

$$\mu\frac{d}{d\mu}\tilde{U}\left(\frac{Q}{N\mu},\alpha_s(\mu)\right) = -\nu\left(\alpha_s(\mu)\right)\tilde{U}\left(\frac{Q}{N\mu},\alpha_s(\mu)\right) \ , \tag{2.41}$$

with ν the anomalous dimension of the composite operator to be introduced in (2.45). The exclusive dependence on the ratio Q/N indicates that $\tilde{U}$ depends only on soft kinematic scales. Solving (2.41) gives

$$\tilde{U}\left(\frac{Q}{N\mu},\alpha_s(\mu)\right) = \tilde{U}\left(\frac{Q}{\mu},\alpha_s(\mu)\right)\exp\left[\int_{\mu}^{\mu/N}\frac{d\lambda}{\lambda}\nu\left(\alpha_s(\lambda)\right)\right] \ , \tag{2.42}$$

with all N-dependence exponentiating. The exponent can also be expressed via momentum space as

$$\tilde{U}\left(\frac{Q}{N\mu},\alpha_s(\mu)\right) = \tilde{U}\left(\frac{Q}{\mu},\alpha_s(\mu)\right)\exp\left[\int_0^1 dz\frac{z^{N-1}-1}{1-z}\nu\left(\alpha_s\left(\left(1-z\right)^2Q^2\right)\right)\right] \ . \tag{2.43}$$

The anomalous dimension is process-dependent, and Q may in other processes be replaced by a different characteristic hard energy scale, e.g. by the mass of the charm quark in open charm production to be discussed in the next sections.

Since ψ contains collinear divergences (to be absorbed by ϕ as shown in (2.39)) and double logarithms (requiring typically something like not one but two scale integrals) its exponentiation is a little more involved. However, for the DY process there exist exponentiation proofs for the complete cross section near threshold [26, 37]. The moments of the eikonal DY cross section exponentiate at the level of integrands [22, 38, 39], with exponents consisting of webs, selections of cut diagrams under criteria defined by graphical topology (irreducibility under cuts of the eikonal lines) and with possibly modified colour weights. Each web is a cut diagram, and can be integrated over the momentum k that it contributes to the final state. The definition of eikonal cross sections requires the concept of Wilson lines, which first occurred in (2.24). The Wilson lines

$$\Phi_\beta^{(f)}(\lambda_2,\lambda_1;X) = \mathrm{P}\exp\left(-ig\int_{\lambda_1}^{\lambda_2} d\eta\ \beta\cdot A^{(f)}(\eta\beta+X)\right)\ . \tag{2.44}$$

required here are again exponentials of integrals over the Lie-algebra valued gluon field, but now over a finite line segment along direction β^μ and passing through spacetime point X. The gauge field is a matrix in the representation of parton f. Such Wilson lines summarize the coupling of soft gluons to a single parton, or an entire jet [15, 24, 25], neglecting recoil, and are therefore the natural building blocks for defining eikonal cross sections[40], which have already been encountered implicitly in section 2.5. For DY, the product

$$\mathcal{W}_{\mathrm{DY}}(X) = \Phi_{\beta_2}^{(\bar q)}(0,-\infty;X)\ \Phi_{\beta_1}^{(q)}(0,-\infty;X) \tag{2.45}$$

represents the QCD radiation generated by the annihilation of the incoming quark and antiquark colour sources, again neglecting recoil. In terms of these operator products, the DY eikonal cross section at fixed gluon radiation energy $w\,Q/2$ can be defined as

$$\begin{aligned}\sigma_{\mathrm{DY}}^{(\mathrm{eik})}(wQ,\epsilon) &= \frac{Q}{6}\int\frac{d\lambda}{2\pi}\,\mathrm{e}^{-i\lambda wQ/2}\\ &\quad\times\mathrm{Tr}\,\langle 0|\,\bar{\mathrm{T}}\left[\mathcal{W}_{\mathrm{DY}}(0)^\dagger\right]\,\mathrm{T}\left[\mathcal{W}_{\mathrm{DY}}(\lambda\hat n)\right]|0\rangle\ ,\end{aligned} \tag{2.46}$$

with $\hat n = (1,\vec 0)$. The trace is over colours and $T,\bar T$ represent time-ordering and anti time-ordering, respectively. The expression is normalized to $\delta(w)$ at lowest order.

The eikonal is related to the full cross section according to

$$\sigma_{\mathrm{DY}} = \psi_V\ \psi_V\ \sigma_{\mathrm{DY}}^{(\mathrm{eik})}\ . \tag{2.47}$$

The purely virtual ψ_V contains poles but no logarithmic threshold enhancements since these require (the imperfect cancellation of) real and virtual contributions. For the Drell-Yan cross section one has

$$\begin{aligned}\sigma_{\mathrm{DY}}^{(\mathrm{eik})}(N,\epsilon) &= \exp\left\{2\int\frac{d^{4-2\epsilon}k}{(2\pi)^{4-2\epsilon}}\,\theta\left(\frac{Q}{\sqrt2}-k^+\right)\,\theta\left(\frac{Q}{\sqrt2}-k^-\right)\right.\\ &\quad\left.\times w_{\mathrm{DY}}\left(k^2,\frac{k\cdot\beta_1 k\cdot\beta_2}{\beta_1\cdot\beta_2},\mu^2,\alpha_s(\mu),\epsilon\right)\left(\mathrm{e}^{-N(2\,k\cdot\zeta_T/Q)}\ -1\right)\right\},\end{aligned} \tag{2.48}$$

where w_{DY} represents the web for DY at fixed total momentum k^μ, and the β_1 and β_2 are the velocities of the colliding eikonal lines. The kinematics vector $\zeta_T = (1,\vec 0)$ projects out the time-like component of soft radiation to be kept fixed, here the energy. The θ functions

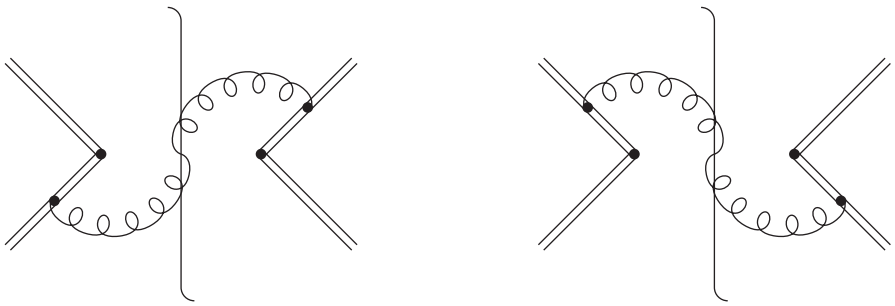

Figure 2.12: *The two webs of the DY eikonal cross section at order α_s.*

serve to limit the plus and minus momenta of total gluon radiation. With this choice the maximum value of k_T^2 is Q^2, which is also the natural value for the renormalization scale in the virtual corrections. Note that these cross sections are defined in $d = 4-2\epsilon$ dimensions, indicated by the argument ϵ, and that collinear singularities are still present.

The one-loop radiative contribution to the web shown in Fig.2.12 is given by

$$w_{DY}^{(1)(\mathrm{real})}(k) = \frac{2C_F\alpha_s}{\pi}\,\left(4\pi\mu^2\mathrm{e}^{-\gamma_E}\right)^{\epsilon}\,\delta_+(k^2)\,\frac{\beta_1\cdot\beta_2}{\beta_1\cdot k\,\beta_2\cdot k}\,. \tag{2.49}$$

Expressing the measure of the momentum integration as $dk_0dk_3d^{2-2\epsilon}k_\perp$ one finds for the eikonal cross section

$$\ln\sigma_{\mathrm{DY}}^{(\mathrm{eik})}(N,\epsilon) = \frac{4C_F\alpha_s}{\pi}\left(4\pi^2\mu^2\right)^{\epsilon}\int\frac{dk_0dk_3d^{2-2\epsilon}k_\perp}{2k_3k_\perp^2}\delta\left(k_3-\sqrt{k_0^2-k_\perp^2}\right)\left(e^{-\frac{Nk_0}{2Q}}-1\right)\,. \tag{2.50}$$

Expanding now in $k_\perp/k_0$ and using the delta function one obtains

$$\begin{aligned}\ln\sigma_{\mathrm{DY}}^{(\mathrm{eik})}(N,\epsilon) &= \frac{4C_F\alpha_s}{\pi\Gamma\left(1-\epsilon\right)}\left(4\pi\right)^{\epsilon}\left(\frac{\mu^2}{Q^2}\right)^{\epsilon}\int\limits_0^1\frac{dw}{w}\int\limits_0^w\frac{d\lambda}{\lambda^{1+2\epsilon}}\left(e^{-Nw/2}-1\right)\\ &= \frac{2C_F\alpha_s}{\pi\Gamma\left(1-\epsilon\right)}\left(4\pi\right)^{\epsilon}\left(\frac{\mu^2}{Q^2}\right)^{\epsilon}\left(-\frac{1}{\epsilon}+\ln^2N+\ldots\right)\,,\end{aligned} \tag{2.51}$$

where in the last line only the poles and the highest power of $\ln N$ have been displayed. The collinear pole arising from the λ integration is cancelled by the distribution ϕ to render the cross section finite. The remaining term $\ln w$ produces a double logarithm in N upon carrying out the w integration. One can now compare the two expressions (2.38) and (2.47) for $\sigma_{\mathrm{DY}}^{(\mathrm{eik})}(N,\epsilon)$ to derive

$$\begin{aligned}\ln\tilde{\psi}\left(N\right) &= \frac{2C_F\alpha_s}{\pi\Gamma\left(1-\epsilon\right)}\left(4\pi\right)^{\epsilon}\left(\frac{\mu^2}{Q^2}\right)^{\epsilon}\int\limits_0^1\frac{dw}{w}\int\limits_0^w\frac{d\lambda}{\lambda^{1+2\epsilon}}\left(e^{-Nw}-1\right)\\ &\quad -\frac{1}{2}\int\limits_0^1dz\frac{z^{N-1}-1}{1-z}\nu\left(\alpha_s\left(\left(1-z\right)^2Q^2\right)\right)\,,\end{aligned} \tag{2.52}$$

the desired exponentiated version of ψ.

Alternatively, a proof of the exponentiation of ψ based on its behaviour under changes of renormalization scale and gauge fixing can be found in [26], where also explicit expression for the new densities are given. They are quite similar but not identical to the ϕ densities, e.g. for a quark in quark one has

$$\begin{aligned}\psi_{q/q}(\xi) &= (2\pi)^{-1} \int_{-\infty}^{\infty} dy^0 \exp(-i\xi p^0 y^0) \\ &\quad \frac{1}{2}\sum_{\sigma}\langle q(p,\sigma) \mid \bar{q}(y^0,\vec{0})\frac{1}{2}\gamma^+ q(0) \mid q(p,\sigma)\rangle_{A_0=0} \ . \end{aligned} \tag{2.53}$$

For the gluon density $\psi_{g/g}$ a similar result is given in [41].

Factorization and resummation have in this chapter been discussed in a general context. These tools can now be applied to the deep inelastic production of heavy quarks in chapters 3 through 5, and to the Drell-Yan process in chapter 6.

Chapter 3

Resummation of deep inelastic charm production

The method of threshold resummation will now be applied to heavy quark production in deep inelastic scattering. This reaction offers a direct probe of the gluon density in the proton, unpolarized as well as polarized. Furthermore, the presence of two energy scales, first that of the exchanged photon Q and second the mass m of the charm quark, is conducive to detailed studies of perturbative QCD dynamics.

Unpolarized charm production has been extensively studied both experimentally [42, 43, 44] and theoretically [45, 46, 47, 48], including a NLL resummation [49]. Spin dependent deep-inelastic lepton-hadron scattering has also received much interest during the past years [50, 51, 52, 53]. Presently, next-to-leading order analyses of the experimental data for the structure function g_1, to be defined in section 3.1, allow for the extraction of polarized parton distributions $\Delta\phi_{i/P}$. Contrary to naive expectation, these measurements indicate that only less than half of the proton spin is carried by the constituent quarks, a fact frequently referred to as the nucleon spin puzzle. Despite progress in recent years, the polarized parton distributions $\Delta\phi_{i/P}$ are still considerably less constrained than their unpolarized counterparts $\phi_{i/P}$. This is particularly true for the gluon spin distribution $\Delta\phi_{g/P}$, the leading candidate on the list of proposed solutions to the spin puzzle, since its first moment contributes to the sum rule for the nucleon's spin content [54, 55], as to be explained in section 3.2. Numerous polarized hard scattering processes are sensitive to the gluon spin distribution. Since the charm upgrade the HERMES experiment measures polarized leptoproduction of charmed hadrons [56, 57, 58, 59]. The COMPASS experiment [60] will measure the polarized gluon density in the proton $\Delta\phi_{g/P}$ through the boson-gluon fusion process and subsequent open charm production. COMPASS will probe both the region of photoproduction ($Q^2 \simeq 0$) as well as deep-inelastic scattering and extend the kinematical range accessible to the HERMES experiment.

In general, fixed target experiments, such as HERMES or COMPASS with centre-of-mass energies of $\sqrt{S} = 7.4$ GeV and 14.1 GeV respectively, operate rather close to the threshold for charm pair-production. In this region of phase space, the perturbatively calculable hard scattering cross section has potentially large higher order double-logarithmic threshold corrections. Thus, a resummation of these Sudakov logarithms to all orders in perturbation theory as explained in the previous chapter is required in order to regain

control over the perturbative expansion. This Sudakov resummation will be carried out to next-to-leading logarithmic (NLL) accuracy in this chapter. The final result provides an approximate sum of the complete perturbative expansion if, at each order, the Sudakov corrections dominate. Studies of threshold resummation for polarized scattering processes have been performed for the polarized Drell-Yan cross section [61]. By re-expanding the resummed cross section in α_s to next-to-leading (NLO) and next-to-next-to-leading order (NNLO) in chapter 4 estimates can be given of the size of the higher order corrections so far unknown exactly.

Section 3.1 deals with the factorization of the kinematics near the charm production threshold and the dynamics of the process at lowest order. Section 3.2 reviews the spin puzzle and expands on the motivation for studying the polarized gluon density. Sections 3.3 and 3.4 describe the computation of the two important ingredients in the resummation calculation, the jet and soft functions, respectively. Finally, section 3.5 presents the full exponent, the result of the resummation.

3.1 Kinematics and Born level dynamics

The process of lepton (l) – proton (P) scattering will in the following be considered in single-particle inclusive (1PI) kinematics

$$\mathrm{l}(l) + \mathrm{P}(p) \to \mathrm{l}(l-q) + \mathrm{Q}(p_1) + X[\overline{\mathrm{Q}}](p_2') \,, \tag{3.1}$$

where Q is a heavy quark and $X[\overline{\mathrm{Q}}]$ denotes any allowed hadronic final state containing at least the heavy antiquark. Since close to the charm threshold the exchange of heavy electroweak bosons is suppressed, only virtual photon exchange

$$\gamma^*(q) + P(p) \longrightarrow Q(p_1) + X[\bar{Q}](p_2') \tag{3.2}$$

is relevant. It will be useful to define the kinematic variables Q^2, x, y by

$$Q^2 = -q^2 > 0 \quad , \quad x = \frac{Q^2}{2p\cdot q} \quad , \quad y = \frac{p\cdot q}{p\cdot l} \,, \tag{3.3}$$

and the hadronic Mandelstam variables as

$$\begin{aligned} S &= (p+q)^2 = 2pq + q^2 = S' - Q^2, & T_1 &= (p-p_1)^2 - m^2 = -2pp_1, \\ U_1 &= (q-p_1)^2 - m^2 = -Q^2 - 2p_1 q \,, & S_4 &= S + T_1 + U_1 + Q^2 \,. \end{aligned} \tag{3.4}$$

These can easily be converted to variables of more applicational interest like transverse momentum or rapidity. The variable S_4 can be shown to measure the off-shellness of the process

$$S_4 = S + T_1 + U_1 + Q^2 = (p+q)^2 - (p_1+p_2)^2 - 2p_1 k_S \,, \tag{3.5}$$

where the relation $p_2' = p_2 + k_S$ for the anti-quark momentum inside the state X has been used.

Before going into the details of the resummation calculation one first needs to work out the partonic cross section and its relation to the partonic structure function at Born level.

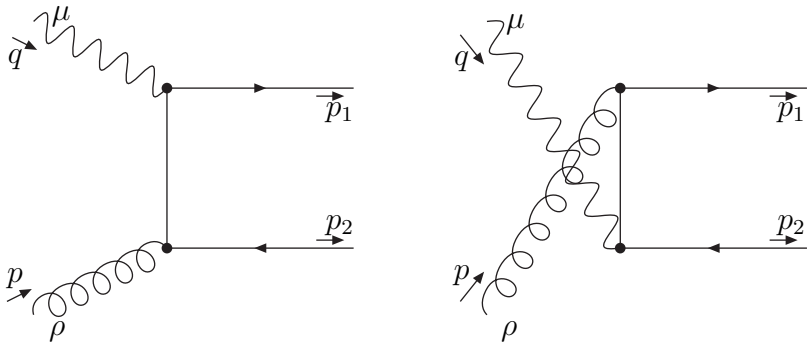

Figure 3.1: *The two diagrammes contributing to the production of heavy quarks through photon-gluon-fusion at Born level.*

The contributions from initial state quarks and antiquarks vanish at leading order and will therefore be neglected in the following. This leaves only the gluon-initiated partonic subprocess

$$\gamma^*(q) + g(k) \longrightarrow \mathrm{Q}(p_1) + X'[\overline{\mathrm{Q}}](p_2'), \tag{3.6}$$

where $k = z\,p$. The two diagrammes contributing to this process at Born level are shown in Fig.3.1. The matrix element for the first of these is given by

$$(\mathcal{M}_1)_{\mu\rho} = \bar{u}\,(p_1, \sigma_1))\,(-ie\gamma_m)\,\frac{i\,(\not{p}_1 - \not{q} + m)}{(p_1 - q)^2 - m^2}\,(-ig_s[t_a]_{ij}\gamma_\rho)\,v\,(p_2, \sigma)\ , \tag{3.7}$$

and by a similar expression for the second diagramme. The colour structure of the squared matrix element is given by $K_{g\gamma}C_AC_F$, where the average over initial state colours is contained in $K_{g\gamma} = 1/8$. The photonic and gluonic Lorentz indices of $\mathcal{M}$ have to be contracted with the appropriate helicity projection operator

$$-\frac{1}{4s'^2}\epsilon_{\mu\nu\rho\sigma}q^\rho p^\sigma \epsilon_{\alpha\beta\gamma\delta}q^\gamma p^\delta \tag{3.8}$$

for $M\,(++) - M\,(+-) = \Delta|\mathcal{M}|$. This gives

$$\Delta|\mathcal{M}|^2_{\mathrm{Born}} = g_s^2 e^2 e_H^2 \Delta B_{\mathrm{QED}} \tag{3.9}$$

with

$$\Delta B_{\mathrm{QED}} = -\left(\frac{t_1}{u_1} + \frac{u_1}{t_1}\right) - 2m^2\left(\frac{1}{t_1} + \frac{1}{u_1} + \frac{t_1}{u_1^2} + \frac{u_1}{t_1^2}\right) + 2q^2\left(\frac{1}{t_1} + \frac{1}{u_1} + \frac{2}{s'}\right)\ , \tag{3.10}$$

in agreement with the result [62, 63] in the $q^2 \longrightarrow 0$ limit. For comparison, the corresponding unpolarized result for $M\,(++) + M\,(+-)$ requires the projector $\frac{1}{4}g_{\mu\nu}g_{\alpha\beta}$ and is given by

$$B_{\mathrm{QED}} = \frac{t_1}{u_1} + \frac{u_1}{t_1} + 4\frac{m^2 s'}{t_1 u_1}\left(1 - \frac{m^2 s'}{t_1 u_1}\right) + 2\frac{s'q^2}{t_1 u_1} + 2\frac{q^4}{t_1 u_1} + 2\frac{m^2 q^2}{t_1 u_1}\left(2 - \frac{s'^2}{t_1 u_1}\right)\ . \tag{3.11}$$

The partonic invariants introduced here are

$$s = (k+q)^2 \equiv s' + q^2, \quad t_1 = (k-p_1)^2 - m^2, \quad u_1 = (q-p_1)^2 - m^2, \quad s_4 = (p_2')^2 - m^2. \tag{3.12}$$

Similar to S_4 the invariant s_4 parametrizes the inelasticity of the partonic reaction (3.6) in 1PI kinematics. This distance from threshold is conveniently measured in terms of a dimensionless weight function w_S [35],

$$w_S = \frac{s_4}{m^2} \simeq \frac{2\bar{p}_2 \cdot k_S}{m^2} \equiv \frac{2\zeta \cdot k_S}{m} \,. \tag{3.13}$$

This is one of the soft weights that will play a central role in the kinematical factorization of the process. The 1PI kinematics vector ζ is defined by splitting the recoil momentum $p_2' = \bar{p}_2 + k_S$ into the momentum $\bar{p}_2$ at threshold, and the momentum k_S of any additional (soft) radiation above threshold.

After phase space integration one obtains for the polarized and unpolarized cross sections

$$\frac{d\,(\Delta)\,\sigma}{dt_1} = \frac{\pi\alpha_s\alpha e_H^2}{s'^2}\,(\Delta)\,B_{\rm QED} \,. \tag{3.14}$$

As was done for inclusive deep inelastic scattering in section 1.2 these partonic results can be expressed as charm contributions to the unpolarized and polarized partonic structure functions. In order to do so, an antisymmetric part has to be added to the symmetric one of the hadronic tensor as given in definition (1.2). The relation of the polarized cross-section to the polarized structure function g_1 depends on the choice of normalization for this antisymmetric part of the hadronic tensor

$$W^A_{\mu\nu} = \frac{1}{pq}\epsilon_{\mu\nu\alpha\beta}p^\alpha q^\beta g_1 \,. \tag{3.15}$$

To project g_1 out from this one can use the projector

$$\frac{1}{s'}\epsilon^{\mu\nu\rho\sigma}q_\rho p_\sigma \,. \tag{3.16}$$

The lowest order differential charm contributions to the polarized partonic structure functions is thus

$$\frac{dg_{1,\rm c}^{(\rm q,0)}}{dt_1} = \frac{\alpha_s e_c^2 Q^2}{8\pi s'^2 x}\Delta B_{\rm QED} = \frac{Q^2}{8\pi^2\alpha x}\frac{d\Delta\sigma}{dt_1} \,. \tag{3.17}$$

Similarly, for the spin-averaged F_2 one finds

$$\frac{dF_{2,\rm c}^{(\rm q,0)}}{dt_1} = \frac{\alpha_s e_c^2 Q^2}{4\pi s'^2}B_{\rm QED} = \frac{Q^2}{4\pi^2\alpha}\frac{d\sigma}{dt_1} \,. \tag{3.18}$$

Neglecting electroweak radiative corrections[1], the difference of cross sections for reaction (3.1) with longitudinally polarized protons is expressed in terms of the double-differential deep-inelastic polarized hadronic heavy quark structure functions $d^2g_k/dT_1\,dU_1,\ k = 1,2$. Only the structure function g_1 is relevant asymptotically for $M/Q \ll 1$. It contains leading twist two operators and has a parton model interpretation, as has been explicitly computed to lowest order above. This justifies considering g_1 only.

[1] QED radiative corrections have been studied in the leading-logarithmic approximation in [64].

The double-differential structure function $d^2g_1^c/dT_1\,dU_1$ factorizes as

$$S'^2\frac{d^2g_1^c(x,Q^2,m^2,T_1,U_1)}{dT_1\,dU_1} = \int_{z^-}^{1}\frac{dz}{z}\,\Delta\phi_{g/P}(z,\mu^2)\,\Delta\omega_g\Big(\frac{x}{z},s_4,t_1,u_1,Q^2,m^2,\mu^2,\alpha_s(\mu)\Big)\,, \tag{3.19}$$

where the polarized gluon distribution in the proton is denoted by $\Delta\phi_{g/P}$ and z is the momentum fraction with $z^- = -U_1/(S'+T_1)$. The corresponding expression for the unpolarized structure function F_2 is given in [49]. The dimensionless function $\Delta\omega_g$ describes the hard scattering process [65, 66, 67, 68, 69] and depends on the partonic invariants t_1, u_1 and s_4, defined in (3.12).

The kinematical is far less complicated than the dynamical factorization but nevertheless crucial for resummation. It follows from a decomposition [33] of the total weight function w in the threshold region of phase space. From four-momentum conservation

$$q + zp = p_1 + p_2 + k_S \tag{3.20}$$

in the partonic process (3.6) one obtains

$$(q + zp - p_1)^2 = (p_2 + k_S)\,, \tag{3.21}$$

which upon dropping terms quadratic in the soft momentum k_S and rearranging becomes

$$S_4 = (1-z)(2pq - 2pp_1) + 2p_2k_S\,. \tag{3.22}$$

Substituting $2pq - 2pp_1 = -u_1$ and $2p_2k_S = s_4$ as can be derived from the defining relations of the partonic Mandelstam variables (3.12), inserting into (3.5) and dividing out m^2 produces

$$\frac{S_4}{m^2} \simeq (1-z)\left(\frac{-u_1}{m^2}\right) + \frac{s_4}{m^2} = w_1\left(\frac{-u_1}{m^2}\right) + w_S\,, \tag{3.23}$$

where the soft weights w_1 and w_S have been introduced. In turn, S_4/m^2 can be interpreted as the overall weight w of the process. It is worth noting for later calculations that in going from hadronic to partonic level two Mandelstam variables scale with z, whereas one remains unchanged, namely

$$t_1 = zT_1, \quad s' = z(S+Q^2), \quad u_1 = U_1\,. \tag{3.24}$$

Near threshold there is thus very little extra energy available for gluon radiation besides creating the heavy pair. Hence the dynamics is almost Born-like with small deviations controlled by the parameter S_4. They can be due either to radiation from the incoming quark, which in this way looses a fraction w_1 of its original four-momentum, or to extra radiation in the final state, i.e. at the soft level and therefore denoted w_s. To obtain a partonic cross section the constituent functions need to be multiplied and overall momentum conservation must be imposed in the form of a delta function according to

$$\Delta\omega_g = \int dw_1 dw_S\;\; \delta\left(\frac{S_4}{m^2} - w_1\left(\frac{-u_1}{m^2}\right) - w_S\right)\;\; H\;\; \Delta\psi_{g/g}\,(w_1)\;\; S\,(w_S)\;\;, \tag{3.25}$$

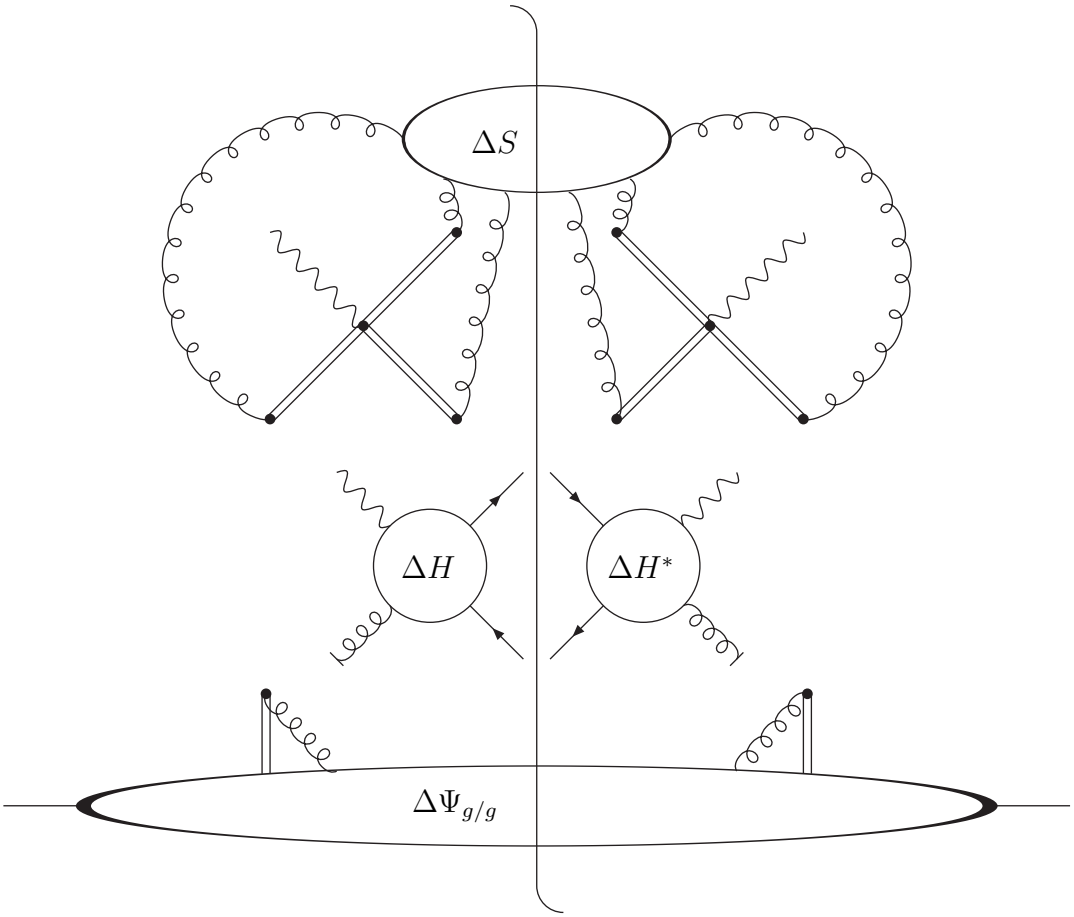

Figure 3.2: *General leading region for polarized deep inelastic heavy quark production through photon-gluon fusion after complete factorization of soft gluons.*

where for clarity all arguments besides the soft weights have been suppressed. Each of the functions $\Delta\psi_{g/g}(w_1)$, $S(w_S)$, and H_g, which are conveniently computed in $\zeta \cdot A = 0$ gauge, organizes contributions corresponding to a particular set of quanta and thereby only depends on its own individual weight function as introduced in (3.23). Fig.3.2 depicts this factorization near threshold.

It is often convenient to consider these functions in moment space, defined by the Laplace transform with respect to the overall weight w, since this operation turns integrals like (3.25) into simple products in moment space. Under the assumption of factorization the partonic cross section $\Delta\omega_g$ in moment space can then be written in a factorized form, up to corrections of order $1/N$, as [35, 28, 33, 49]

$$\begin{aligned} &\Delta\tilde{\omega}_g(N, t_1, u_1, Q^2, m^2, \mu^2, \alpha_s(\mu)) \; = \\ &\qquad H_g(\zeta, Q^2, m^2, \alpha_s(\mu)) \left[\frac{\Delta\tilde{\psi}_{g/g}(N_u, k\cdot\zeta/\mu)}{\Delta\tilde{\phi}_{g/g}(N_u, \mu)}\right] \tilde{S}\left(\frac{m}{N\mu}, \zeta\right) . \end{aligned} \tag{3.26}$$

where $N_u = N(-u_1/m^2)$. The N-dependence in each of the functions of (3.26) exponentiates.

The jet and soft functions, $\Delta\psi_{g/g}$ and S in (3.26), can each be represented as operator matrix elements [26, 28, 33, 49]. Dependence on the spin degrees of freedom can be kept

explicit in these elements, such that the methods of [35, 26, 28, 33] for the resummation of the singular functions in (3.25) via appropriate evolution equations can be generalized to account for initial state polarizations. The jet-function $\Delta\tilde{\psi}_{g/g}$ obeys two evolution equations, namely the renormalization group equation and an equation describing the energy dependence via gauge-dependence [35, 26, 24]. Solving both equations sums Sudakov double logarithms. Mass factorization introduces the density $\Delta\tilde{\phi}_{g/g}$ as a counterterm and requires the choice of a scheme. In the $\overline{\text{MS}}$-scheme $\Delta\tilde{\phi}_{g/g}$ has no double logarithms. The soft function S obeys a renormalization group equation, which resums all NLL logarithms originating from soft gluons not already accounted for in $\Delta\tilde{\psi}_{g/g}$. In general, the soft and the hard functions S and H_g depend also on the colour structure of the underlying scattering reaction, but for deep-inelastic production of heavy quarks this dependence is trivial [49].

3.2 The spin puzzle and the axial anomaly

Before explicitly computing in sections 3.3 and 3.4 the soft and jet functions, the ingredients in the resummation of polarized deep inelastic charm production, this section reviews the spin puzzle and its relation to the axial anomaly. In contrast to the precision data available on the spin-averaged structure functions of the proton, polarized measurements have proven a lot more difficult, and consequently the polarized structure functions are much less constrained [50, 70, 71]. Even today the seemingly simple question which constituents of the proton make which contribution to its overall spin is still awaiting its final verdict. The first moment

$$\Gamma_1^P(Q^2) = \int_0^1 dx g_1^P(x, Q^2) \tag{3.27}$$

of the polarized structure function g_1^P can serve to illustrate the puzzles which resulted in the so called nucleon spin crisis in the 1980-ies. Current best measurements (cf. [70] and references therein) find the first moment to lie in the range

$$0.130 \leq \Gamma_1^P\left(Q^2 = 10\text{GeV}^2\right) \leq 0.142 \; . \tag{3.28}$$

From an operator product approach to the spin-dependent part of the proton's hadronic tensor it follows that

$$\Gamma_1^P\left(Q^2\right) = \frac{1}{12}\left[\left(a_3 + \frac{a_8}{\sqrt{3}}\right) E_{\text{NS}}(Q^2) + \frac{4}{3} a_0(Q^2) E_{\text{S}}(Q^2)\right] \; , \tag{3.29}$$

where the indices i on the a_i indicate which operators the contribution arises from, $i = 1 \ldots 8$ corresponding to the components of an $SU(3)$ octet of flavours and $i = 0$ to the singlet. The coefficients $E_{\text{NS}}(Q^2)$ and $E_{\text{S}}(Q^2)$ are power series in the strong coupling. As far as global $SU(3)$ flavour symmetry holds the octet currents are conserved, and a_3 and a_8 are scale-independent. They can therefore be determined at a rather different energy scale from weak β-decay. With all except for one constant on the right hand side of (3.29) known, the measurement of $\Gamma_1^P\left(Q^2\right)$ can be turned into one of a_0, yielding

$$0.22 \leq a_0\left(Q^2 = 10\text{GeV}^2\right) \leq 0.34 \; . \tag{3.30}$$

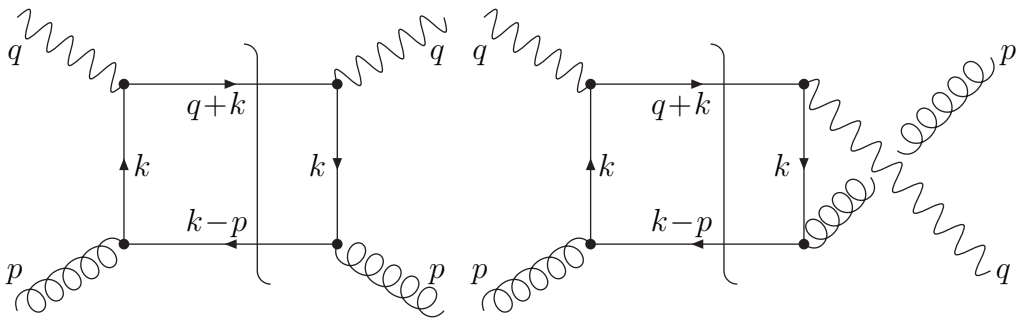

Figure 3.3: *The two cut diagrammes contributing to photon gluon fusion (massless quarks in the final state).*

In the naive parton model

$$a_0 = \Delta\Sigma \ , \tag{3.31}$$

where

$$\Delta\Sigma = \int_0^1 dx \left(\Delta u(x) + \Delta\bar{u}(x) + \Delta d(x) + \Delta\bar{d}(x) + \Delta s(x) + \Delta\bar{s}(x)\right) \ , \tag{3.32}$$

and thus a_0 receives contributions exclusively from light quarks. Hence to account for the total proton spin one would expect $a_0 = 1$, in clear contradiction with (3.30). The first EMC results [72] had even indicated $a_0 \approx 0$, leaving almost no room at all for a quark contribution to the proton spin. But the somewhat larger values in (3.30) still call for an explanation. This is sometimes phrased as a violation of the Ellis-Jaffe sum rule, which starting from the naive parton model makes the further assumption that the strange polarization vanishes. Combining this as before with the weak β-decay data one would predict $\Gamma_1^P = 0.185 \pm 0.003$, clearly incompatible with the measurements as stated in (3.28). On the other hand, if one considers a neutron instead of a proton only the sign of a_3 changes in (3.29), leading to

$$\Gamma_1^P - \Gamma_1^N = \int_0^1 dx \left(g_1^P(x,Q^2) - g_1^N(x,Q^2)\right) = \frac{a_3}{6} E_{NS}(Q^2) \ . \tag{3.33}$$

This Bjorken sum rule is in good agreement with experiment, augmenting confidence in the theoretical result (3.29).

In view of the striking incapability of the naive parton model to explain experimental results theoretical interest was drawn to possible gluonic contributions [73, 74]. The lowest-order cut graphs relevant to this process are shown in Fig.3.3. They depict the same process as Fig.3.1, but final state quark masses are to be neglected. This modifies (3.31) to

$$a_0 = \Delta\Sigma - \frac{n_f \alpha_s\left(Q^2\right)}{2\pi} \Delta G\left(Q^2\right) \ , \tag{3.34}$$

with n_f the number of light quark flavours and the polarized gluon contribution $\Delta G\left(Q^2\right) = \int_0^1 dx \Delta\phi_{g/P}\left(Q^2, x\right)$. Hence data and theory can be brought to agreement if the gluonic contribution to the proton spin is sizable and positive. One could at $Q^2 = 10\mathrm{GeV}^2$ take e.g. $\Delta\Sigma \approx 0.6$ and obtain $2.2 \leq \Delta G \leq 3.3$.

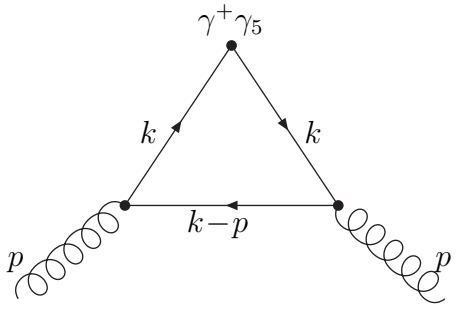

Figure 3.4: *The triangle graph for the axial anomaly (quarks could also circulate in the opposite direction).*

As was stressed already in [73, 74] the contribution from Fig.3.3 is actually proportional to the axial anomaly triangle graph as shown in Fig.3.4. Because of the axial anomaly the four-divergence of the current $j_5^\mu = \sum_{i=1}^{n_f} \tilde{q}_i \gamma^\mu \gamma_5 q_i$ does not vanish, but can be expressed as a product of the gluonic field strength and dual field strength tensors. Since the partonic contribution to the overall spin follows from evaluating this current as sandwiched between gluonic states, $\langle g(p,\lambda)|j_5^\mu|g(p,\lambda)\rangle$, its non-conservation corresponds with the additional term in (3.34) as compared to (3.31).

Having re-interpreted the experimental results as data on the spin contributions not only from quarks but also from gluons, one would like to quantitatively assess each individual share. Since the gluon term in (3.34) comes endowed with an explicit (running) α_s, it may seem that increasing the interaction energy scale should suffice to extract exclusively the quark spin, with the ΔG dilution being suppressed by the decreasing strong coupling. However, this naive expectation is not borne out by a more careful analysis. The evolution of ΔG itself is within the DGLAP framework governed by the first moment of the polarized gluon splitting function [75, 76, 77]

$$\Delta P_{gg}(x) = C_A \left[\frac{2}{(1-x)_+} - 4x + 2 \right] + \delta(1-x) \frac{11 C_A - 4 n_f T_R}{6} \ . \tag{3.35}$$

Now

$$\int_0^1 dx \Delta P_{gg}(x) = \frac{11 C_A - 4 n_f T_R}{6} \ , \tag{3.36}$$

which is exactly the negative of the first coefficient of the QCD β-function determining the evolution of the strong coupling[2]. Unlike in the spin-averaged case the contributions from the two factors thus mutually cancel in the product rendering

$$Q^2 \frac{d}{dQ^2} \left[\alpha_s\left(Q^2\right) \Delta G\left(Q^2\right) \right] = 0 \ . \tag{3.37}$$

It has been suggested to extract the gluon density by considering large transverse momentum jets (cf. [78, 79, 80] and references therein). Alternatively, one could require the final state quarks in Fig.3.3 to be not light but heavy and look for charmed hadrons. The heavy quark production mechanism is at lowest order sensitive only to the polarized

[2]Note that $\int_0^1 dx \Delta P_{qq}(x) = \int_0^1 dx \Delta P_{qg}(x) = 0$.

gluon distribution and therefore plays a central role in the solution of the proton spin puzzle. The phenomenological importance of this process constitutes a key motivation for its resummation analysis carried out in the present work.

3.3 The jet function

The jet function is the first non-trivial ingredient in the resummation calculation for polarized and unpolarized deep inelastic charm production. The jet function $\Delta\psi_{g/g}$ is in its definitions very similar to the gluon distribution $\Delta\phi_{g/g}$. Both are matrix elements of some renormalized operator in a gluonic state, and they display identical collinear poles. Since the polarized gluon/gluon splitting function $\Delta\phi_{g/g}$ is available in the literature, and its poles should cancel those of $\Delta\psi_{g/g}$, it provides a valuable cross-check in the computation of the jet function. Fixing instead of the + a timelike component of the secondary gluon's momentum one can proceed from $\Delta\phi_{g/g}$ to $\Delta\psi_{g/g}$ as will become clear shortly. Note that in the computation of the logarithmic terms in this section no γ_5 ambiguities arise, since these are suppressed by $1/N$.

Recall first the definition of the density of quarks in hadrons as an operator matrix element in (1.21). A very similar expression gives the corresponding polarized gluon density

$$\begin{aligned}\Delta\phi_{g/h}(\xi) &= \left(2\pi\xi p^+\right)^{-1} \int\limits_{-\infty}^{\infty} dy^- \exp\left(-i\xi p^+ y^-\right) \\ &\quad \langle h(p,\sigma) \mid F_\mu^+(0,y^-,\vec{0}) F^{\mu+}(0) \mid h(p,\sigma)\rangle_{A^+=0} \ , \end{aligned} \tag{3.38}$$

a discussion of which can be found e.g. in [5] for the spin-averaged case. Here p and σ denote the incoming hadron's momentum and spin respectively. The gluon carries a fraction ξ of the initial hadronic momentum in the + direction. The matrix element (3.38) is not accessible perturbatively since for the partonic structure of hadrons the low-energy regime of QCD accounts for important contributions. However, if instead of an initial hadronic a gluonic state is considered,

$$\Delta\phi_{g/g}(\xi) = \left(2\pi\xi p^+\right)^{-1} \int\limits_{-\infty}^{\infty} dy^- \exp\left(-i\xi p^+ y^-\right) A \ , \tag{3.39}$$

where

$$A = \langle g(p,\sigma) \mid F_\mu^+(0,y^-,\vec{0}) F^{\mu+}(0) \mid g(p,\sigma)\rangle_{A^+=0} \ , \tag{3.40}$$

the calculation becomes feasible. Before going to higher orders in the coupling consider this expectation value at lowest order to determine its normalization, in (3.39) given by the factor $(2\pi\xi p^+)^{-1}$. To fix the +- component of the secondary gluon's momentum an explicit expression for (3.40) is required. This is accomplished noting that a gluonic state can be created from the vacuum by applying a creation operator

$$\mid g(p,\sigma)\rangle = a_\lambda^\dagger(p) \mid 0\rangle \ , \quad \langle g(p,\sigma) \mid = \langle 0 \mid a_\lambda(p) \ ,$$

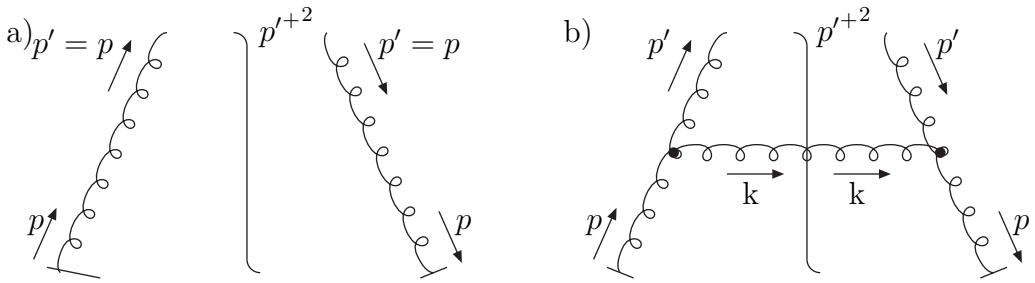

Figure 3.5: *Diagrammes required in the computation of the gluon densities $\Delta\psi_{g/g}$ and $\Delta\phi_{g/g}$ a) Lowest order diagramme required for the normalization b) Real gluon emission contribution.*

where the second expression follows from taking the conjugate. Inserting the gluon field in the form

$$A^{\mu}(x) = \int \frac{d^3\vec{k}}{2\omega_k}\Big[a_\lambda(\vec{k},x_0)\epsilon^{\mu}(k,\lambda)e^{-i\omega(k)x^0+i\vec{k}\cdot\vec{x}} + a^{\dagger}_\lambda(\vec{k},x_0)\epsilon^{\star\mu}(k,\lambda)e^{i\omega(k)x^0-i\vec{k}\cdot\vec{x}}\Big] \tag{3.41}$$

into the definition of the field strength tensor $F^{\mu+} = \partial^{\mu}A^{+} - \partial^{+}A^{\mu} + [A^{\mu}, A^{+}]$ and using $A^{+} = 0$ and[3] $\partial^{+} = \partial_{-}$ one obtains

$$F^{\mu+}(x) = \int \frac{d^3\vec{p'}}{2\omega_{p'}}(ip'^{+})\Big[a'_\lambda(\vec{p'},x_0)\epsilon^{\mu}(p',\lambda')e^{-ip'_\alpha x^\alpha} - a^{\dagger}_{\lambda'}(\vec{p'},x_0)\epsilon^{\star\mu}(p',\lambda')e^{ip'_\alpha x^\alpha}\Big]\ , \tag{3.42}$$

as well as

$$F_{\mu}{}^{+}(x) = \int \frac{d^3\vec{p''}}{2\omega_{p''}}(-ip''^{+})\Big[a''_\lambda(\vec{p''},x_0)\epsilon_{\mu}(p'',\lambda'')e^{-ip''_\alpha x^\alpha} - a^{\dagger}_{\lambda}(\vec{p''},x_0)\epsilon^{\star}_{\mu}(p'',\lambda'')e^{ip''_\alpha x^\alpha}\Big]\ . \tag{3.43}$$

Upon insertion of a complete sum over states $\sum_\lambda \mid \lambda\rangle\langle\lambda \mid$ one obtains for A a rather lengthy expression, which can be simplified making use of the commutation relation $\Big[a_\lambda(\vec{k},x_0), a^{\dagger}_{\lambda'}(\vec{k'},x_0)\Big] = \delta_{\lambda\lambda'}2\omega_k\delta^3(\vec{k}-\vec{k'})$ obeyed by the creation and annihilation operators to obtain

$$A = p^{+2}\left(-\sum_\lambda \epsilon^{\star}_{\mu}(\lambda)\epsilon^{\mu}(\lambda)\right)e^{ip^+x^-}\ . \tag{3.44}$$

Since the incident gluon is polarized the sum in this expression collapses to $\sum_\lambda \epsilon^{\star}_{\mu}(\lambda)\epsilon^{\mu}(\lambda) = -1$. Note also that at this stage it is somewhat arbitrary whether to call this momentum p^+ (the initial gluon's momentum) or p' (the momentum of the gluon participating in the hard scattering) since at lowest order the two are equal due to the absence of radiation. One can picture this at the level of Feynman diagrammes as in Fig.3.5a. Requiring at lowest order $\Delta\phi^{(0)}_{g/g}(\xi) = \delta(1-\xi)$, expressing the consistency condition that the gluon should remain itself in the absence of interactions, one can determine the normalization constant c in

$$\Delta\phi^{(0)}_{g/g}(\xi) = cp^{+2}\int_{-\infty}^{\infty} dy^- e^{-i\xi p^+y^- + ip^+y^-} = c2\pi\xi p^+\delta(1-\xi)\ , \tag{3.45}$$

[3]This follows from the fact that in light-cone coordinates $p\cdot k = p^+k^- + p^-k^+ - \vec{p_\perp}\cdot\vec{k_\perp}$ leading to the metric $g_{+-} = g_{-+} = 1$ and $g_{\perp\perp} = -1$.

where an extra factor of $\xi = 1$ has been introduced. However, note that in (3.39) the partial derivatives which eventually produce the momenta act on the wavefunction of the gluon taking part in the scattering, making plausible the insertion of ξ in (3.45).

Having found the normalization constant from a lowest order calculation one is now in a position to compute the one-loop correction to $\Delta\phi_{g/g}(\xi)$. $F^+_\mu(0, y^-, \vec{0}_\perp)F^{\mu+}(0)$ can be regarded as a Heisenberg operator evolving with the full Hamiltonian H of the theory considered. Expanding in the strong coupling brings down interaction terms from the exponentials the operator is sandwiched in between. This can then be expressed graphically through corresponding Feynman diagrammes. Consider first the diagramme of real gluon emission, Fig.3.5b, and denote by p and p' the momenta of the initial and interacting gluons, respectively, and by k that of the real gluon crossing the final state cut. The gauge-fixing vector u is chosen as $u = (0, 1, \vec{0}_\perp)$. In principle it is possible to also at higher orders work with explicit representations of the polarization vectors. However, this can become quite tedious and also to some extent conceals the generality of the polarized splitting functions or probability distributions. It is much more convenient to work with the projection operator

$$\frac{1}{2}\frac{\epsilon_{\gamma\delta\kappa\lambda}p^\kappa u^\lambda}{p\cdot u}\frac{\epsilon_{\mu\nu\pi\tau}p^\pi u^\tau}{p\cdot u} \ . \tag{3.46}$$

With this the result for real gluon emission becomes

$$\Delta\phi^{(1)}_{g/g}(\xi) = \frac{\alpha_s}{\pi^2}C_A\int d^{d-2}\vec{k}_\perp B \ , \tag{3.47}$$

where

$$\begin{aligned} B \ = \ & -\frac{1}{4\xi p^+}\int dk^+dk^-\frac{\epsilon_{\gamma\delta\kappa\lambda}p^\kappa u^\lambda}{p\cdot u}\left[g^{\delta\alpha}\left(-p-p'\right)^\rho + g^{\alpha\rho}\left(p'-k\right)^\delta + g^{\rho\delta}\left(k+p\right)^\alpha\right] \\ & \frac{N^{\alpha\mu}\left(p'\right)}{2k^-}\frac{\epsilon_{\mu\nu\pi\tau}p^\pi u^\tau}{p\cdot u}\xi^2\frac{N^{\nu\beta}\left(p'\right)}{2k^-}\left[g^{\gamma\beta}\left(p+p'\right)^\sigma + g^{\beta\sigma}\left(-p'+k\right)^\gamma + g^{\sigma\gamma}\left(-k-p\right)^\beta\right] \\ & N^{\rho\sigma}\left(k\right)2\pi\delta_+\left(k^2\right)\delta\left(k^+-\left(1-\xi\right)p^+\right) \ . \end{aligned} \tag{3.48}$$

The colour structure $C_A = 3$ of (3.47) can be derived from $SU(3)$ group identities.

The algebra is best left to a symbolic manipulation programme, such as FORM [81], yielding

$$B = \frac{2\xi - 3\xi^2 + 2\xi^3}{\vec{k}^2_\perp\xi\left(1-\xi\right)}$$

and hence

$$\Delta\phi^{(1)}_{g/g}(\xi) = \frac{\alpha_s}{2\pi}\left(\frac{-1}{\epsilon}\right)2N_C\left(\frac{1}{1-\xi}+1-2\xi\right) \ . \tag{3.49}$$

In deriving (3.49) scaleless integrals have been split into two parts according to

$$\int\frac{d^{d-2}\vec{k}_\perp}{\vec{k}^2_\perp} = \int\frac{d^{d-2}\vec{k}_\perp}{\vec{k}^2_\perp+M^2} + M^2\int\frac{d^{d-2}\vec{k}_\perp}{\vec{k}^2_\perp\left(\vec{k}^2_\perp+M^2\right)} = \pi\epsilon^{-1} + \pi\left(-\epsilon\right)^{-1} + ... \ ,$$

where the ultraviolet pole $\pi\epsilon^{-1}$ is cancelled by the $\overline{\rm MS}$ counterterm but the infrared $\pi\left(-\epsilon\right)^{-1}$ remains. M is an arbitrary mass needed to split the integrand. There are in

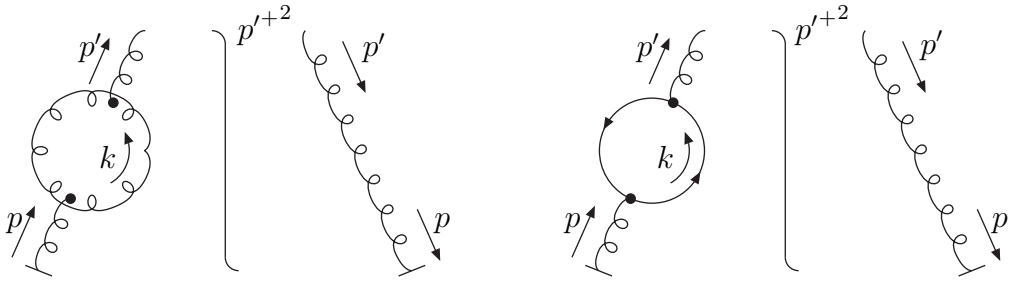

Figure 3.6: *The virtual gluon emission and virtual quark pair creation diagrammes.*

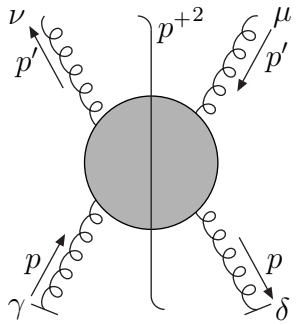

Figure 3.7: *The matrix element needed for both the unpolarized and polarized gluon distributions viewed as a Green function. The indices are indicated explicitly and to be contracted with either the projectors $\mathcal{P}$ or $\Delta\mathcal{P}$.*

principle also finite terms in (3.49) involving logarithms of the (suppressed) regularization scale μ and the 4π from the n-dimensional phase space, but in the following discussion of soft gluon resummation only the poles of $\phi^{(1)}_{g/g}$ will be important. Also, there are still the virtual diagrammes of Fig.3.6 contributing, namely the virtual gluon emission and the virtual quarks-antiquark pair loops. When these are added they turn functions ill-defined at threshold $\xi = 1$ into +-distributions, but otherwise contribute to neither the divergence nor the large logarithms. They add only delta-function terms of the type $\delta(1-\xi)$, and in this way generate in (3.49) the full polarized one-loop gluon-gluon splitting function.

To compare with the unpolarized case and to round up the physical picture it is instructive to take a look at the index structure of (3.48) in more detail. With the Lorentz indices not yet contracted, and suppressing overall signs, symmetry factors as well as spacetime arguments, it reads

$$A^{(1)}_{\text{real}} = \underbrace{\langle g(p,\sigma) \mid g_s A_\gamma}_{\propto \epsilon^*_\gamma(p,\sigma)} \overbrace{\underbrace{A_\rho}\, \underbrace{A_\alpha \partial^+ A_\nu}_{\propto N_{\alpha\nu}}\, \partial^+ \underbrace{A_\mu g_s A_\beta}_{\propto N_{\mu\beta}}\, \underbrace{A_\sigma}}^{\propto N_{\rho\sigma}} \underbrace{A_\delta \mid g(p,\sigma)\rangle}_{\propto \epsilon_\delta(p,\sigma)} , \tag{3.50}$$

which can be recognized as a four-point Green function with two external legs μ and ν and two on-shell fields γ and δ (cf. Fig.3.7). Here the effect of Wick contractions and the gluon field operator acting on a state containing one gluon have been indicated by over- and underbraces. These are to be interpreted as $\langle g(p,\sigma) \mid A_\gamma \propto \epsilon^*_\gamma(p,\sigma)$, $A_\rho A_\sigma \propto N_{\rho\sigma}$, $A_\alpha A_\nu \propto N_{\alpha\nu}$, $A_\mu A_\beta \propto N_{\mu\beta}$ and $A_\delta \mid g(p,\sigma)\rangle \propto \epsilon_\delta(p,\sigma)$. Different contractions of fields are also possible. These other possible combinations either represent nothing but a renaming of indices at the level of Feynman diagrammes and are properly taken care of by the

symmetry factors hitherto omitted, or they lead to disconnected diagrammes. From (3.50) it is also clear that the two partial derivatives lead to primed momenta p' since the fields they act on always pair up with fields coming out of the vertex. To be more precise assume that in (3.50) A^μ paired up with the initial state gluon $g(p,\sigma)$ to give $\epsilon^{*\mu}$. Then this incoming gluon would not connect with the rest of the diagramme. But corresponding to a disconnected diagramme this combination of fields would not contribute to the physical process.

To derive from (3.50) the unpolarized expression one needs to contract with projectors

$$\mathcal{P}^{(1)}_{\gamma\delta}\mathcal{P}^{(2)}_{\mu\nu} = \left(-g_{\gamma\delta} + \frac{u_\gamma p_\delta + p_\gamma u_\delta}{u\cdot p}\right)(-g^{\mu\nu}) \ ,$$

averaging over initial and summing over final state polarizations. To obtain the polarized result, however, one must use $\Delta\mathcal{P}^{(1)}_{\gamma\delta}\Delta\mathcal{P}^{(2)}_{\mu\nu}$ as given by (3.46). It can be seen that $\Delta\mathcal{P}^{(1)}_{\gamma\delta}$ has the desired effect of projecting out the difference between polarization states by going to the specific frame $p = (p^+, 0, \vec{0})$ and $u = (0, u^-, \vec{0})$, whence $\epsilon_{\gamma\delta\kappa\lambda}p^\kappa u^\lambda/(p\cdot u) = \epsilon_{\gamma\delta 30} = (\delta_{\gamma 1}\delta_{\delta 2} - \delta_{\gamma 2}\delta_{\delta 1})$, which gives the difference in polarizations $\epsilon^*_1(\sigma,p)\epsilon_2(\sigma,p) - \epsilon^*_2(\sigma,p)\epsilon_1(\sigma,p)$. It can also be checked explicitly that as to be expected mixing polarized and unpolarized projectors in one calculation leads to a vanishing result. As remarked earlier with respect to γ_5 ambiguities in the dimensional regularization of the antisymmetric tensor are $1/N$ effects.

The jet function $\Delta\psi$ is similar to the $\Delta\phi$ computed above but differs in the momentum component of the secondary gluon fixed through integration and exponential. Again, a constant of normalization has to be computed first, as given by (cf. equation (16) in [49])

$$\begin{aligned}\Delta\psi_{g/g}(\xi) &= c\int_{-\infty}^{\infty} dy^0 \exp\left(-i\xi p^0 y^0\right) \\ &\qquad \langle g(p,\sigma) \mid F^+_\mu(y_0,0,0,0)F^{\mu+}(0) \mid g(p,\sigma)\rangle_{A^0=0} \ . \end{aligned} \tag{3.51}$$

As previously one wants to normalize such that $\Delta\psi_{g/g}(\xi) = \delta(1-\xi)$. The algebra required to work out the operator in the gluonic state is exactly the same as in the previous case but the different exponents lead to

$$\Delta\psi^{(0)}_{g/g}(\xi) = cp^{+2}\int_{-\infty}^{\infty} dy^0 e^{-i\xi p^0 y^0 + ip^0 y^0} = c4\pi\xi p^0\delta(1-\xi) \ , \tag{3.52}$$

where as before there arises at this lowest order an ambiguity since $\xi = 1$. Hence the result $c = (4\pi\xi p^0)^{-1}$ takes into account that scattering takes place off the secondary gluon.

In the one-loop calculation it turns out that the delta function fixing the k^0 is a little more involved to impose than the one with k^+. Also this time track needs to be kept of more powers in ϵ since besides the pole terms also the finite contributions, typically containing logarithms of e.g. the regularization scale μ, are of interest. The momentum component squared produced by the two partial derivatives at the final state cut remains the +- component which, however, in this case cannot simply be expressed as $\xi^2 p^{+2}$ since it is no longer fixed by the delta function. The expression to compute is thus, using the

same projector as in the calculation of $\Delta\phi$,

$$\begin{aligned}\Delta\psi^{(1)}_{g/g}(\xi) &= \left(2\xi 2p^0\right)^{-1} N_C g^2 \mu^{2\epsilon} \int \frac{d^n k}{(2\pi)^{n-1}} \frac{\epsilon_{\gamma\delta\kappa\lambda} p^\kappa u^\lambda}{2p\cdot u} N^{\rho\sigma}(k)\,\delta_+\left(k^2\right)\delta\left(k^0-(1-\xi)\,p^0\right) \\ &\left[g^{\delta\alpha}(-p-p')^\rho + g^{\alpha\rho}(p'-k)^\delta + g^{\rho\delta}(k+p)^\alpha\right]\frac{N^{\alpha\mu}(p')}{2p\cdot k}\frac{\epsilon_{\mu\nu\pi\tau}p^\pi u^\tau}{p\cdot u} \\ &\left(p^+-k^+\right)^2\frac{N^{\nu\beta}(p')}{2p\cdot k}\left[g^{\gamma\beta}(p+p')^\sigma + g^{\beta\sigma}(-p'+k)^\gamma + g^{\sigma\gamma}(-k-p)^\beta\right] \\ &N^{\rho\sigma}(k)\,\delta_+\left(k^2\right)\delta\left(k^0-(1-\xi)\,p^0\right)\ , \end{aligned} \tag{3.53}$$

where unlike in (3.48) the gauge-fixing vector $u=(1,\vec{0})$ is now time-like. The delta functions can be reexpressed as

$$\delta_+\left(k^2\right)\delta\left(k^0-(1-\xi)\,p^0\right) = \frac{1}{\sqrt{2}}\delta_+\left(k^- - \frac{\vec{k_\perp}^{\,2}}{2k^+}\right)\delta\left(k^{+2}+\frac{1}{2}\vec{k_\perp}^{\,2}-(1-\xi)\sqrt{2}p^0k^+\right)\ ,$$

where

$$k^+_{1,2} = \frac{(1-\xi)\,p^0}{\sqrt{2}}\left(1\pm\sqrt{1-\frac{\vec{k_\perp}^{\,2}}{(1-\xi)^2\,p^{0\,2}}}\right)\ ,$$

leading to an upper limit $\vec{k_\perp}^{\,2} < \frac{1}{a} = (1-\xi)^2\,p^{0\,2}$ on the transverse components. Since the two cases k_1 and k_2 have to be considered separately the delta functions become somewhat more tedious to impose. Again utilizing FORM for the algebra there occur at intermediate stages roots of $(1-\xi)$, but such terms cancel upon integration over k^+ and k^-. One obtains

$$\begin{aligned}\Delta\psi^{(1)}_{g/g}(\xi) &= \frac{\alpha_s}{2\pi}2N_C\left(\frac{\mu^2}{p^{0\,2}}\right)^\epsilon\frac{\pi^\epsilon}{(1-\xi)^{2\epsilon}}\left(1-\gamma_E\epsilon\right) \\ &\left[-\frac{1}{\epsilon}\left(\frac{1}{1-\xi}+1-2\xi\right)-\frac{1}{1-\xi}+\mathcal{O}(1-\xi)+\mathcal{O}(\epsilon)\right]\ . \end{aligned} \tag{3.54}$$

The pole is exactly the same as that of $\Delta\phi$, as it should be. Now in the eikonal limit $\xi\to 1$

$$\frac{1}{1-\xi}+1-2\xi = \frac{2\xi-3\xi^2+2\xi^3}{\xi\,(1-\xi)} \longrightarrow \frac{1}{1-\xi} = \frac{1}{w}\ , \tag{3.55}$$

which gives the result

$$\Delta\psi^{(1),\mathcal{O}(NLL)}_{g/g}(\xi) = \frac{\alpha_s}{\pi}N_C\left[\left(-\frac{1}{\epsilon}+\gamma_E-\ln 4\pi\right)\left(\frac{1}{w}\right)+2\frac{\ln(w)}{w}+\frac{1}{w}\left(\ln\left(\frac{4p^{0\,2}}{\mu^2}\right)-1\right)\right]\ . \tag{3.56}$$

To this level of accuracy, it agrees with $\psi^{(1),\mathcal{O}(NLL)}_{g/g}(\xi)$ as given in [49].

3.4 The soft function

The soft function for (polarized) heavy quark production receives contributions from the diagrammes shown in Fig.3.8 and from the heavy (anti-)quark self-energy graphs. However, not the full results for these composite operators are required. Only their anomalous

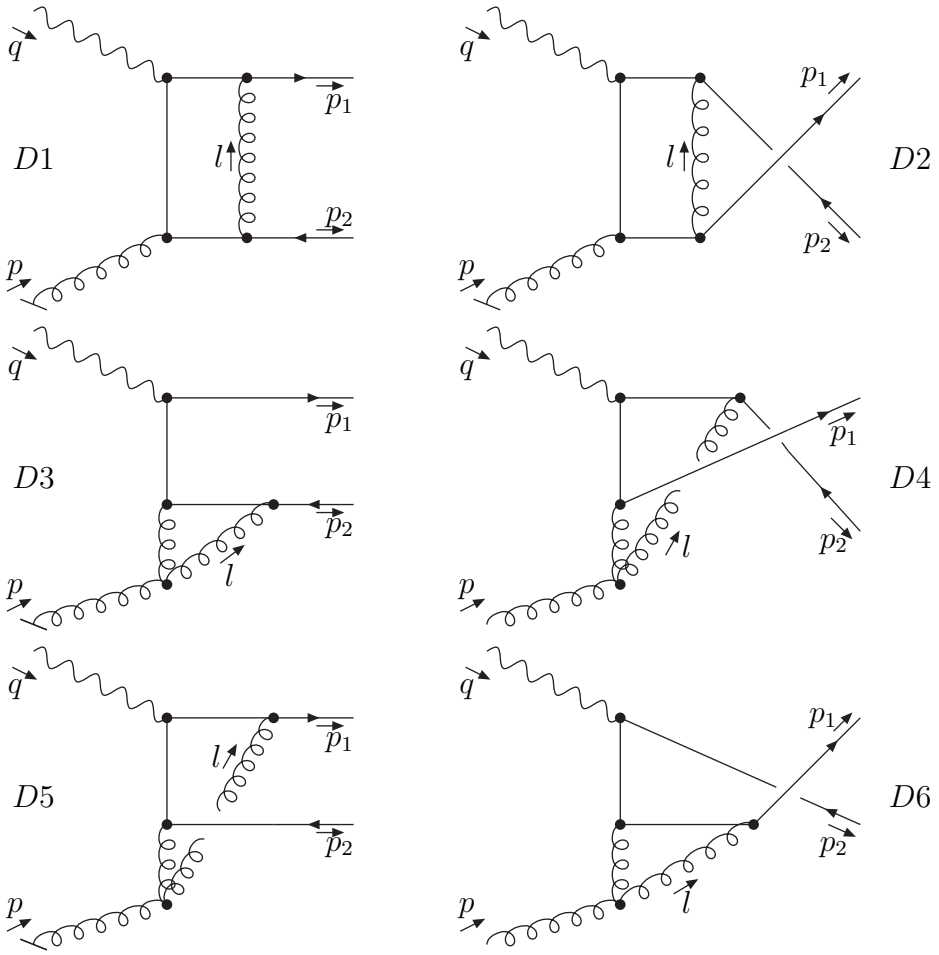

Figure 3.8: *The six diagrammes contributing to the soft function of heavy quarks production through photon-gluon-fusion.*

dimension in the soft limits, i.e. the coefficient of the ultraviolet pole, is required for resummation. Also, as discussed in section 2.5 the soft function really couples only to eikonal lines. It is instructive to see how here this general result will follow from explicitly making the soft approximation in a one loop calculation. Adding the contributions (3.7) and its counterpart from the second Born level diagramme as in Fig.3.1 gives

$$\mathrm{Born}_{\mu\alpha} = -ieg[t_a]_{ij}\left(\frac{\bar{u}(p_1)\gamma_\mu(\not{p}_1-\not{q}+m)\gamma_\alpha v(p_2)}{(p_1-q)^2-m^2+i\epsilon}+\frac{\bar{u}(p_1)\gamma_\alpha(\not{p}_1-\not{p}+m)\gamma_\mu v(p_2)}{(p_1-p)^2-m^2+i\epsilon}\right). \tag{3.57}$$

This expression will factor out off the one loop results to be computed next.

As an example consider the first two diagrammes from Fig. 3.8. These add up to

$$\begin{aligned} D1+D2 \;=\; & eg^3\left(C_F-\frac{C_A}{2}\right)[t_a]_{ij}\int\frac{d^nl}{(2\pi)^n}\frac{N^{\beta\gamma}(l)}{l^2+i\epsilon} \\ & \left[\frac{\bar{u}(p_1)\gamma_\beta(\not{p}_1-\not{l}+m)\gamma_\mu(\not{p}_1-\not{l}-\not{q}+m)\gamma_\alpha(-\not{p}_2-\not{l}+m)\gamma_\gamma v(p_2)}{((p_1-l)^2-m^2+i\epsilon)((p_1-l-q)^2-m^2+i\epsilon)((p_2+l)^2-m^2)+i\epsilon}\right. \\ & \left.+\frac{\bar{u}(p_1)\gamma_\gamma(\not{p}_1+\not{l}+m)\gamma_\alpha(\not{p}_1+\not{l}-\not{p}+m)\gamma_\mu(-\not{p}_2+\not{l}+m)\gamma_\beta v(p_2)}{((p_1+l)^2-m^2+i\epsilon)((p_1+l-p)^2-m^2+i\epsilon)((p_2-l)^2-m^2)+i\epsilon}\right]. \end{aligned}$$

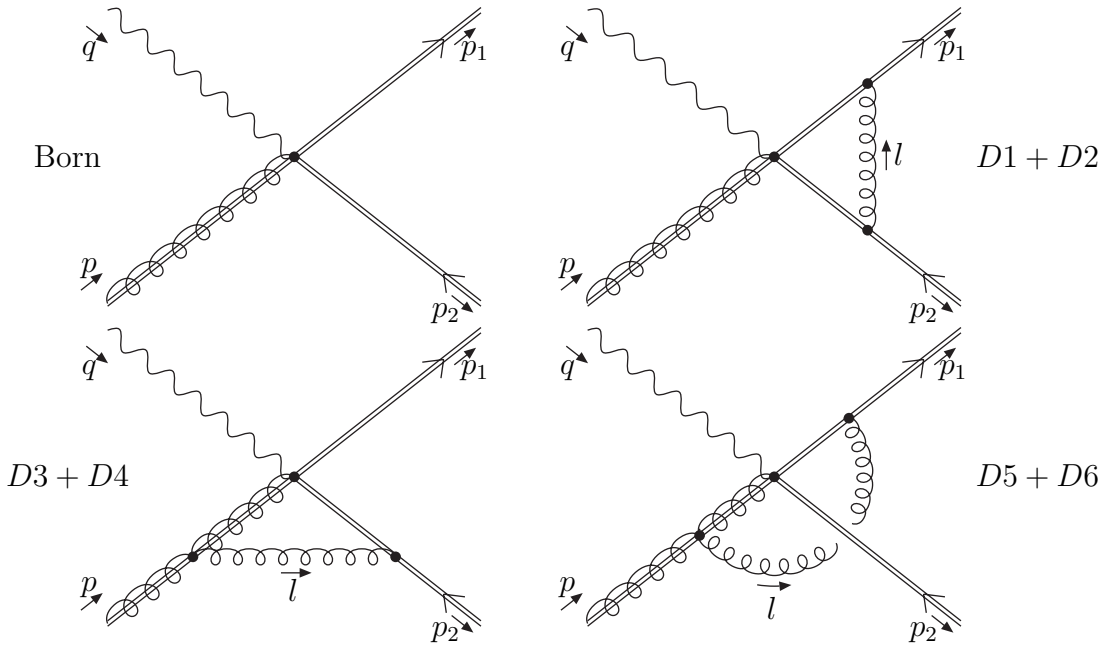

Figure 3.9: *Reduced diagrammes obtained from Figs. 3.1 and 3.8, eikonal lines are indicated as double.*

(3.58)

In axial gauge the gluon propagator term is given by

$$N^{\mu\nu}(l) = -g^{\mu\nu} + \frac{n^\mu l^\nu + n^\nu l^\mu}{n\cdot l} - n^2\frac{l^\mu l^\nu}{(l\cdot n)^2} \tag{3.59}$$

with n some gauge-fixing vector. Now the soft momentum l can be neglected with respect to the hard momenta p, p_1, p_2 and q. Using the Dirac equation for the external spinors $u(p_1)$ and $v(p_2)$ further simplifies (3.58) to

$$D1 + D2 = \mathrm{Born}_{\mu\alpha} i g^2 \left(C_F - \frac{C_A}{2}\right) \int \frac{d^n l}{(2\pi)^n} \, \frac{N^{\beta\gamma}(l)}{l^2 + i\epsilon} \, \frac{p_1^\beta}{-p_1 l + i\epsilon} \, \frac{-p_2^\gamma}{p_2 l} \, , \tag{3.60}$$

where the Born contribution (3.57) has been factored out. The same can be done with the other diagrammes. Results are similar to (3.60) but will not be given in detail. However, it is instructive to consider the reduced diagrammes resulting from the contraction of off-shell lines in Figs.3.1 and 3.8. The soft gluon(s) couple to the eikonal lines in Fig. 3.8 with a single polarization component only. Besides the diagrammes $D1$ to $D6$ also the self-energies of the final state heavy quarks contribute to the soft function.

After some lengthy algebra, carefully applying the principle value prescription to the denominators of expressions like (3.60) one obtains the soft anomalous dimension to order α_s as

$$\Delta\Gamma_S(\alpha_s) \;=\; \frac{\alpha_s}{\pi}\left\{\left(\frac{C_A}{2} - C_F\right)(L_\beta + 1) - \frac{C_A}{2}\left(\ln\left(\frac{4(k\cdot\zeta)^2}{m^2}\right) + \ln\frac{m^4}{t_1\, u_1}\right)\right\} \, , \tag{3.61}$$

with $\beta = \sqrt{1 - 4\,m^2/s}$ and $L_\beta = (1 - 2\,m^2/s)\{\ln(1-\beta)/(1+\beta) + \mathrm{i}\pi\}/\beta$. Clearly, in expressions like (3.57) and (3.60) contraction with a projector to extract spin-averaged or

spin-dependent contributions would just affect the Born term, which can be factored out off the order α_s expressions. This explains why the expression for $\Delta\Gamma_S$ is identical to its unpolarized counterpart.

3.5 The full exponent

The ingredients of the calculation can now be assembled as described in [49, 1, 4]. The final result for $\Delta\tilde{\omega}_g$ in the $\overline{\rm MS}$-scheme in moment space resums all $\ln N$ in single-particle inclusive kinematics and is given by

$$\begin{aligned}
\Delta\tilde{\omega}_g^{\rm res}(N,t_1,u_1,Q^2,m^2,\mu^2,\alpha_s(\mu)) \;=\; & \\
& H_g(\zeta,Q^2,m^2,\alpha_s(m))\;\tilde{S}(1,\zeta)\exp\left\{2\int_\mu^m\frac{d\mu'}{\mu'}\gamma_g\left(\alpha_s(\mu')\right)\right\} \\
& \times\;\exp\left\{\int_0^\infty\frac{dw}{w}\Big(1-{\rm e}^{-N_u w}\Big)\Big[\int_{w^2}^1\frac{d\lambda}{\lambda}A^g(\alpha_s(\sqrt{\lambda}2k\cdot\zeta))+\frac{1}{2}\nu_g(\alpha_s(w2k\cdot\zeta))\Big]\right\} \\
& \times\;\exp\left\{\int_m^{m/N}\frac{d\mu'}{\mu'}2\,{\rm Re}\Delta\Gamma_S\left(\alpha_s(\mu')\right)\right\} \\
& \times\;\exp\left\{-2\int_\mu^{2k\cdot\zeta}\frac{d\mu'}{\mu'}\Big(\gamma_g\left(\alpha_s(\mu')\right)-\gamma_{g/g}\Big(N_u,\alpha_s(\mu')\Big)\Big)\right\},
\end{aligned} \tag{3.62}$$

with $N_u = N(-u_1/m^2)$ as defined below (3.26). To NLL accuracy, the product H_gS on the second line of (3.62) is determined from matching to the Born result at the scale $\mu = m$. To this accuracy the product H_gS is also insensitive to the choice of treatment of γ_5. The second exponent in (3.62) gives the leading N-dependence of the ratio $\Delta\tilde{\psi}_{g/g}/\Delta\tilde{\phi}_{g/g}$ with

$$A_g(\alpha_s) \;=\; C_A\frac{\alpha_s}{\pi}+\frac{1}{2}C_AK\left(\frac{\alpha_s}{\pi}\right)^2+\ldots\,, \qquad\qquad \nu^g(\alpha_s) \;=\; 2C_A\frac{\alpha_s}{\pi}+\ldots\,, \tag{3.63}$$

where $K = C_A(67/18-\pi^2/6)-5/9n_f$ can be inferred from [82, 83] using [84] (cf. also [61]). The scale evolution of the ratio $\Delta\tilde{\psi}_{g/g}/\Delta\tilde{\phi}_{g/g}$ is governed by

$$\gamma_g(\alpha_s) \;=\; b_2\frac{\alpha_s}{\pi}+\ldots\,, \tag{3.64}$$

$$\gamma_{g/g}(N,\alpha_s) \;=\; -\frac{\alpha_s}{\pi}(C_A\ln N-b_2)-\left(\frac{\alpha_s}{\pi}\right)^2\left(\frac{1}{2}C_AK\ln N\right)+\ldots\,, \tag{3.65}$$

with $\gamma_{g/g}$ calculated in [82, 83], and the soft anomalous dimension to order α_s is given by (3.61). Note that the various anomalous dimensions given above are identical to NLL accuracy to the corresponding quantities of soft gluon resummation for unpolarized scattering [49].

The resummed expression (3.62) represents the central result of this chapter. It provides the sum of Sudakov logarithms due to soft gluon emission to all orders in the perturbative expansion and accurate to the next-to-leading logarithm. Finally, (3.62) can

be brought into a form allowing for an easy finite order inversion to s_4 space or, alternatively, a numerical computation. This will facilitate the discussions in chapters 4 and 5, respectively. The integrals in the exponents of (3.62) may be carried out, upon which the sum of the three exponents becomes

$$\begin{aligned}
&\frac{A_g^{(1)}}{2\pi b_0^2\alpha_s}\left[2\lambda_u+\lambda_u\ln\lambda_u\right]-\frac{A_g^{(1)}}{\pi b_0}\gamma_E\ln\lambda_u-\frac{B_g^{(1)}}{2\pi b_0}\ln\lambda_u\\
&-\frac{A_g^{(2)}}{2\pi^2 b_0^2}\left[2\lambda_u+\ln\lambda_u\right]-\frac{A_g^{(1)}}{\pi b_0}\lambda_u\ln\left(\frac{M_u^2}{\mu_F^2}\right)+\frac{A_g^{(1)}}{2\pi b_0}\ln\left(\frac{M_u^2}{\mu_R^2}\right)\left[2\lambda_u+\ln\lambda_u\right]\\
&+\frac{A_g^{(1)}b_1}{2\pi b_0^3}\left[\frac{1}{2}\ln^2\lambda_u+\ln\lambda_u+2\lambda_u\right]+\frac{\mathrm{Re}\Gamma_S^{(1)}}{\pi b_0}\ln\left(1-2\lambda\right)\ , \qquad (3.66)
\end{aligned}$$

with $\lambda_u=b_0\alpha_s\ln N_u$, $\lambda=b_0\alpha_s\ln N$, and coefficients

$$\begin{aligned}
A_g^{(1)} &= C_A\,,\quad A_g^{(2)}=\frac{1}{2}C_A\left[\left(\frac{67}{18}-\zeta_2\right)C_A-\frac{5}{9}N_f\right]\ .\\
B_g^{(1)} &= C_A\left(1+\ln\left(\frac{u_1^2}{sm^2}\right)\right)\ . \qquad (3.67)
\end{aligned}$$

Defining $L_u=\ln(-u_1/m^2)$ and substituting

$$\ln\left(\frac{M_u^2}{\mu_{F,R}^2}\right)=\ln\left(\frac{m^2}{\mu_{F,R}^2}\right)+2L_u,\qquad \lambda_u=\lambda+b_0\alpha_s L_u \qquad (3.68)$$

one arrives, to NLL accuracy, at

$$\begin{aligned}
\omega\Big(N,s,t_1,u_1,\mu_F^2,\mu_R^2\Big) &= \omega_0(s,t_1,u_1)\\
&\quad\times\exp\left[\ln N\,h_1(\lambda)+h_2\left(\lambda,\frac{m^2}{\mu_R^2},\frac{m^2}{\mu_F^2},s,t_1,u_1\right)\right] \qquad (3.69)
\end{aligned}$$

where

$$\begin{aligned}
h_1(\lambda) &= \frac{A_g^{(1)}}{2\pi b_0\lambda}\Big[2\lambda+(1-2\lambda)\ln(1-2\lambda)\Big]\\
h_2(\lambda) &= -\frac{A_g^{(1)}}{\pi b_0}\gamma_E\ln\left(1-2\lambda\right)-\frac{\bar{B}_g^{(1)}}{2\pi b_0}\ln\left(1-2\lambda\right)-\frac{A_g^{(2)}}{2\pi^2 b_0^2}\left[2\lambda+\ln\left(1-2\lambda\right)\right]\\
&\quad-\frac{A_g^{(1)}}{\pi b_0}\lambda\ln\left(\frac{m^2}{\mu_F^2}\right)+\frac{A_g^{(1)}}{2\pi b_0}\ln\left(\frac{m^2}{\mu_R^2}\right)\left[2\lambda+\ln\left(1-2\lambda\right)\right]\\
&\quad-\frac{C_A}{2\pi b_0}\ln\left(1-2\lambda\right)\left(2L_u-\ln\left(\frac{s}{m^2}\right)\right)+\frac{\mathrm{Re}\Gamma_S^{(1)}}{\pi b_0}\ln\left(1-2\lambda\right)\ , \qquad (3.70)
\end{aligned}$$

with $\bar{B}_g^{(1)}=C_A$.

This exponent can be used as a generating functional to obtain estimates of finite order corrections in chapter 4. A numerical evaluation of the full exponent will be presented in chapter 5.

Chapter 4

Finite order results for charm production

In the previous chapter a resummed expression describing polarized deep inelastic charm production to all orders in perturbation theory has been derived. This full result will in this chapter be utilized as a generating functional yielding upon re-expansion approximate first and second order expressions. Albeit at first sight appearing like a step backwards from the all-orders result, these finite order estimates will prove highly valuable in assessing the phenomenological relevance of the resummation calculation. Whereas exact NLO corrections to polarized heavy quark photoproduction are known [63, 62, 85, 86], the calculation for finite Q^2 has not yet been completed [65, 66]. In the absence of a complete one loop calculation for the process, the resummation results constitute current best estimates beyond lowest order and allow to quantitatively investigate the discriminative power of heavy quark production in measuring the polarized gluon density of the proton as envisaged by HERMES and COMPASS. The estimates are valid in the region dominated by threshold logarithms, where their impact on the charm structure function g_1^c can be studied. The approximate partonic finite order results, accurate to NLL, are derived in section 4.1 and integrated over phase space to produce partonic coefficient functions in section 4.2. They are convoluted with different available parameterizations of the gluon density to give estimates for the charm contribution to the polarized structure function g_1^c in section 4.3.

4.1 Re-expansion of the exponent

To derive finite order results the resummed exponent (3.70) is expanded to the desired order in α_s, taking into account also the running of the strong coupling. In the following this will be done up to second order so as to provide NLO and NNLO approximations to NLL accuracy for the partonic single-particle inclusive double-differential cross section difference $\Delta\sigma_{\gamma^* g}$. There are in principle no limits as to the order of this re-expansion, but mostly it is carried out one or two orders beyond those computed exactly to provide estimates of the numerical importance of the unknown terms. NNLO should be sufficient for the process under consideration since the full one loop calculation is still pending [65,

66]. Once it becomes available, it can be combined with the two loop estimate. Should need be, a three loop contribution can be generated from (3.70).

For the process $\gamma^* + g \longrightarrow \mathrm{Q} + \overline{\mathrm{Q}}$, the single-particle inclusive double-differential cross section difference is related to the hard function $\Delta\omega_g$ as in equation (3.19). To NLL accuracy it can be written in a factorized form as

$$s'^2 \frac{d^2\Delta\sigma_{\gamma^* g}(s', t_1, u_1)}{dt_1\, du_1} = 8\pi^2\,\alpha\,\frac{x}{Q^2}\,\Delta\omega_g\Big(x, s_4, t_1, u_1, Q^2, m^2, \mu^2, \alpha_s(\mu)\Big) \simeq$$
$$\Delta B^{\mathrm{Born}}_{\gamma^* g}(s', t_1, u_1)\left\{\delta(s' + t_1 + u_1) + \frac{\alpha_s(\mu)}{\pi} K^{(1)}(s', t_1, u_1) + \left(\frac{\alpha_s(\mu)}{\pi}\right)^2 K^{(2)}(s', t_1, u_1)\right\}, \tag{4.1}$$

with the Born level hard part $\Delta B^{\mathrm{Born}}_{\gamma^* g} = \alpha\alpha_s e_c^2 \pi \Delta B_{\mathrm{QED}}$ as from (3.10), in agreement with [87, 88].

The NLO and NNLO soft gluons corrections to NLL accuracy are

$$K^{(1)}(s', t_1, u_1) = \tag{4.2}$$
$$2\,C_A\left[\frac{\ln(s_4/m^2)}{s_4}\right]_+ + \left[\frac{1}{s_4}\right]_+ \left\{C_A\left(\ln\left(\frac{t_1}{u_1}\right) + \mathrm{Re}L_\beta - \ln\left(\frac{\mu^2}{m^2}\right)\right) - 2\,C_F\,(\mathrm{Re}L_\beta + 1)\right\}$$
$$+ \delta(s_4)\,C_A \ln\left(\frac{-u_1}{m^2}\right)\ln\left(\frac{\mu^2}{m^2}\right),$$

$$K^{(2)}(s', t_1, u_1) = \tag{4.3}$$
$$2\,C_A^2\left[\frac{\ln^3(s_4/m^2)}{s_4}\right]_+ + \left[\frac{\ln^2(s_4/m^2)}{s_4}\right]_+ \left\{3\,C_A^2\left(\ln\left(\frac{t_1}{u_1}\right) + \mathrm{Re}L_\beta - \ln\left(\frac{\mu^2}{m^2}\right)\right)\right.$$
$$\left. -2\,C_A\,(b_2 + 3\,C_F\,(\mathrm{Re}L_\beta + 1))\right\} + \left[\frac{\ln(s_4/m^2)}{s_4}\right]_+ \ln\left(\frac{\mu^2}{m^2}\right)\left\{C_A^2\left(-2\ln\left(\frac{t_1}{u_1}\right)\right.\right.$$
$$\left.\left. -2\mathrm{Re}L_\beta + 2\ln\left(\frac{-u_1}{m^2}\right) + \ln\left(\frac{\mu^2}{m^2}\right)\right) + 2\,C_A\,(b_2 + 2\,C_F\,(\mathrm{Re}L_\beta + 1))\right\}$$
$$+ \left[\frac{1}{s_4}\right]_+ \ln^2\left(\frac{\mu^2}{m^2}\right)\left\{-C_A^2 \ln\left(\frac{-u_1}{m^2}\right) - \frac{1}{2}\,C_A\,b_2\right\},$$

with μ the $\overline{\mathrm{MS}}$-mass factorization scale, $b_2 = (11C_A - 2n_f)/12$ and L_β given below (3.61). A comparison with the preliminary results for the exact $\mathcal{O}(\alpha_s)$ corrections calculated in [65, 66] provides a valuable cross check of equation (4.2).

In deriving (4.2) and (4.3) the necessary inversion from Laplace moments to momentum space was done by successively matching the highest power in $\ln N$ (or $\ln \tilde{N}$) to an s_4 distribution, as given in (A.2) in appendix A. The lower powers of the moment space logarithm required to make up the s_4 expression are subtracted before continuing with the matching at the next order in $\ln N$. Since by the way it is set up resummation is always carried out to a particular power of the large logarithm the perturbative expansion is truncated in a well defined way. Its structure is of the form

$$1 + \frac{\alpha_s}{\pi}\left(L^2 + L\,(1 + L_M) + L_M\right) + \frac{\alpha_s^2}{\pi^2}\left(L^4 + L^3\,(1 + L_M) + L^2\left(L_M + L_M^2\right) + LL_M^2\right),$$

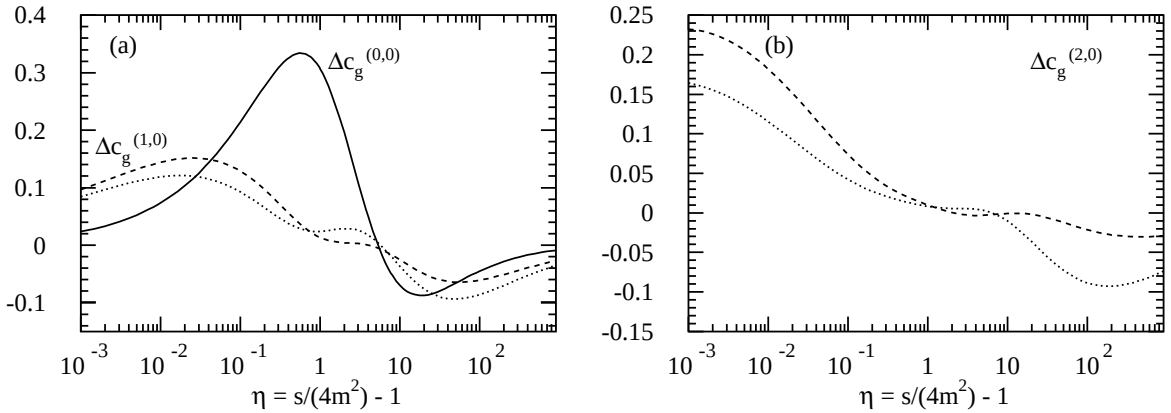

Figure 4.1: *(a) The η-dependence of the coefficient functions $\Delta c_g^{(k,0)}(\eta,\xi)$, $k=0,1$ for $Q^2 = 10\,\mathrm{GeV}^2$ with $m = 1.5\,\mathrm{GeV}$. Plotted are the exact result for $\Delta c_g^{(0,0)}$ (solid line) and the LL approximation (dotted line) and NLL approximation to $\Delta c_g^{(1,0)}$ (dashed line). (b) The η-dependence of the coefficient function $\Delta c_g^{(2,0)}(\eta,\xi)$ for $Q^2 = 10\,\mathrm{GeV}^2$ with $m = 1.5\,\mathrm{GeV}$. Plotted are the LL approximation (dotted line) and NLL approximation.*

where for simplicity $\ln N = L$, $\ln\left(\frac{\mu^2}{m^2}\right) = L_M$, and coefficients have been suppressed. Hence e.g. L^2 is dropped if not multiplied into a scale-dependent logarithm. To obtain hadronic results the partonic functions need to be convoluted with the polarized parton distributions. However, in the next section the partonic results will first be presented separately.

4.2 The partonic coefficient functions

In this section the partonic results (4.2) and (4.3) will be integrated over phase space and investigated numerically. To this end, it is convenient to define dimensionless coefficient functions $\Delta c_g^{(k,l)}$,

$$\Delta\sigma_{\gamma^* g}(s',q^2,m^2) \;=\; \frac{\alpha\,\alpha_s\,e_q^2}{m^2}\sum_{k=0}^{\infty}(4\pi\alpha_s(\mu))^k\sum_{l=0}^{k}\Delta c_g^{(k,l)}(\eta,\xi)\ln^l\frac{\mu^2}{m^2}\,. \tag{4.4}$$

Hence the superscript k indicates the order in α_s and l the power of the scale-dependent logarithm. As completely inclusive quantities the functions $\Delta c_g^{(k,l)}$ depend only on the scaling variables

$$\eta \;=\; \frac{s}{4m^2} - 1\,, \qquad\qquad \xi \;=\; \frac{Q^2}{m^2}\,, \tag{4.5}$$

where η is a measure of the distance to the partonic threshold.

Only for the lowest order coefficient function $\Delta c_g^{(0,0)}$ is it possible to analytically integrate over phase space. At higher orders one has to resort to numerical methods. There occur integrals of +-distributions in s_4 against test functions, at this point the Born contribution, whose subleading dependence on s_4 comes in through $u_1 = s_4 - t_1 - s'$. To

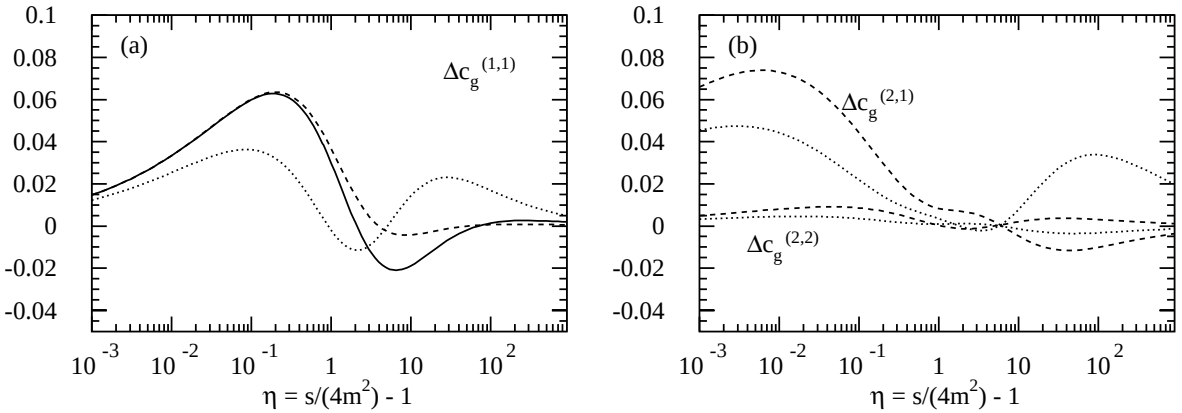

Figure 4.2: *(a) The η-dependence of the coefficient function $\Delta c_g^{(1,1)}(\eta,\xi)$ for $Q^2 = 10\,\mathrm{GeV}^2$ with $m = 1.5\,\mathrm{GeV}$. Plotted are the exact result (solid line), the LL approximation (dotted line) and the NLL approximation (dashed line). (b) The η-dependence of the coefficient functions $\Delta c_g^{(2,l)}(\eta,\xi)$, $l = 1,2$ for $Q^2 = 10\,\mathrm{GeV}^2$ with $m = 1.5\,\mathrm{GeV}$. Plotted are the LL approximation (dotted line) and the NLL approximation (dashed line).*

increase numerical stability such integrals are split into difference and boundary terms according to

$$\int_0^{s_4^+} ds_4 \left[\frac{\ln^n(s_4/m^2)}{s_4}\right]_+ f(s_4) = \int_\Delta^{s_4^+} ds_4 \frac{\ln^n(s_4/m^2)}{s_4}\left(f(s_4) - f(s_4=0)\right) + \frac{1}{n+1}\ln^{n+1}\left(s_4^+/m^2\right) f(s_4=0) \ , \qquad (4.6)$$

with the test function f regulating the divergence at $s_4 \longrightarrow 0$. For sufficiently smooth f the regulator Δ can even be taken to zero.

In Fig.4.1 all coefficient functions $\Delta c_g^{(k,0)}; k = 0,1,2$, i.e. those not accompanied by scale-dependent logarithms, are plotted for $Q^2 = 10\,\mathrm{GeV}^2$ and $m = 1.5\,\mathrm{GeV}$. Only the Born function $\Delta c_g^{(0,0)}$ in Fig.4.1a is known exactly [87, 88]. For $\Delta c_g^{(1,0)}$ in Fig.4.1a and $\Delta c_g^{(2,0)}$ in Fig.4.1b estimates to LL and NLL accuracy are given. In the LL case, only the highest powers in the logarithm are kept, i.e. $[\ln(s_4/m^2)/s_4]_+$ and $[\ln^3(s_4/m^2)/s_4]_+$ terms in equations (4.2) and (4.3), respectively. Clearly, both $\Delta c_g^{(1,0)}$ and $\Delta c_g^{(2,0)}$ are sizable near threshold. Here the large logarithms dominate, while they tend to be numerically rather small at larger values of η. As mentioned above, for a complete resummation to NNLL accuracy one would need to match the resummed result (3.70) at NLO, which requires knowledge of all one-loop soft and virtual corrections. These are not yet available [65, 66]. However, it is possible to investigate some next-to-next-to leading (NNLL) logarithmic contributions, such as the Coulomb corrections [65, 66, 69] for $\Delta c_g^{(1,0)}$ and for $\Delta c_g^{(2,0)}$ those NNLL terms obtainable from the expansion of (3.70). Numerically, these NNLL terms were found to have an effect on $\Delta c_g^{(1,0)}$ or $\Delta c_g^{(2,0)}$ of the order of 5% only as compared to the NLL corrections and are therefore not displayed here.

Since no exact results for $\Delta c_g^{(1,0)}$ and $\Delta c_g^{(2,0)}$ are available it is impossible to judge directly the quality of the LL and NLL approximations. However, similar investigations

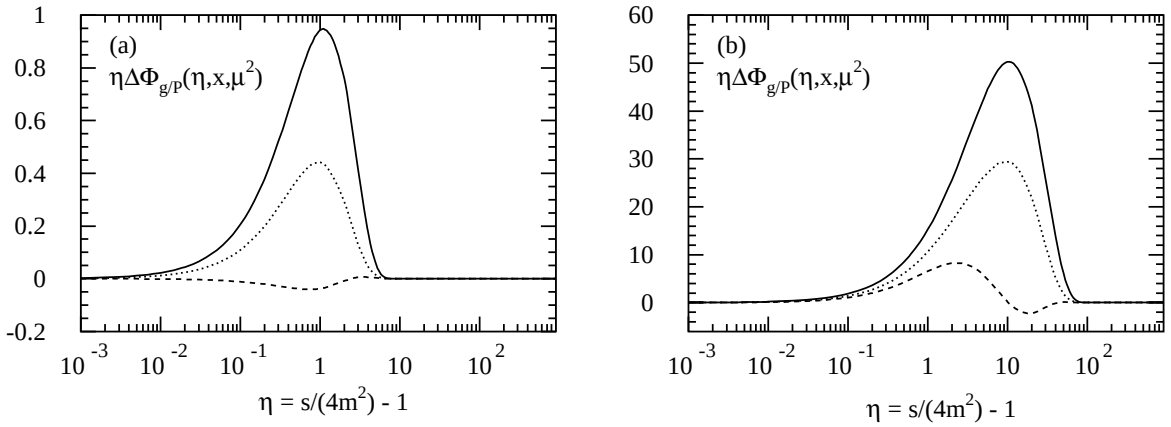

Figure 4.3: *(a) The polarized gluon distribution $\eta\Delta\phi_{g/P}(\eta, x, \mu^2)$ for $x = 0.1$ and $\mu = 1.5\,\mathrm{GeV}$. Plotted are the parameterizations GS A of [11] (solid), GS C of [11] (dashed) and GRSV valence of [12] (dotted). (b) Same as (a) for $x = 0.01$.*

in the case of unpolarized heavy quark production [49], where exact one-loop results are known [89], suggest that generally NLL accuracy provides a very good approximation of the true result for Q^2 not too large[1]. A strong indication that the same is true in the polarized case is provided by the fact that $K^{(1)}$, $K^{(2)}$ are identical to the unpolarized case, with only $B^{\mathrm{Born}}_{\gamma^* g}$ differing from $\Delta B^{\mathrm{Born}}_{\gamma^* g}$.

The coefficient functions multiplying scale-dependent logarithms are displayed in Fig.4.2a for $\Delta c_g^{(1,1)}$ and in Fig.4.2b for $\Delta c_g^{(2,1)}$ and $\Delta c_g^{(2,2)}$. For the parameters the same values as in Fig.4.1 are chosen. In particular the estimates for $\Delta c_g^{(1,1)}$ and $\Delta c_g^{(2,1)}$ to NLL accuracy can be seen to be large near threshold. Additionally, for the function $\Delta c_g^{(1,1)}$ the exact result can be obtained from renormalization group methods,

$$\Delta c_g^{(1,1)}\left(\eta(x),\xi\right) \;=\; \frac{1}{4\pi^2}\int\limits_{ax}^{1} dz\;\left(b_2\,\delta(1-z)-\frac{1}{2}\Delta P_{gg}^{(0)}(z)\right)\,\Delta c_g^{(0,0)}\left(\eta\Big(\frac{x}{z}\Big),\xi\right)\,, \quad (4.7)$$

with $a = 1 + 4m^2/Q^2$ and the one-loop splitting function as given by (3.35). Splitting into difference and boundary terms improves numerical stability, as before with the approximate coefficient functions. Fig.4.2a clearly shows that the approximation based on NLL accuracy traces the exact result (4.7) extremely well even at larger η. Again, for $\Delta c_g^{(2,1)}$ NNLL terms obtained from the expansion of the resummed result (3.70) have only a small effect.

4.3 The hadronic structure function

In this section the impact of the approximate higher order perturbative corrections on the inclusive hadronic structure function g_1 will be investigated. In terms of coefficient

[1] In the regime of large Q^2/m^2 on the other hand, the coefficient functions $\Delta c_g^{(k,0)}$ can be approximated with different methods based on the operator product expansion [69].

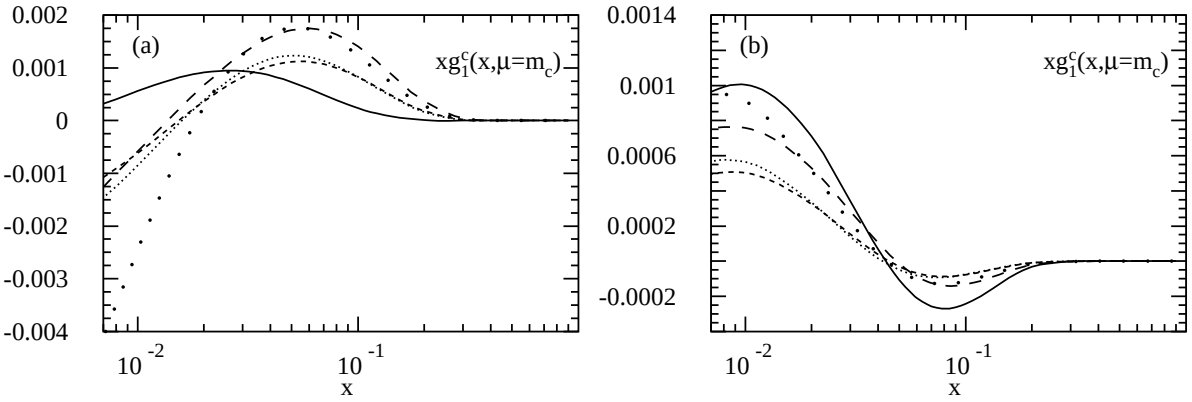

Figure 4.4: *(a) The x-dependence of the charm structure function $xg_1^c(x, Q^2, m^2)$ with the gluon distribution GS A [11] for $\mu = m = 1.5\,\mathrm{GeV}$ and $Q^2 = 10\,\mathrm{GeV}^2$. Plotted are the results at leading order (solid), at NLO to LL accuracy (dotted), at NLO to NLL accuracy (dashed), at NNLO to LL accuracy (spaced dotted) and at NNLO to NLL accuracy (spaced dashed). (b) Same as (a) with the gluon distribution GS C [11].*

functions, the charm structure function g_1^c can be expanded as

$$\begin{aligned} & g_1^c(x, Q^2, m^2) \qquad (4.8) \\ & = \frac{\alpha_s(\mu)\, e_c^2 Q^2}{8\pi^2 m^2 x} \int_{ax}^{1} dz \Delta\phi_{g/P}(z, \mu^2) \sum_{k=0}^{\infty} (4\pi\alpha_s(\mu))^k \sum_{l=0}^{k} \Delta c_g^{(k,l)}(x/z, \xi) \ln^l \frac{\mu^2}{m^2} \\ & = \frac{\alpha_s(\mu)\, e_c^2}{2\pi^2} \int_{-\infty}^{A} d(\log_{10}\eta) \ln 10\ \eta \Delta\phi_{g/P}(\eta, x, \mu^2) \sum_{k=0}^{\infty} (4\pi\alpha_s(\mu))^k \sum_{l=0}^{k} \Delta c_g^{(k,l)}(\eta, \xi) \ln^l \frac{\mu^2}{m^2}\ , \end{aligned}$$

where $a = 1 + 4m^2/Q^2$, $A = \log_{10}(\xi\{1/x - 1\}/4 - 1)$, and $\Delta\phi_{g/P}$ the polarized gluon distribution as before. Recall that the $\overline{\mathrm{MS}}$-scheme has been chosen and that contributions from light initial state quarks are neglected. For $\Delta\phi_{g/P}$ the parameterizations of [11, 12] are compared. This choice is not intended to express any particular preference, but to illustrate the discriminative power of a structure function measurement in this kinematic regime with respect to the various gluon distributions consistent with data currently available. In the analysis at NLO (LO) a 2-loop (1-loop) running coupling with $n_f = 3$ light flavours, a charm (pole) mass of $m = 1.5\,\mathrm{GeV}$ [89], and $\Lambda_{\mathrm{QCD}} = 0.232$ GeV are used.

The somewhat non-standard expression in the last line of (4.8) facilitates the investigation of partonic threshold effects on g_1^c. At the cost of introducing the logarithmic measure the standard convolution of g_1^c has been turned into a point-wise multiplication of the coefficient functions with $\eta\Delta\phi_{g/P}$. The latter is plotted as a function of η in Fig.4.3. The support it provides through (4.8) can be estimated by overlaying it with the partonic coefficient functions. Comparing Fig.4.3 with Figs.4.1 and 4.2 one can tell over which ranges of η the function $\eta\Delta\phi_{g/P}$ becomes large and hence where it samples the $\Delta c_g^{(k,l)}$. Fig.4.3 reveals that for values $x \gtrsim 0.01$ and at scales around $Q^2 \simeq 10\,\mathrm{GeV}^2$ this happens indeed in the region where the resummed approximation looks trustworthy, irrespective of the parameterization considered for the gluon density. It seems therefore reasonable

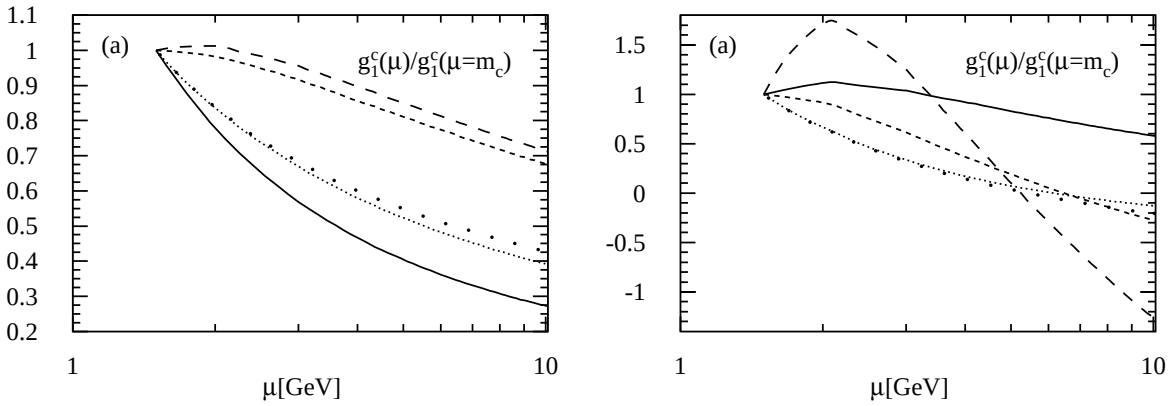

Figure 4.5: *(a) The factorization scale dependence of the charm structure function* $g_1^c(x,Q^2,m^2,\mu^2)/g_1^c(x,Q^2,m^2,\mu^2=m^2)$ *with the gluon distribution GS A [11] for* $m = 1.5\,\mathrm{GeV}$, $Q^2 = 10\,\mathrm{GeV}^2$ *and* $x = 0.05$. *Plotted are the results at leading order (solid), at NLO to LL accuracy (dotted), at NLO to NLL accuracy (dashed), at NNLO to LL accuracy (spaced dotted) and at NNLO to NLL accuracy (spaced dashed). (b) Same as (a) with the gluon distribution GS C [11].*

to expect the LL and NLL estimates for $\Delta c_g^{(k,l)}$ to provide good descriptions of the true higher order corrections for g_1^c for $x \gtrsim 0.01$. The gluon densities from set A of [11] and the valence scenario of [12] are both positive and similar in shape, while the gluon density from set C of [11] relaxes the positivity constraint on $\Delta\phi_{g/P}$ and oscillates.[2]

A comparison of the x-dependence of g_1^c as computed from the NLO and NNLO estimates (4.2) and (4.3) with the leading order result [87, 88, 91] is given in Fig.4.4a over a range $0.007 \leq x \leq 1$. Here $Q^2 = 10\,\mathrm{GeV}^2$, a fixed value of the factorization scale $\mu = m = 1.5\,\mathrm{GeV}$, as well as the gluon parameterization GS A of [11] have been chosen. Similar results are obtained with the gluon distribution in the valence scenario of [12] but not displayed here. The perturbative corrections are found to be sizable, both in the region of intermediate x, around 0.05 and at smaller x, where however, the approximation is less certain to work well. To assess the quality of the approximation, at each order results to LL and to NLL accuracy are compared. At intermediate x, the small differences between LL and NLL accuracy show a very good stability of the threshold approximation for the description of g_1^c. Towards smaller x however, these deviations increase and indicate that the underlying approximations fail for $x \leq 0.01$. In Fig.4.4b the calculation of xg_1^c is repeated for the same parameters as in Fig.4.4a but with the gluon density GS C of [11]. Again, the perturbative corrections are sizable over the whole range in x, but the shapes of the curves completely different. Both the coefficient functions and the gluon density oscillate, which leads in particular at intermediate x around 0.1 to destructive interference, with g_1^c being only marginally different from zero.

As can be seen from these plots the charm contribution to the polarized structure function can serve also beyond leading order to distinguish different gluon density scenarios. Two more checks of these results are worthwhile to gauge their reliability. First,

[2]Recent results from the HERMES collaboration [90] indicate a positive ratio of polarized over unpolarized gluon distribution $\Delta\phi_{g/P}/\phi_{g/P}$ at intermediate x.

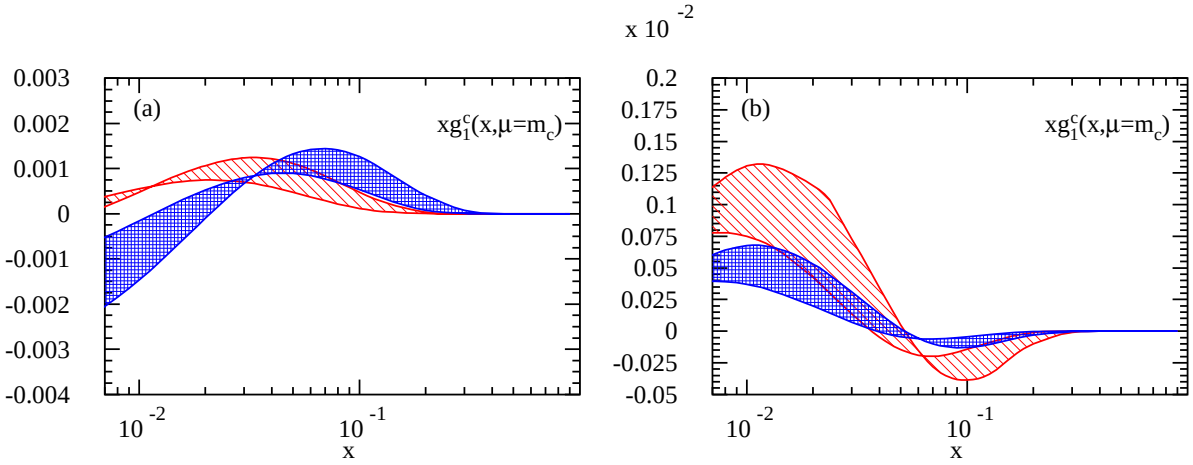

Figure 4.6: *(a) The charm mass dependence of the charm structure function* $xg_1^c(x, Q^2, m^2, \mu^2 = m^2)$ *with the gluon distribution GS A [11] for* $m = 1.3 \ldots 1.7\,\mathrm{GeV}$, $Q^2 = 10\,\mathrm{GeV}^2$, *for LL (striped band) and NLL (hatched band). (b) Same as (a) but with the gluon distribution GS C [11].*

one can study the dependence of g_1^c on the mass factorization scale, and second, its dependence on the (rather poorly constrained) charm quark mass. In general, leading order calculations exhibit a strong sensitivity on the factorization scale, which is usually reduced once higher order corrections are taken into account. In addition, there are general arguments supporting a reduction in scale dependence from including soft gluon effects [92]. Therefore, it is important to assess the effect of the NLL-approximate NLO and NNLO results (4.2) and (4.3) on the scale dependence of g_1^c in comparison to the leading order calculation [87, 88, 91]. Note however, that the arguments of [92] leading to genuine NLO soft gluon resummations rely on NNLL accuracy, which is not yet available for g_1^c [66, 63]. The ratio $g_1^c(\mu)/g_1^c(\mu = m)$ is shown over a range $m \leq \mu \leq 10\mathrm{GeV}$ with $m = 1.5\,\mathrm{GeV}$, $Q^2 = 10\,\mathrm{GeV}^2$, and $x = 0.05$ held fixed. In Fig.4.5a the parameterization GS A of [11] were used, but the following conclusions hold also for the gluon density in the valence scenario of [12]. At NLO the corrections based on LL accuracy only are not found to be sufficient to reduce the scale dependence. Clearly, soft gluon effects need to be approximated at least to NLL accuracy to achieve the desired result, a feature also noticed in studies of unpolarized heavy quark production [49]. The best estimate available for g_1^c makes use of the exact expression for the coefficient function $\Delta c^{(1,1)}$ of equation (4.7). However, since it differs only slightly from the NLO result to NLL accuracy for the chosen parameters in Fig.4.5, it will not be displayed here. In Fig.4.5b this analysis is repeated for the parameterization GS C of [11]. In this case, the NLO and NNLO approximations do not reduce the scale dependence. This is due to the oscillating gluon density, which leads to g_1^c being close to zero at the x-value chosen, and even causes g_1^c to change sign, depending on the scale. The dependence of the NLO results for g_1^c on the charm quark mass is shown in Fig.4.6 for both the GS A and GS C gluon distributions (4.6(a) and (b), respectively) at $Q^2 = 10\,\mathrm{GeV}^2$. The variation of g_1^c with m is sizeable across almost the complete range of x as investigated previously. Most of this mass dependence originates from the Born cross section.

To summarize, the study of the charm structure function as in Figs.4.4 and 4.5 shows that the soft gluon estimates of higher order corrections to the coefficient functions are well

under control and give stable predictions for g_1^c at scales Q^2 not too large and $x \gtrsim 0.01$. On the other hand, in the chosen kinematical range the effects of higher orders do not upset the sensitivity to the polarized gluon distribution function, with different gluon parameterizations leading to qualitatively different behaviour for g_1^c. Therefore, measurements of the charm structure function allow to further constrain the polarized gluon density. Including higher order contributions significantly reduces the scale dependence of g_1^c, in particular when computed with the GS A set of parton distributions. However, the sizable charm quarks mass dependence of g_1^c at leading order is not reduced upon including approximate higher order corrections. Nevertheless, analysis of g_1^c as presented here is well applicable in the kinematical range accessible to the HERMES and COMPASS experiments. In this region, the NLO and NNLO estimates given can help to reduce theoretical uncertainties and may assist in the theoretical interpretation of future g_1^c measurements.

Chapter 5

Charm production at all orders

As has been stressed in chapters 3 and 4 the resummed expressions for heavy quark electroproduction have so far been made use of only as generating functionals for approximate finite order corrections. Indeed, resummation approaches to numerically investigate full exponents have so far been mostly limited to inclusive processes. As a matter of principle, the more differential a cross section, the better suited it is for phenomenology, because one may incorporate detector-specific acceptance cuts and thereby reduce the need for extrapolation. Therefore, to fully exploit threshold-resummation as a quantitative tool of phenomenology, it seems desirable to understand better the behaviour of threshold-resummed expressions for double-differential cross sections. Resummed expressions have been derived for many double-differential hadronic cross sections, but most have only been used as generators of approximate finite order perturbation theory. A notable exception is provided by the double differential (in transverse momentum and rapidity) prompt photon production cross section, for which a study was performed [93] that employed an elegant analytic representation of the cross section involving two moment variables. Unfortunately, for many other cross sections, in particular involving heavy quarks, such a representation is not as readily possible.

The following sections contain results of a study concerned with a numerical evaluation of the full resummed exponent in heavy quark electroproduction. Section 5.1 presents an expression for the hadronic structure function conducive to numerical investigation. Section 5.2 introduces the minimal prescription employed in the numerical inversion from moment space. Section 5.3 contains numerical results. Section 5.4 presents the tower expansion, an alternate strategy to extracting information out off the all-order expression. Finally, section 5.5 concludes with an outlook to future investigations.

5.1 Refactorization revisited

Double differential single particle inclusive cross sections for $2 \to 2$ processes can be characterized by the property that their lowest order partonic hard scattering functions are constants as functions of the moment variable N. This is equivalent to the statement that the lowest order partonic subprocess at fixed external momenta *defines* the threshold condition. In this chapter the resummed form of a cross section with this property will

be investigated, the double-differential unpolarized cross section for the by now familiar single heavy quark inclusive electroproduction process. In this chapter polarization will not be considered, but this generalization should pose no further problems. The quantities of interest here are $d^2F_k^Q/dT_1\,dU_1,\ k=2,L$, the double-differential deep-inelastic heavy quark structure functions. The kinematic ranges of the hadronic variables T_1 and S_4 (at fixed T_1), introduced in (3.4), are given by

$$\begin{aligned} T_1^{\min} &= -\frac{S'}{2}(1+\beta) < T_1 < -\frac{S'}{2}(1-\beta) = T_1^{\max} \\ & 0 < S_4 < \frac{S}{S'T_1}\left(T_1+\frac{S'}{2}(1-\beta)\right)\left(T_1+\frac{S'}{2}(1+\beta)\right) = S_4^{\max} \end{aligned} \tag{5.1}$$

with $\beta=\sqrt{1-4m^2/S}$. The following study will be limited to considering F_2^Q, because the F_L^Q contribution is very small [89]. Just like in the polarized case, this structure function factorizes to leading power in $\Lambda_{\rm QCD}/Q$ as

$$\begin{aligned} S'^2\,\frac{d^2F_2^Q(x,S_4,T_1,U_1,Q^2,m^2)}{dT_1\,dU_1} &= \\ \sum_{i=q,\bar q,g}\int_{z^-}^1\frac{dz}{z}\,\phi_i(z,\mu_F^2)\,\omega_i\Big(&\frac{x}{z},s_4,t_1,u_1,Q^2,m^2,\mu_F^2,\mu_R^2\ ,\Big) \end{aligned} \tag{5.2}$$

where the lower limit z^- is given by $-U_1/(S'+T_1)$. The dimensionless hard scattering function ω_i describes as before the parton scattering process

$$\gamma^*(q)+\ i(k)\longrightarrow {\rm Q}(p_1)+\ X'[\overline{\rm Q}](p_2')\,. \tag{5.3}$$

with $k=z\,p$. Unlike in the polarized case, exact results for ω_i are known to NLO [89, 45]. For fully differential result cf. [47]. The convolution in (5.2) may also be written in the form

$$\begin{aligned} S'^2\,\frac{d^2F_2^Q(x,W,T_1,U_1,Q^2,m^2)}{dT_1\,dU_1} &= \\ \int_{y_{\min}}^1\frac{dy}{y}\int_0^W dw\sum_{i=q,\bar q,g}\phi_i(y)\omega_i\Big(w,y,T_1,U_1\Big)\,&\delta\left(W-w-(1-y)\frac{S'+T_1}{m^2}\right) \end{aligned} \tag{5.4}$$

with $y_{\min}=1-Wm^2/(S'+T_1)$, $W=S_4/m^2$, and $w=s_4/m^2$. After a Laplace transform this convolution *almost* factorizes

$$\begin{aligned} S'^2\,\frac{d^2F_2^Q(x,N,T_1,U_1,Q^2,m^2)}{dT_1\,dU_1} &= \int_0^1 dw_1 e^{-N\left(\frac{S'+T_1}{m^2}w_1\right)}\sum_{i=q,\bar q,g}\bar\phi_i(w_1)\,\omega_i\Big(N,w_1,T_1,U_1\Big) \\ \omega_i\Big(N,w_1,T_1,U_1\Big) &= \int_0^\infty dw\,e^{-Nw}\,\omega_i\Big(w,w_1,T_1,U_1\Big) \end{aligned} \tag{5.5}$$

with $w_1\equiv 1-y$ and $\bar\phi_i(w_1)=\phi_i(y)/y$. Near threshold, to leading power in N, the sum can be restricted to the dominant, gluonic contribution $i=g$ [49]. Since no confusion can arise, this subscript on ω_g will be dropped from now on. Were it not for the y (or w_1) dependence in ω_i, the factorization in (5.5) would be exact. However, at large N, the

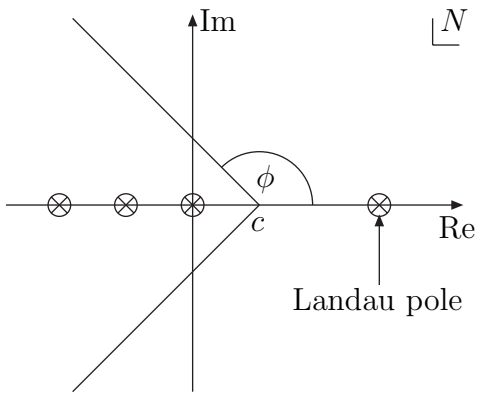

Figure 5.1: *The complex N plane and contour used for the numerical inversion from moments according to the minimal prescription. All except for the Landau poles lie to the left of the contour.*

dependence on w_1 in $\omega(N, w_1)$ is not singular, and can be approximated by setting w_1 equal to some fixed, optimal value $w_1^{\rm opt}$. This allows one to write

$$S'^2 \frac{d^2 F_2^Q(x, N, T_1, U_1, Q^2, m^2)}{dT_1\, dU_1} \simeq \bar{\phi}_g \left(N \frac{S' + T_1}{m^2} \right) \omega\Big(N, w_1^{\rm opt}, T_1, U_1\Big) . \tag{5.6}$$

In section 5.3 $w_1^{\rm opt}$ will be determined and the quality of this approximation assessed. For $\omega(N, w_1^{\rm opt}, T_1, U_1)$ one can now use (3.69) or any of its finite order expansions in α_s. The latter allow comparisons with momentum space results generated by analytical inversion from moment space and subsequent integration. In the following sections it will often be useful and illustrative to exhibit contributions of a particular order in the strong coupling and the large logarithms. To avoid confusion, the notation

$$\mathrm{N}^k\mathrm{LO} - l\mathrm{L}_{+,N} \tag{5.7}$$

will be employed for finite order results, where k indicates the order in the strong coupling, the subscripts + and N denote +-distributions and moments, respectively, and l expresses if only the leading term ($l = 1$), or also the next-to-leading term ($l = 2$) is included. Since the variables x, Q^2, and m in expressions like (5.6) will in the following be kept fixed, they will henceforth no longer be displayed explicitly in the list of arguments.

5.2 The minimal prescription

Threshold-resummed expressions are derived in N space. At finite orders the analytic conversion to momentum space is simple, since the moments corresponding to the usual +-distributions are known in closed form to the necessary accuracy in N [37, 94]. However, for the full resummed exponent this is not the case. The conversion to momentum space then requires a numerical inverse Laplace transform, for the case at hand after the $w_1^{\rm opt}$ approximation as in (5.6) one needs to compute

$$S'^2 \frac{d^2 F_2^Q(W, T_1, U_1)}{dT_1\, dU_1} = \int\limits_{c-i\infty}^{c+i\infty} \frac{dN}{2\pi i} e^{NW} \bar{\phi}_g \left(N \frac{S' + T_1}{m^2} \right) \omega\Big(N, w_1^{\rm opt}, T_1, U_1\Big) , \tag{5.8}$$

	$\ln^7(x)/x$	$\ln^5(x)/x$	$\ln^3(x)/x$
$\ln^8 \tilde{N}$	0.125	-	-
$\ln^7 \tilde{N}$	-	-	-
$\ln^6 \tilde{N}$	5.76	0.167	-
$\ln^5 \tilde{N}$	16.8	-	-
$\ln^4 \tilde{N}$	128	4.11	0.25
$\ln^3 \tilde{N}$	451	8.01	-
$\ln^2 \tilde{N}$	1424	36.5	2.47
$\ln \tilde{N}$	2815	64.4	2.4
const	2829	67.8	3.65

Table 5.1: *Coefficients of powers of* $\ln \tilde{N}$ *in moment space expression corresponding to plus-distributions in momentum space.*

with c the intercept of the contour with the real N axis. Usually, the parameter c is to be chosen so that the contour passes to the right of all singularities. Such singularities typically result not only from the logarithms $\ln N$ at $N = 0$, but also from the moments of the parton densities at negative values of N, as will become clear in section 5.3. All these singularities are physical and should thus be sampled by the inverse transformation. However, the functions h_i in (3.70) also exhibit singularities at $N^* = \exp(1/a\, b_0 \alpha_s)$, for $a = 1, 2$. Such unphysical Landau pole singularities, resulting from integrals over functions of the running coupling, signal the limitations of perturbation theory at leading power in $\Lambda_{\rm QCD}/Q$ and prevent one from choosing the standard contour to the right of all singularities. A *minimal* choice of contour [95] avoids these singularities by passing them on the left and thereby constitutes a definition of resummed perturbation theory at leading power of $\Lambda_{\rm QCD}/Q$. Fig.5.1 illustrates this choice of contour in the complex N plane. Moment space resummation using a minimal contour has many attractive features, which have been amply demonstrated for a number of inclusive and single-differential observables, and one double-differential cross section [93]. Specifically, the inverse is given by

$$f(z) = \frac{1}{\pi} \mathrm{Im} \int_0^\infty dz e^{i\phi} e^{wN} f(N(z)) \,, \qquad N = c + z e^{i\phi} \,. \tag{5.9}$$

To improve convergence properties and numerical precision the contour is thus often tilted [96], with $\phi = 3\pi/4$ a typical value for the studies in subsequent sections. Generically, this leads to inversions acquiring most of their final result for z values not too far from zero, i.e. for none-too large values of $\ln N$. Also, numerical precision can often be improved by shifting the intercept c. Explicit values for these parameters will be given in the next section.

5.3 Numerical studies

While the mapping from polynomials in $\ln N$ to +-distributions (cf. (1.10)) and vice versa is unique, and relates the highest power of the plus-distribution to the highest power of $\ln N$ as can be seen from the list in appendix A, it was observed already in [97] that

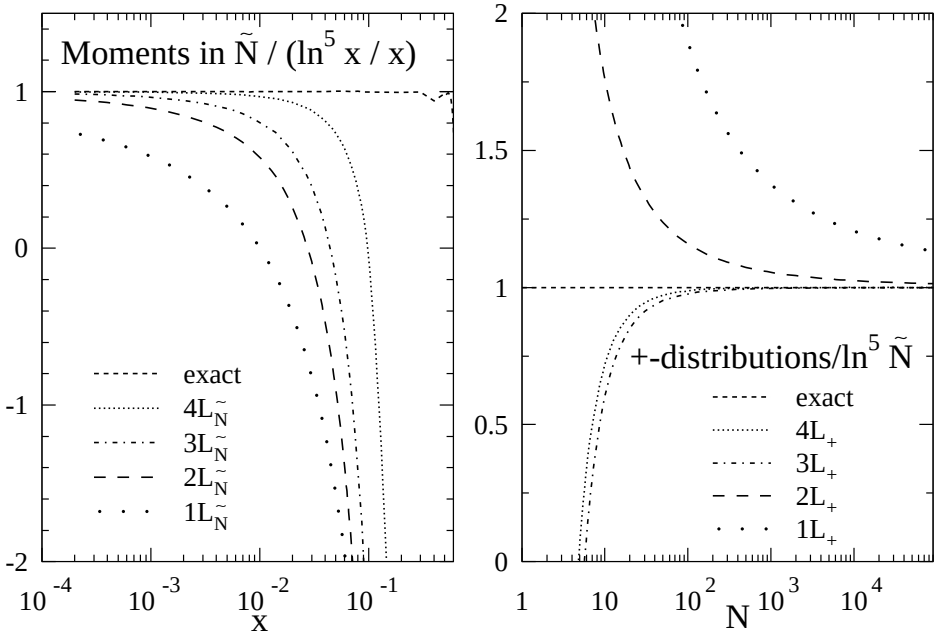

Figure 5.2: *a) The quality of the numerical inversion from moment space normalized by the exact result* $\ln^5(x)/x$ *for* $kL_{\tilde{N}}$. *b)* $\ln^5 \tilde{N}$ *generated from a numerical Mellin transformation of its corresponding sum of +-distributions for* kL_+.

subleading terms in moment space become numerically important if they come endowed with large coefficients. This is shown for a few $[\ln^i(x)/x]_+$ in Table 5.1. The quality of the numerical inversion from moment space can be seen from Fig. 5.2 for $\ln^5(x)/x$, where instead of N proper the more natural $\tilde{N}$ is considered (cf. appendix A). Other distributions lead to similar graphs. The figure shows that neglecting subleading terms in moment space leads to serious relative deviations from the correct result when approaching the point $x = 1$. Of course, the absolute values of $\ln^5(x)/x$ decrease on approaching $x = 1$, so the influence of the hierarchy-reversing coefficients depends very much on the particular process under consideration; its kinematics might effect a sampling of regions which are indeed sufficiently accurately approximated by the first terms of the moment space expression. However, a first indication that subleading powers of the logarithms in moment space do make relevant contributions is provided by Fig.5.3. It assess the importance of such terms for the partonic coefficient function $c^{2,0}$, the unpolarized counterpart of the $\Delta c^{2,0}$ introduced in (4.4). For easy comparison with the literature, the scale in these plots is the same as that chosen in [49]. Note that when generating expressions like (4.2) and (4.3) by numerical inversion according to (5.9), constants in moment space expressions make no contribution.

Really one is interested not so much in the inclusive but more in the double differential structure function. Before this can be investigated, some parameter choices have to be made. The following default values apply unless indicated otherwise. The value of the strong coupling is fixed at $\alpha_s = 0.2$. Furthermore, a simplified gluon distribution of the form $\phi(z) = 6(1-z)^5/z$ will be adopted. The Laplace transform of $\bar{\phi}(w) = kw^p\theta(1-w)$ is given by

$$\bar{\phi}(N) = k\left(-\frac{d}{dN}\right)^p \frac{1}{N}\left(1 - e^{-N}\right) \ , \tag{5.10}$$

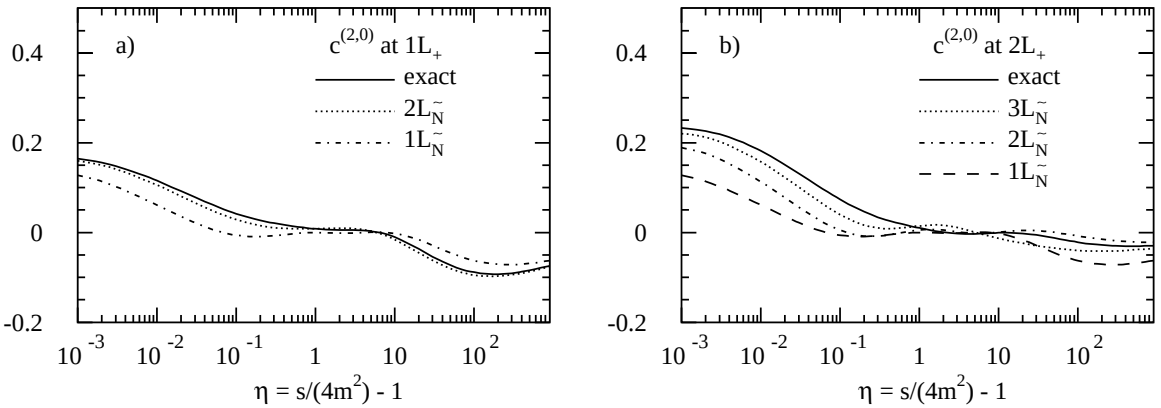

Figure 5.3: *a) The coefficient function $c^{2,0}$ at $1L_+$ as reproduced by $kL_{\tilde{N}}$ with $k \in \{1,2,3\}$. b) Same as a, but at $2L_+$.*

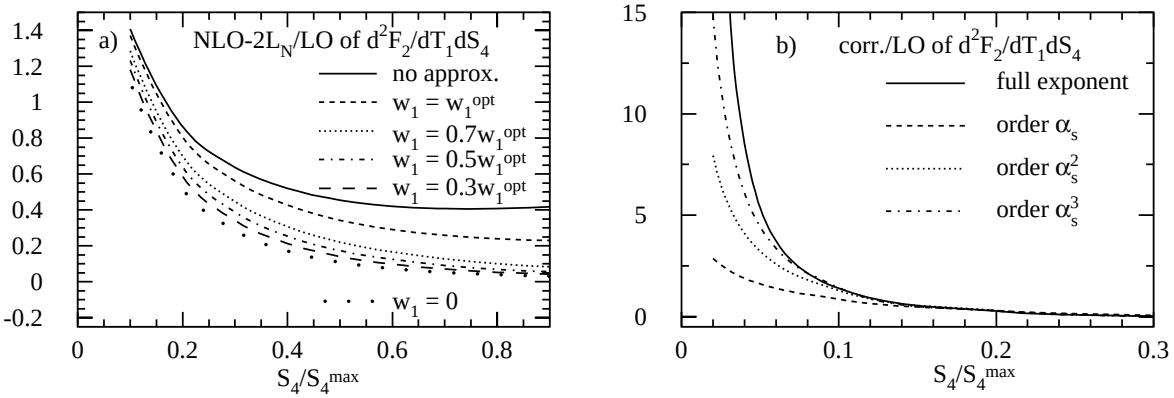

Figure 5.4: *a) Comparison of different choices for the variable $w_1^{\rm opt}$, for the ratio of NLO$-2L_N$ to LO of $d^2F_2^Q/dT_1dS_4$. The solid curves are results without approximation, computed with (5.2), the dashed curves represent the choice (5.11). b) Expandability of the resummed expressions for $d^2F_2^c/dT_1dS_4$ with NLL exponent (ratio to LO) with contour parameters $\phi = 0.75$, $c = 1$ for $S_4/S_4^{\rm max} \geq 0.1$, and $c = 10$ for $S_4/S_4^{\rm max} < 0.1$.*

with $\bar{\phi}$ defined below (5.5). In this feasibility study scale-independent, fixed distributions will be considered. The effects of their Laplace space DGLAP evolution should not be too large and can be included at a later point [4]. Default scale choices are $\mu = m$, with m the charm mass, 1.5 GeV. The default value for Q^2 is 10 GeV^2. For the Bjorken variable the value $x = 0.1$ is chosen. When T_1 is kept fixed, this is done at $(T_1^{\rm min} + T_1^{\rm max})/2$. Most studies involve the distribution in the hadronic distance to threshold $S_4/S_4^{\rm max}$ of K-factors, i.e. hadronic observables corrected to higher orders divided by their leading order versions.

Before investigating the double differential structure function proper one first needs to find the optimal value of $w_1^{\rm opt}$ as in (5.6). To this end, Fig.5.4a shows for $d^2F_2^Q/dT_1dS_4$ how well the ratio of the NLO $-$ $2L_N$ results to the LO one, both computed according to (5.2), compares with various choices of $w_1^{\rm opt}$ for this ratio, if both approximate NLO $-$ $2L_N$ and LO are computed according to (5.8). It can be concluded that an optimal choice,

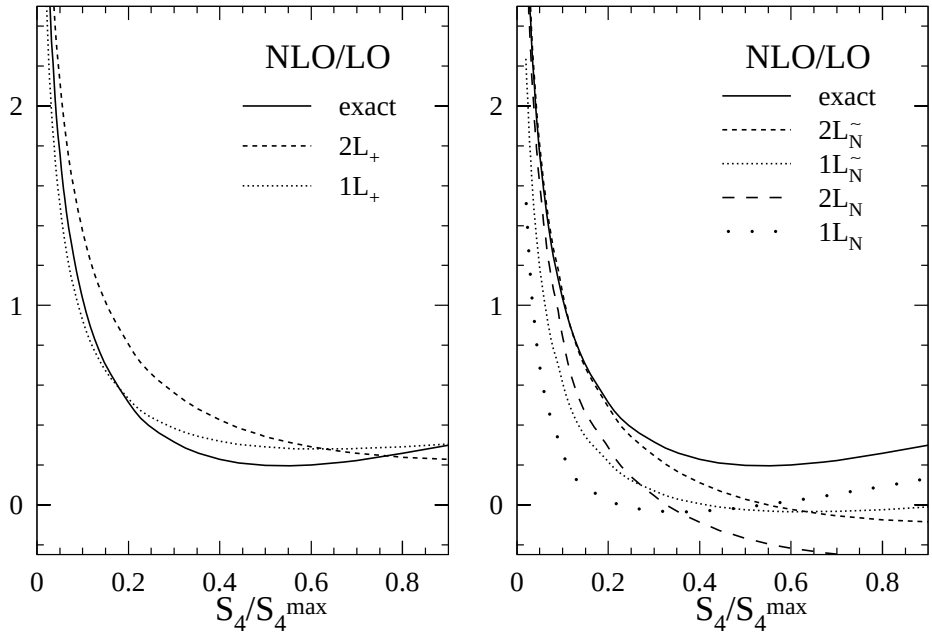

Figure 5.5: NLO$-k\mathrm{L}_{+,N}$ *corrections divided by LO contribution to* $d^2F_2^c/dT_1dS_4$ *as functions of* $S_4/S_4^{\max}$ *at* $w_1^{\rm opt}$. *The contour parameters are* $\phi = 0.75$, $c = 1$ *for* $S_4/S_4^{\max} \geq 0.1$, *and* $c = 10$ *for* $S_4/S_4^{\max} < 0.1$. *All results computed with simplified gluon density* $y\phi(y) = 6(1-y)^5$. *a)* L_+ *b)* L_N *and* $\mathrm{L}_{\tilde{N}}$.

quite close to the exact result for this finite order for small $S_4/S_4^{\max}$ (with deviations of order 10% in the threshold region), is given by

$$w_1^{\rm opt} = \frac{S_4}{S' + T_1} \ , \tag{5.11}$$

which will be the default choice from now on. This allows an evaluation of the resummed exponent as shown in Fig.5.4b, but the further discussion of this graph will be postponed. Consider first Fig.5.5, which shows the hierarchies of NLO $- k\mathrm{L}_{+,N}$ for $k = 1, 2$ in comparison with the exact result [91, 45]. Especially in moment space, omitting only one term already leads to serious deviations at moderated distance from threshold. On the other hand, the progression from $k = 1$ via $k = 2$ to the exact result is more uniform in N than in s_4. The moments tend to be somewhat smaller than the exact result, whereas momentum space estimates tend to exceed it. Also, the behaviour differs slightly for N and $\tilde{N}$. To really judge this, a process computed to higher orders and to higher accuracy in the logarithms has to be investigated. The inclusive deep inelastic structure function F_2 has these properties. This will be investigated and compared to the result for heavy quark production in [4].

Clearly, lower powers of $\ln N$ make a substantial contribution. This is true irrespective of which parton distribution one considers, although the choice does influence the absolute value of the result. Note that including an N-dependent Born function, which would correspond to a more inclusive cross section and different threshold condition, would have a similar effect, since such functions typically behave like the inverse of some low power of N [95], i.e. very similar to the moment space parton distributions. As to be expected, closer to partonic threshold incomplete expressions approximate the full result better than

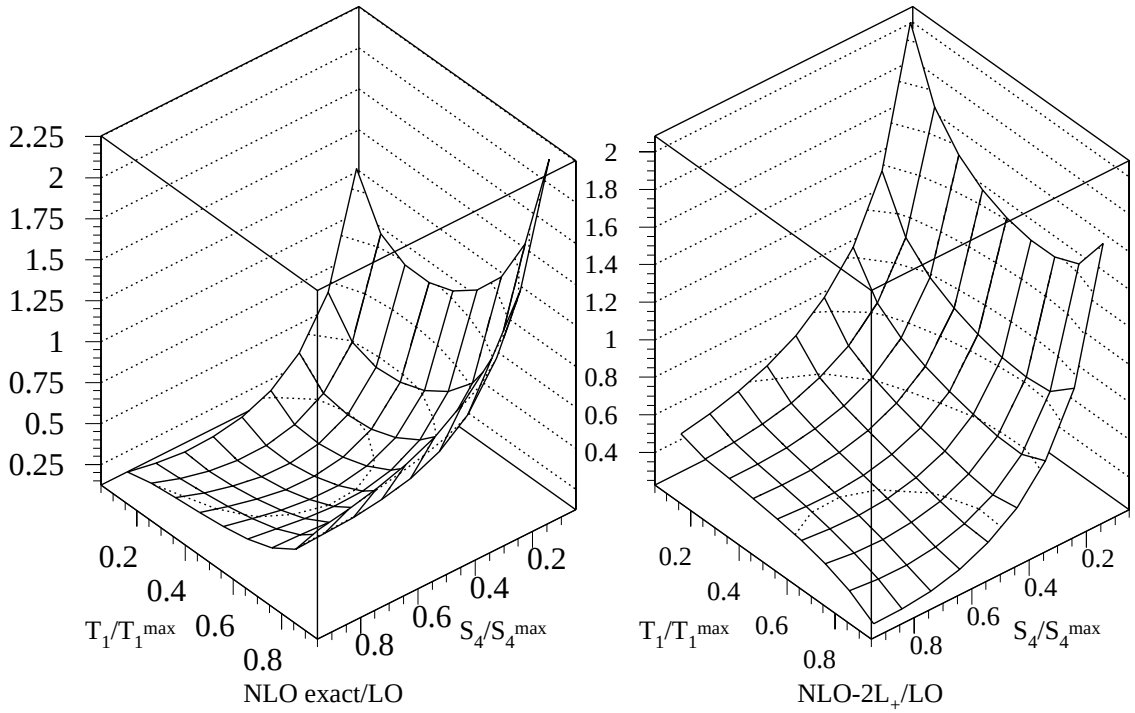

Figure 5.6: *NLO corrections divided by LO contribution to* $d^2F_2^c/dT_1dS_4$ *as function of* $S_4/S_4^{\max}$ *and* $T_1/T_1^{\max}$ *for a) exact, and b)* $2L_+$.

further away from threshold.

Instead of inverting a hadronic observable, one can perform the inverse Laplace transform at the parton level, and then use the result in (5.2). The benefit of such a *hybrid* approach would lie in the fact that no approximations for w_1 would be necessary, and it would be easier to include realistic parton distributions, as numerical routines are not usually supplied in the form of moments. Although this approach is in fact quite straightforward at any finite order, the observables considered here present a minor complication, associated with the fact that its lowest order parton level version does not have N dependence. In passing from finite order terms $\sim \ln^k N$ to resummed expressions $\exp(\ln^2 N)$ both the large and small N divergences become much more severe. They require an extra damping which can be provided by the parton densities, but is absent at the parton level. The hybrid approach will not be pursued any further in the following, for details consult [4].

While the plots obtained at fixed T_1 show only a single slice through the two-dimensional kinematics (T_1, S_4) parameter space, Fig.5.6 presents two-dimensional plots. It shows the ratio of the NLO and LO contributions, for the exact as well as for the NLO$-2L_N$ values. As expected, one finds large corrections, in fact of the order of one or even higher, for small S_4, across the full range of T_1. At the T_1 edges of phase space no enhancements occur.

One can now turn to Fig.5.4b, the expandability in the strong coupling of the full resummed expression. The graph shows that with NLL in the resummed exponent, a NNLO approximation in the strong coupling already traces very well the full exponent. Resummed exponents computed to LL are approximated even more accurately by

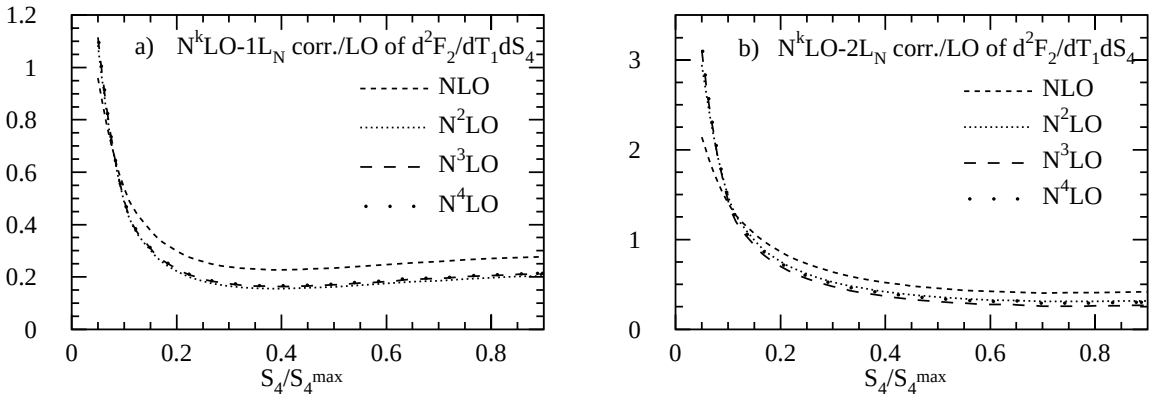

Figure 5.7: *Tower resummed expressions as functions of $S_4/S_4^{\max}$ for a) $\mathrm{N^kLO-1L}_N$, and b) $\mathrm{N^kLO-2L}_N$, all normalized by LO.*

their expansions in the strong coupling. In absolute values the resummed expressions are a little above the $\mathrm{NLO-2L}_+$ corrections around $S_4/S_4^{\max} \simeq 0.1$, but fall below the $\mathrm{NNLO-2L}_+$ corrections (not presented graphically here). This is consistent with the results found for the partonic coefficient function $c^{(2,0)}$ in Fig.5.3 and for the NLO corrections to $d^2F_2^c/dT_1dS_4$ in Fig.5.5. Nevertheless, for the resummed exponent integration over the full phase space to generate inclusive quantities is not possible, since unlike powers of $\ln N$ the divergence of an $\exp(\ln^2 N)$-type of expression cannot be compensated by polynomials or rational functions (e.g. parton distributions). To be more precise, the exponent $\exp NS_4$ or $\exp Ns_4$ (for hadronic or partonic phase space integrations, respectively) provides no damping of the integrand at the lower limit of integration $S_4 = 0$ or $s_4 = 0$. In any case, possible difficulties encountered in relating the perturbation series in moment and momentum space have already been stressed in the discussion of the finite order examples.

5.4 Tower expansion

Expansions of the resummed expression (3.70) offer an alternative way of representing the all-order result, namely as a sum of towers of logarithms. The combination of these expressions with exact finite order results determines the number of towers for which all coefficients are exactly known. For the inclusive F_2 this method was studied in [97] with four towers known exactly. In this section only heavy quark production will be considered.

Expansion of the functions in (3.70) results in

$$\begin{aligned} \omega_0(s,t_1,u_1,\alpha_s) &= \left(\frac{\alpha_s}{\pi}\right) h_{00}(s,t_1,u_1) + \left(\frac{\alpha_s}{\pi}\right)^2 h_{01}(s,t_1,u_1) + \ldots \\ h_i &= \sum_{k=1}^{\infty} \left(\frac{\alpha_s}{\pi}\right)^k L^k\, h_{ik}, \;\; i = 1,2 \end{aligned} \tag{5.12}$$

After substitution of these expansions into (3.70) one can express the hard scattering

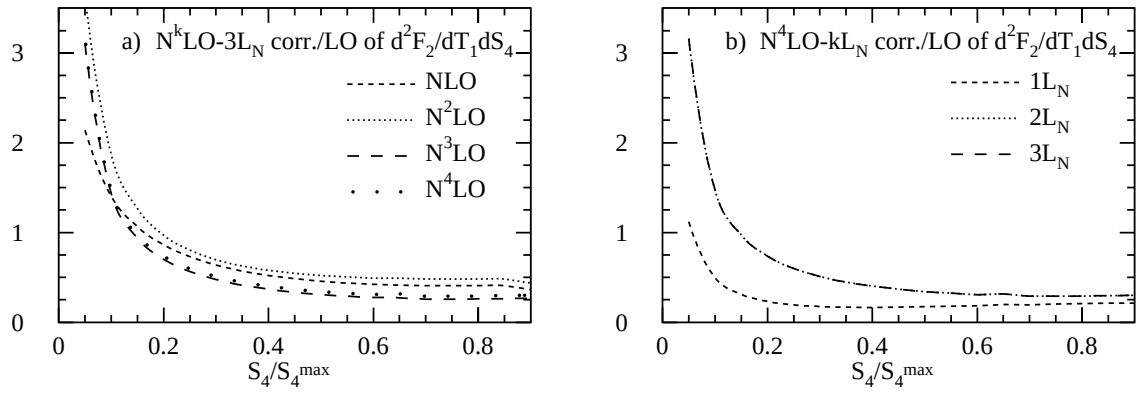

Figure 5.8: *Tower resummed expression as functions of $S_4/S_4^{\max}$ for a) $\mathrm{N^kLO} - 3\mathrm{L}_N$, and b) at $\mathrm{N^4LO} - k\mathrm{L}_N$, $k \in \{1,2,3\}$ ($\mathrm{N^4LO} - 2\mathrm{L}_N$ and $\mathrm{N^4LO} - 3\mathrm{L}_N$ almost coincide), all normalized by LO.*

function ω in towers of $L = \ln N$.

$$\omega = h_{00}(\alpha_s)\left[1 + \sum_{k=1}^{\infty}\left(\frac{\alpha_s}{\pi}\right)^k \left(c_{k1}\,L^{2k} + c_{k2}\,L^{2k-1} + c_{k3}\,L^{2k-2} + \ldots\right)\right]. \tag{5.13}$$

One finds

$$c_{k1} = \frac{(h_{11})^k}{k!} \tag{5.14}$$

$$c_{k2} = \frac{(h_{11})^{k-1}}{(k-1)!}h_{21} + \theta_{k2}\frac{(h_{11})^{k-2}}{(k-2)!}h_{12} \tag{5.15}$$

$$\begin{aligned} c_{k3} &= \frac{(h_{11})^{k-2}}{(k-2)!}\frac{1}{2}(h_{21})^2\theta_{k2} + \frac{(h_{11})^{k-3}}{(k-3)!}h_{13}\theta_{k3} + \frac{(h_{11})^{k-2}}{(k-2)!}h_{22}\theta_{k2} \\ &+ \frac{(h_{11})^{k-3}}{(k-3)!}h_{12}h_{21}\theta_{k3} + \frac{(h_{11})^{k-4}}{(k-4)!}\frac{1}{2}(h_{12})^2\theta_{k4} + \frac{(h_{11})^{k-1}}{(k-1)!}h_{01} \end{aligned} \tag{5.16}$$

where

$$\begin{aligned} h_{1k} &= \frac{A^{(1)}}{\pi b_0}\frac{(2b_0\pi)^k}{k(k+1)} \\ h_{2k} &= \frac{(2\pi b_0)^k}{k}\left(\gamma\theta_{k2}\left(S_1(k-1) - \beta\theta_{k2} - \alpha\right)\right) \end{aligned} \tag{5.17}$$

with

$$\alpha = \frac{1}{\pi b_0}\left(-A^{(1)}\gamma_E - \frac{1}{2}\bar{B}^{(1)} - \frac{C_A}{2}(2L_u - \ln\frac{s}{m^2}) + \mathrm{Re}\Gamma_S^{(1)}\right) \tag{5.18}$$

$$\beta = -\frac{A^{(2)}}{2\pi^2 b_0^2} \tag{5.19}$$

$$\gamma = \frac{A^{(1)}b_1}{2\pi b_0^3} \tag{5.20}$$

Here $\theta_{kj} = 1$ for $k \geq j$ and zero otherwise, and $S_1(k) = \sum_{j=1}^{k} 1/j$. These results are very similar to those in [97]. The coefficient h_{01} was determined by careful matching of the $\mathcal{O}(\alpha_s^2)$ term in (5.13) to the exact $\mathcal{O}(\alpha_s^2)$ expressions for ω given in [89].

Note that (5.13) is expressed as tower expansions in $\ln^i N$. By using the correspondence between the two spaces as e.g. in Appendix A one might generate similar expressions expanded in plus-distributions, with an equal numbers of towers. In Figs.5.7 and 5.8 of this section first results for tower expansions in N are displayed. They show good convergence qualities already at not too high orders in the strong coupling. Hence, the tower resummation can be regarded as a viable definition alternative to that used in section 5.3. In the tower approach the intrinsic ambiguity of the numerical inversion, resulting in the occurrence of a Landau pole, is handled in a way different from the minimal prescription. In a sense, renormalon ambiguities are shifted out to infinite tower number.

5.5 Conclusions and outlook

The results presented in this chapter form constitute part of [4]. Comparing with similar inclusive functions, for which higher orders in both the strong coupling and the threshold logarithms are known, should provide further insight into the results. Furthermore, a significant reduction of renormalization scale dependence is a genuine benefit of resummed expressions [98, 92]. This effect can only be investigated with realistic parton distributions and a running coupling constant. Also, a conversion from T_1, U_1 to some more physical variables like rapidity and transverse momentum and the use of realistic parton distributions would make the differential quantities computed directly applicable in phenomenology.

Chapter 6

Resummation for the Drell-Yan process

The resummation calculations of previous chapters were aimed at organizing and estimating logarithmic corrections dominant near partonic threshold. It has been observed that in the DIS scheme the refactorization of the DY cross section leading to exponentiation of threshold logarithms can also be used to organize a class of constant terms, most of which arise from the ratio of the timelike Sudakov form factor to its spacelike counterpart. This exponentiation will be extended here to include *all* constant terms. Also, it will be demonstrated how a similar organization may be achieved in the $\overline{\rm MS}$ scheme.

This chapter is structured as follows. Section 6.1 starts with a short review of previous work on the subject and gives some motivation for the study to follow. In section 6.2 the resummation of the quark Sudakov form factor and its embedding in the DIS–scheme DY cross section will be reviewed. The exponentiation in this scheme will be extended to include all constant terms. In section 6.3 the result for the $\overline{\rm MS}$ cross section will be derived. In section 6.5 the numerical relevance of the exponentiations will be studied in a two-loop analysis, while section 6.6 contains some conclusions.

6.1 Introduction

In previous chapters large threshold corrections to partonic cross sections have been identified and resummed. Also in similar processes such large terms almost always take the form of logarithms of ratios of kinematical scales. As partonic threshold is approached, these enhancements are parametrically guaranteed to increasingly dominate the perturbative contributions to the cross section. Often, however, also constant terms, which do not depend on scale ratios vanishing at threshold and which arise predominantly from purely virtual diagrams, are numerically important in the cross section. Some of these large constants originate from the same infrared singularities that give rise to the large logarithms, and consequently are resummable.

The threshold resummation for the partonic DY cross section is derived using as usual the procedure of refactorization: the Mellin transform of the cross section is expressed

as a product of well–defined functions, each organizing a class of soft and collinear enhancements. The refactorizations are valid up to corrections vanishing at threshold, and thus suppressed by powers of the Mellin variable N at large N. Terms independent of N can then be treated, in principle, by the same methods used to resum terms enhanced by logarithms of N. For the DY cross section and the deep–inelastic structure function F_2, such a refactorization was achieved in [26]. The resulting resummation of constant terms established to all orders the earlier observation [10] that, in the DIS–scheme DY cross section, the largest constants are related to the ratio of the timelike Sudakov form factor and its spacelike continuation. By solving an appropriate evolution equation [99], an exponential representation for this form factor, and thus also for the ratio, was derived [100], allowing easy numerical evaluation. Comparison with exact two–loop results [101] showed in that case that N–independent contributions at two loops are indeed dominated by the exponentiation of the one–loop result, combined with running coupling effects [102, 103].

In this chapter this analysis is refined for the DIS scheme, and extended to the $\overline{\rm MS}$ scheme. The challenge in the latter case lies in the fact that the finite subtraction constants of this scheme are not related to a physical scattering process involving the electromagnetic quark coupling at lowest order. Therefore, ratios of form factors do not naturally occur in the $\overline{\rm MS}$ scheme. The practical prevalence and relative simplicity of the $\overline{\rm MS}$ scheme would, however, make such an organization desirable. It will be shown that the refactorization formalism of [26] leads to the exponentiation of *all* N–independent contributions to the inclusive DY cross section, in both the $\overline{\rm MS}$ and the DIS schemes. As a corollary, one may note that all constant terms in the $\overline{\rm MS}$–scheme non-singlet deep-inelastic structure function F_2 have been organized into an exponential form as well. Furthermore, it is possible to organize the factorization procedure so that real and virtual contributions are individually made finite; one can then disentangle various sources of constants, such as π^2 terms arising from unitarity cuts and similar terms arising from expansions of phase–space related Γ functions.

One might object that there is no kinematic limit in which N–independent terms dominate parametrically, so that an organization of such terms cannot be of much practical use. The view taken here is that whenever all–order information is available one should make use of it, at least to gauge the potential impact of generic higher order corrections on the cross section at hand. One should bear in mind that the pattern of exponentiation, even for N–independent terms, is highly nontrivial, and includes all–order information arising from renormalization group evolution and the requirements of factorization; for example, a considerable fraction of nonabelian effects (i.e. terms not proportional to C_F^2) arising at two loops can be shown to follow from running coupling effects implemented on the (essentially abelian) one–loop result. In the present case one could be bolder and argue that, since all constants have been shown to exponentiate, using the exponentiated expression should provide a better approximation to the exact answer. This is in fact the case for generic values of higher order perturbative coefficients, even for asymptotic series such as those arising in QCD. It cannot, however, be proven for any particular cross section, although it works in practice for the cases that have been tested. At the very least, differences between results for the physical cross section with or without the exponentiation of constant terms can provide nontrivial estimates of errors due to (uncalculated) higher order corrections. Notice in passing that constant terms are not affected by the Landau pole and thus factor out of the inverse Mellin transform needed

to construct the physical cross section.

6.2 The DIS scheme and the Sudakov form factor

Consider the N–th moment of the partonic DY cross section, taken with respect to $z = Q^2/s$, with Q the measured invariant mass and s the partonic invariant mass squared. Mass factorization of this quantity, in the DIS scheme, is performed by simply dividing its dimensionally regularized ($d = 4 - 2\epsilon$ as usual), unsubtracted version by the square of the N–th moment (taken with respect to the partonic Bjorken–x variable) of the non–singlet partonic deep–inelastic structure function F_2

$$\widehat{\omega}_{\rm DIS}(N) = \frac{\omega(N,\epsilon)}{\left[F_2(N,\epsilon)\right]^2} \,. \tag{6.1}$$

While numerator and denominator are each infrared and collinear divergent, their ratio is finite to all perturbative orders [15], so the ϵ dependence of the *l.h.s.* can be neglected. Explicit dependence on the hard scale Q and on the strong coupling $\alpha_s(\mu^2)$ will generally be understood.

The Sudakov form factor naturally arises in $\omega(N,\epsilon)$, before mass factorization, following the reasoning of [26]. One observes that near threshold (*i.e.* at large N) $\omega(N,\epsilon)$ can be refactorized according to

$$\omega(N,\epsilon) = |H_{\rm DY}|^2\, \psi(N,\epsilon)^2\, U(N) + \mathcal{O}(1/N) \,. \tag{6.2}$$

The $\psi(N,\epsilon)$ and $U(N)$ functions contain the N dependence associated with initial state radiation at fixed energy and coherent soft radiation, respectively. They are well–defined as operator matrix elements [26], and are calculable in perturbation theory. Both functions are gauge–dependent, but their product in (6.2) is not; implicitly, the presentation here will be in axial gauge. Using gauge invariance and renormalization group (RG) arguments, one can show that both the parton distribution $\psi(N,\epsilon)$ as well as the eikonal function $U(N)$ obey evolution equations. These can be solved near threshold in an exponential form, up to corrections suppressed by powers of N. The function $|H_{\rm DY}|^2$, collecting all hard–gluon corrections, has no N dependence and may be determined by matching to exact calculations order by order. Divergences are only present in the parton distribution function $\psi(N,\epsilon)$.

To identify the Sudakov form factor, it is useful to separate virtual (V) and real (R) contributions to the resummed ψ and U functions, according to

$$\begin{aligned} \psi(N,\epsilon) &= \mathcal{R}(\epsilon)\, \psi_R(N,\epsilon) \,, \\ U(N) &= U_V(\epsilon)\, U_R(N,\epsilon) \,, \end{aligned} \tag{6.3}$$

where $\mathcal{R}(\epsilon)$ is the real part of the residue of the quark two-point function in an axial gauge. Using the analysis of Section 8 of [26] one can now write

$$\begin{aligned} \omega(N,\epsilon) &= |H_{\rm DY}\, \mathcal{R}(\epsilon) \sqrt{U_V(\epsilon)}|^2\, \psi_R(N,\epsilon)^2\, U_R(N) + \mathcal{O}(1/N) \\ &= |\Gamma(Q^2,\epsilon)|^2\, \psi_R(N,\epsilon)^2\, U_R(N,\epsilon) + \mathcal{O}(1/N) \,. \end{aligned} \tag{6.4}$$

In fact, the residue of the quark propagator coincides with the virtual jet function summarizing virtual collinear contributions to the form factor, while the square root of the virtual eikonal function appearing in the cross section is responsible for the soft enhancements of Γ. The dimensionally regularized time–like Sudakov form factor $\Gamma(Q^2,\epsilon)$ has thus been identified in the refactorized, unsubtracted Drell–Yan cross section. Near threshold, the only remaining contributions to the cross section come from real radiation, and are summarized by the real parts of the ψ and U functions. At this point one can already observe that $\omega_{\rm DY}(N,\epsilon)$ exponentiates up to corrections suppressed by powers of N: the exponentiation of the form factor in dimensional regularization was proven in [100], while the exponentiation of ψ_R and U_R to this accuracy was proven in [26]. Specifically, the real part of the fixed–energy parton density $\psi_R(N,\epsilon)$ can be written as

$$\psi_R(N,\epsilon) = \exp\left\{\int_0^1 dz\ \frac{z^{N-1}}{1-z}\int_z^1 \frac{dy}{1-y}\ \kappa_\psi\left(\overline{\alpha}\left((1-y)^2Q^2\right),\epsilon\right)\right\}. \tag{6.5}$$

Similarly

$$U_R(N,\epsilon) = \exp\left\{-\int_0^1 dz\ \frac{z^{N-1}}{1-z}\, g_U\left(\overline{\alpha}\left((1-z)^2Q^2\right),\epsilon\right)\right\}. \tag{6.6}$$

Note that in writing (6.5) and (6.6) one makes use of the fact that both functions are renormalization–group invariant, since real emission diagrams in this case do not have ultraviolet divergences. For the function ψ_R this is a consequence of the fact that it fixes the energy of the final state, so that transverse momentum is also limited; for the function U_R it is a consequence of the structure of nonabelian exponentiation [26]. The functions κ_ψ and g_U are both finite at one loop in the limit $\epsilon\to 0$: all IR and collinear singularities are generated by the integrations over the scale of the d–dimensional running coupling, which at one loop is given by

$$\overline{\alpha}\left(\frac{\xi^2}{\mu^2},\alpha_s(\mu^2),\epsilon\right) = \alpha_s(\mu^2)\ \left[\left(\frac{\xi^2}{\mu^2}\right)^{2\epsilon} - \frac{1}{\epsilon}\left\{1-\left(\frac{\xi^2}{\mu^2}\right)^{2\epsilon}\right\}\ \frac{b_0}{4\pi}\alpha_s(\mu^2)\right]^{-1}, \tag{6.7}$$

and will often be abbreviated by $\overline{\alpha}(\xi^2)$, as in (6.5) and (6.6).

A similar refactorization can be performed on the deep inelastic structure function F_2. One finds [26]

$$F_2(N,\epsilon) = |H_{\rm DIS}|^2\,\chi(N,\epsilon)\,V(N)\,J(N) + \mathcal{O}(1/N). \tag{6.8}$$

Here the parton distribution $\chi(N,\epsilon)$ has the same collinear singularities as the one adopted for the DY process, but, according to the general strategy of [26], it fixes a different component of the incoming parton momentum, viz. the plus–component, and is computed in a different axial gauge. $V(N)$ summarizes the effects of coherent soft radiation in the DIS process, while $J(N)$ contains the effects of final state collinear radiation emitted by the struck parton. Separating real and virtual contributions as above one finds

$$\begin{aligned} F_2(N,\epsilon) &= |H_{\rm DIS}|^2\,|\mathcal{R}(\epsilon)V_V(\epsilon)|\,\chi_R(N,\epsilon)\,V_R(N,\epsilon)\,J(N) + \mathcal{O}(1/N) \\ &= |H_{\rm DIS}||\Gamma(-Q^2,\epsilon)|\,\chi_R(N,\epsilon)\,\sqrt{V_V(\epsilon)}\,V_R(N,\epsilon)\,J(N) + \mathcal{O}(1/N)\,. \end{aligned} \tag{6.9}$$

To this extent virtual contributions to F_2 have been organized already in [26]. One now sees that *all* virtual contributions can be organized in terms of $\Gamma(-Q^2,\epsilon)$, by observing

that the purely virtual part of the light–cone distribution χ is identical to the purely virtual part of the outgoing jet J. Both consist essentially of the full two–point function for a lightlike fermion. Note that both virtual jets in (6.9) are computed with the same gauge choice. Gathering all virtual parts, one finds then

$$F_2(N,\epsilon) = |\Gamma(-Q^2,\epsilon)|^2\, \chi_R(N,\epsilon)\, V_R(N,\epsilon)\, J_R(N,\epsilon) + \mathcal{O}(1/N)\,. \tag{6.10}$$

Again, exploiting the results of [26, 100] this form of the refactorization is sufficient to prove the exponentiation of the full cross section up to corrections suppressed by powers of N. In fact F_2 now involves, to this accuracy, only the form factor, and a product of real functions which have been shown to exponentiate by using their respective evolution equations.

This result can be further verified in the following way. A comparison of (6.9) and (6.10) implies that $H_{\rm DIS}$ itself acquires an exponential form. In fact, an analysis along the lines of [99] reveals that it may be expressed as

$$H_{\rm DIS}(Q^2) = Z_H(\alpha_s,\epsilon)\, \frac{\Gamma(-Q^2,\epsilon)}{S^{(0)}(\epsilon)\; G_2^{(0)}(Q^2,\epsilon)}\;, \tag{6.11}$$

where $S^{(0)} = S\, Z_S$ and $G_2^{(0)} = G_2 Z_q$ are the unrenormalized, dimensionally regularized virtual soft function and virtual quark jet function appearing in the factorization of the form factor, and where

$$Z_H = Z_S\, Z_q^2 \tag{6.12}$$

is the UV counterterm function for $H_{\rm DIS}$. The Sudakov form factor Γ does not require a separate Z factor to cancel QCD UV divergences, by virtue of the electromagnetic current conservation. Now, each factor in (6.11) has an exponential form. For the virtual soft function this was shown in [38, 39]. The unrenormalized virtual jet function $G_2^{(0)}(Q^2,\epsilon)$ obeys an evolution equation of the same form as the one used for the full form factor [99], which can be explicitly solved in dimensional regularization by the same methods, using as initial condition the fact that all radiative corrections vanish at $Q^2 = 0$. $G_2^{(0)}(Q^2,\epsilon)$ must then exponentiate by itself. Finally, any Z factor arising in multiplicative renormalization may be represented in terms of the associated anomalous dimension $\gamma = (1/2) d(\ln Z)/d\ln\mu$ as

$$Z_i = \exp\left\{\int_0^{Q^2} \frac{d\xi^2}{\xi^2}\gamma_i\left(\overline{\alpha}\left(\frac{\xi^2}{\mu^2},\alpha_s(\mu^2),\epsilon\right)\right)\right\}\;, \tag{6.13}$$

where again UV poles are generated by integration over the scale of the d–dimensional coupling.

Turning to the evaluation of (6.1), one observes that it requires the ratio of (6.4) and the square of either (6.9) or (6.10). In practice, the expression (6.9) is more convenient than (6.10), because the resulting form (6.15) for $\widehat{\omega}_{\rm DIS}(N)$ is a product of finite functions. Had one used instead the result in (6.10), the resulting expression for $\widehat{\omega}_{\rm DIS}(N)$ would have involved cancelling divergences between the real and virtual parts. Using then (6.9), and the additional information that $U_V(\epsilon) = V_V(\epsilon)$, both being given by pure counterterms to the same eikonal vertex, one can write

$$\widehat{\omega}_{\rm DIS}(N) = \frac{1}{|H_{DIS}|^2}\left|\frac{\Gamma(Q^2,\epsilon)}{\Gamma(-Q^2,\epsilon)}\right|^2 \left(\frac{\psi_R(N,\epsilon)}{\chi_R(N,\epsilon)}\right)^2 \frac{U(N)}{V^2(N)}\frac{1}{J^2(N)}\;. \tag{6.14}$$

The exponentiation and RG running of the various factors of (6.14) are described in detail in [26], with the exception of the ratio ψ_R/χ_R, which there was exponentiated according to (6.5), but evaluated only at leading order. Running coupling effects on this ratio are briefly discussed in section 6.4: they generate a contribution at NNL level at two loops, as well as further N–independent terms. Furthermore, one is now in a position to exponentiate also the one–loop contribution to the matching function, $H^{(1)}_{DIS} = -C_F$. Gathering all factors, and formulating the answer according to standard notation [37], the result for the hard partonic Drell–Yan cross section in the DIS scheme takes the form

$$\begin{aligned}\widehat{\omega}_{\rm DIS}(N) &= \left|\frac{\Gamma(Q^2,\epsilon)}{\Gamma(-Q^2,\epsilon)}\right|^2 \exp\Big[F_{DIS}(\alpha_s)\Big] \\ &\times \exp\left[\int_0^1 dz\,\frac{z^{N-1}-1}{1-z}\left\{2\int_{(1-z)Q^2}^{(1-z)^2Q^2}\frac{d\xi^2}{\xi^2}\,A\Big(\alpha_s(\xi^2)\Big)\right.\right. \\ &- \left.\left. 2B\Big(\alpha_s\Big((1-z)Q^2\Big)\Big) + D\Big(\alpha_s\Big((1-z)^2Q^2\Big)\Big)\right\}\right] + \mathcal{O}(1/N)\,. \qquad (6.15)\end{aligned}$$

Equation (6.15) resums all terms in the perturbative expansion which contain enhancements of the form $\alpha_s^n \log^k N$, with $k \le 2n$, provided the perturbative expansions of the functions A, B and D are known to the desired order in the strong coupling. The perturbative coefficients of the functions A, B, D are in fact all known up to two loops [35, 104, 105] Concerning the three-loop coefficient $A^{(3)}$, the n_f–dependent part is known exactly [105, 36], while good numerical estimates exist for the n_f–independent term [106]. For example, expanding the functions involved as

$$f(\alpha_s) \;=\; \sum_{k=1}^{\infty} f^{(k)}\left(\frac{\alpha_s}{\pi}\right)^k\,, \qquad (6.16)$$

one needs

$$\begin{aligned} A^{(1)} &= C_F \quad , & A^{(2)} &= \frac{1}{2}\left[C_A C_F\left(\frac{67}{18}-\zeta(2)\right) - n_f C_F\left(\frac{5}{9}\right)\right] \\ B^{(1)} &= -\frac{3}{4}C_F \quad , & D^{(1)} &= 0\,. \end{aligned} \qquad (6.17)$$

for resummation to next–to–leading logarithmic accuracy.

Equation (6.15) also exponentiates N–independent terms, which have three sources: they come from unitarity cuts, as in the analytic continuation of the form factor; or from phase space integrations, since for example the parton distributions ψ and χ differ slightly in their phase space measure; finally they arise from the Mellin transformation in the exponent, which generates not only logarithms of N, but also contributions proportional to γ_E and to $\zeta(n)$. One can now examine in more detail the first two classes of exponentiated constants.

The absolute value of the ratio of form factors is finite to all orders and exponentiates [100]. To illustrate this, note that the (timelike) Sudakov form factor $\Gamma(Q^2,\epsilon)$ for the electromagnetic coupling of a massless quark of charge e_q is defined via

$$\Gamma_\mu(p_1,p_2;\mu^2,\epsilon) \equiv \langle 0|J_\mu(0)|p_1,p_2\rangle = -{\rm i}e\,e_q\,\overline{v}(p_2)\gamma_\mu u(p_1)\;\Gamma\Big(Q^2,\epsilon\Big)\;, \qquad (6.18)$$

with $Q^2 = (p_1 + p_2)^2$. Based on [107, 108, 109], it was shown [100] that the dimensionally regularized Sudakov form factor may be written as an exponential of integrals over functions only of α_s,

$$\Gamma(Q^2, \epsilon) = \exp\left\{\frac{1}{2}\int_0^{Q^2}\frac{d\xi^2}{\xi^2}\left[K\left(\alpha_s, \epsilon\right) + G\left(\overline{\alpha}\left(\xi^2\right), \epsilon\right) + \frac{1}{2}\int_{\xi^2}^{\mu^2}\frac{d\lambda^2}{\lambda^2}\gamma_K\left(\overline{\alpha}\left(\lambda^2\right)\right)\right]\right\}. \quad (6.19)$$

The function K in (6.19) is defined to consist of counterterms only, while G is finite for $\epsilon \to 0$. Double logarithms of the hard scale Q arise from the double integral over the anomalous dimension $\gamma_K(\alpha_s)$.

Using (6.19) one can derive a particularly simple expression for the absolute value of the ratio appearing in (6.15). One finds

$$\left|\frac{\Gamma(Q^2, \epsilon)}{\Gamma(-Q^2, \epsilon)}\right| = \exp\left\{\left|\frac{\mathrm{i}}{2}\int_0^{\pi}\left[G\left(\overline{\alpha}\left(\mathrm{e}^{\mathrm{i}\theta}Q^2\right), \epsilon\right) - \frac{\mathrm{i}}{2}\int_0^{\theta} d\phi\, \gamma_K\left(\overline{\alpha}\left(\mathrm{e}^{\mathrm{i}\phi}Q^2\right)\right)\right]\right|\right\} . \quad (6.20)$$

Performing the scale integrals, at the two–loop level this yields

$$\begin{aligned}\left|\frac{\Gamma(Q^2, \epsilon)}{\Gamma(-Q^2, \epsilon)}\right|^2 &= 1 + \frac{\alpha_s(Q)}{\pi}\frac{3\zeta(2)\gamma_K^{(1)}}{2} \\ &+ \left(\frac{\alpha_s(Q)}{\pi}\right)^2\left[\frac{9}{8}\zeta^2(2)\left(\gamma_K^{(1)}\right)^2 + \frac{3}{4}\zeta(2)b_0 G^{(1)}(0) + \frac{3}{2}\zeta(2)\gamma_K^{(2)}\right] ,\end{aligned} \quad (6.21)$$

where

$$\begin{aligned}\gamma_K^{(1)} &= 2\, C_F , \\ G^{(1)}(\epsilon) &= C_F\left(\frac{3}{2} - \frac{\epsilon}{2}\left[\zeta(2) - 8\right] + \epsilon^2\left[8 - \frac{3}{4}\zeta(2) - \frac{7}{3}\zeta(3)\right] + \mathcal{O}(\epsilon^3)\right) , \\ \gamma_K^{(2)} &= C_A C_F\left(\frac{67}{18} - \zeta(2)\right) - n_f C_F\left(\frac{5}{9}\right) = 2A^{(2)},\end{aligned} \quad (6.22)$$

while $b_0 = (11C_A - 2n_f)/3$. The anomalous dimension γ_K is the "cusp" anomalous dimension of a Wilson line in the $\overline{\mathrm{MS}}$ renormalization scheme [84, 110, 111].

Equation (6.21) illustrates the potential relevance of exponentiation of N–independent terms: first of all, the two–loop contribution is numerically dominated by one–loop effects, both through exponentiation and the running of the coupling (the first two terms of the two–loop coefficient numerically make up roughly three quarters of the total); furthermore, for this particular ratio, genuine two–loop effects are given only in terms of $\gamma_K^{(2)}$, thus they are UV–dominated and much simpler to calculate than the full form factor.

Finally, the function $F_{DIS}(\alpha_s)$ collects constant terms arising from phase space integrations in the various functions involved in the factorization, as well as from the exponentiation of the matching function H_{DIS}. One finds at one loop

$$F_{DIS}^{(1)} = C_F\left(\frac{1}{2} + \zeta_2\right) , \quad (6.23)$$

while at two loops some terms can be predicted by taking into account the running of the coupling, which yields

$$F_{DIS}^{(2)} = -\frac{3}{16}C_F b_0\left(4 + \zeta(2) - 2\zeta(3)\right) + \delta F_{DIS}^{(2)} . \quad (6.24)$$

These two–loop contributions should not be taken too literally since, as indicated in (6.24), there is at this level an uncalculated contribution $\delta F_{DIS}^{(2)}$ arising from a pure two–loop calculation, which could easily overwhelm the effects which have been included. Further discussion of the impact of these two–loop effects is given in section 6.5.

6.3 Exponentiation in the $\overline{\rm MS}$ scheme

As remarked in the introduction, one should not expect that the constants associated with the Sudakov form factor in the $\overline{\rm MS}$–scheme DY cross section can be organized as in the previous section, by a simple ratio of the timelike to spacelike versions of the same form factor. The reason for this is that the $\overline{\rm MS}$ quark distribution function is not directly related to a physical process involving quark electromagnetic scattering at lowest order. It is nevertheless possible to organize these constants in a closely related manner.

Mass factorization of the DY cross section in the $\overline{\rm MS}$ scheme is straightforward in moment space: one simply divides $\omega(N,\epsilon)$ by $\phi^2_{\overline{\rm MS}}(N,\epsilon)$, the square of the $\overline{\rm MS}$ quark density, defined by

$$\begin{aligned}\phi_{\overline{\rm MS}}(N,\epsilon) &= \exp\left[\int_0^{Q^2}\frac{d\mu^2}{\mu^2}\left\{\int_0^1 dz\,\frac{z^{N-1}-1}{1-z}A\left(\overline{\alpha}\left(\frac{\mu^2}{\mu_F^2},\alpha_s(\mu_F^2),\epsilon\right)\right)\right.\right.\\ &+ \left.\left. B^\delta\left(\overline{\alpha}\left(\frac{\mu^2}{\mu_F^2},\alpha_s(\mu_F^2),\epsilon\right)\right)\right\}\right] + \mathcal{O}(1/N)\,, \end{aligned} \tag{6.25}$$

with A the same function as appearing in (6.15), while B^δ is the virtual part of the non–single quark–quark splitting function. As appropriate for an $\overline{\rm MS}$ parton density, one can easily verify that $\phi_{\overline{\rm MS}}(N,\epsilon)$ in (6.25) is a series of pure counterterms. Q is the factorization scale, which for simplicity throughout this paper is set equal to the DY invariant mass [1]. One can now factor this density into virtual and real parts

$$\phi_{\overline{\rm MS}}(N,\epsilon) = \phi_V(\epsilon)\,\phi_R(N,\epsilon)\,, \tag{6.26}$$

in such a way that in the (finite) ratio

$$\widehat{\omega}_{\overline{\rm MS}}(N) \equiv \frac{\omega(N,\epsilon)}{\phi_{\overline{\rm MS}}(N,\epsilon)^2} = \left(\frac{|\Gamma(Q^2,\epsilon)|^2}{\phi_V(\epsilon)^2}\right)\left(\frac{\psi_R(N,\epsilon)^2\,U_R(N,\epsilon)}{\phi_R(N,\epsilon)^2}\right) + \mathcal{O}(1/N) \tag{6.27}$$

the ratios of virtual functions and of real functions, displayed in the large brackets, are separately finite. To be precise, the factorization in (6.26) is uniquely defined by the following criteria: first, the ratio of virtual functions must be finite; second, factorizing a series of pure counterterms one would like also $\phi_V(\epsilon)$ to consist only of poles. The real part $\phi_R(N,\epsilon)$ is then defined by (6.26). Note that $\phi_V(\epsilon)$ defined in this way is process–dependent, in contrast to $\phi_{\overline{\rm MS}}(N,\epsilon)$; note also that, while $\phi_{\overline{\rm MS}}$ has only simple poles of collinear origin, the real and virtual contributions will have cancelling double poles. The real and virtual contributions to the cross section will now be analyzed separately.

[1] It is straightforward to repeat the analysis below keeping these scales different.

6.3.1 Cancellation of virtual poles

The timelike Sudakov form factor has imaginary parts, which are the source of the largest contributions to the ratio in (6.21), while the $\overline{\rm MS}$ distribution is real. The analysis can thus be simplified by writing

$$\frac{|\Gamma(Q^2,\epsilon)|^2}{\phi_V(\epsilon)^2} = \left|\frac{\Gamma(Q^2,\epsilon)}{\Gamma(-Q^2,\epsilon)}\right|^2 \left(\frac{\Gamma(-Q^2,\epsilon)}{\phi_V(\epsilon)}\right)^2 \ . \tag{6.28}$$

The benefit of this lies in the fact that the first factor on the *r.h.s.* is finite, and already explicitly resummed in (6.21). The second factor, on the other hand, is purely real. Inspired by the explicit expression for the form factor, (6.19), one starts with the ansatz

$$\begin{aligned}\phi_V(Q^2,\epsilon) &= \exp\left\{\frac{1}{2}\int_0^{Q^2}\frac{d\xi^2}{\xi^2}\left[K\left(\alpha_s(\mu^2),\epsilon\right)+\widetilde{G}\left(\overline{\alpha}\left(\frac{\xi^2}{\mu^2},\alpha_s(\mu^2),\epsilon\right)\right)\right.\right.\\ &+ \left.\left.\frac{1}{2}\int_{\xi^2}^{\mu^2}\frac{d\lambda^2}{\lambda^2}\gamma^{(K)}\left(\overline{\alpha}\left(\frac{\lambda^2}{\mu^2},\alpha_s(\mu^2),\epsilon\right)\right)\right]\right\}\ ,\end{aligned} \tag{6.29}$$

which has the same structure as the Sudakov form factor in (6.19), with the difference that $\widetilde{G}$ has no order ϵ terms.

One now has to show, to all orders in the strong coupling, that the perturbative coefficients of the function $\widetilde{G}$ can be chosen so as to render (6.28) finite. At the end of this section an explicit construction will be provided as well. Since the first ratio on the *r.h.s.* of (6.28) is finite, it is sufficient to prove the cancellation of poles for the second ratio,

$$\frac{|\Gamma(-Q^2,\epsilon)|^2}{\left(\phi_V(\epsilon)\right)^2}\ . \tag{6.30}$$

First of all, one observes that all divergences arising from the terms K and γ_K manifestly cancel between $|\Gamma(-Q^2,\epsilon)|^2$ and $\left(\phi_V(Q^2,\epsilon)\right)^2$, since they result from the limits of integration independent of the particular energy scale considered. Hence divergences could only be generated by the G terms. Now express

$$G\left(-1,\alpha_s,\epsilon\right) = \sum_{m=1}^{\infty}\sum_{n=0}^{\infty} G_m^{(n)}\epsilon^n\left(\frac{\alpha_s}{\pi}\right)^m \tag{6.31}$$

and note that the integration over the energy scale can be rewritten as one over the running coupling making use of

$$\frac{d\mu^2}{\mu^2} = 2\frac{d\bar{\alpha}_s}{\beta\left(\bar{\alpha}_s\right)} = -\frac{1}{\epsilon}\frac{d\alpha_s}{\alpha_s}\frac{1}{1+\frac{1}{4\epsilon}\sum\limits_{m=1}^{\infty} b_{m-1}\left(\frac{\alpha_s}{\pi}\right)^m}\ . \tag{6.32}$$

Considering the integrands of both expressions and keeping in mind the overall factor of $1/\epsilon$ it remains to be shown that $\widetilde{G}$ can be chosen so that

$$\frac{\sum\limits_{m=1}^{p}\widetilde{G}_m\left(\frac{\alpha_s}{\pi}\right)^m}{1+\frac{1}{4\epsilon}\sum\limits_{m=1}^{p-1} b_{m-1}\left(\frac{\alpha_s}{\pi}\right)^m} - \frac{\sum\limits_{m=1}^{p}\sum\limits_{l=0}^{\infty}G_m^l\epsilon^l\left(\frac{\alpha_s}{\pi}\right)^m}{1+\frac{1}{4\epsilon}\sum\limits_{m=1}^{p-1} b_{m-1}\left(\frac{\alpha_s}{\pi}\right)^m} = 0+\mathcal{O}\left(\epsilon\right) \tag{6.33}$$

for any p. The proof proceeds by induction. Assume that it holds for some fixed order $p = k$ in perturbation theory, and show that $\widetilde{G}_{k+1}$ may be chosen such that (6.33) holds also for order $p = k + 1$. Now examine (6.33) for $p = k + 1$. One can write

$$\sum_{m=1}^{k+1} \widetilde{G}_n \Big(\frac{\alpha_s}{\pi}\Big)^m = \sum_{m=1}^{k} \widetilde{G}_m \Big(\frac{\alpha_s}{\pi}\Big)^m + \widetilde{G}_{k+1} \Big(\frac{\alpha_s}{\pi}\Big)^{k+1} . \tag{6.34}$$

The following identity will be useful

$$\begin{aligned} \frac{1}{1 + \frac{1}{4\epsilon} \sum\limits_{m=1}^{k} b_{m-1} \Big(\frac{\alpha_s}{\pi}\Big)^m} &= \frac{1}{1 + \frac{1}{4\epsilon} \sum\limits_{m=1}^{k-1} b_{m-1} \Big(\frac{\alpha_s}{\pi}\Big)^m} \\ &- \frac{\frac{1}{4\epsilon} b_{k-1} \Big(\frac{\alpha_s}{\pi}\Big)^k}{\left(1 + \frac{1}{4\epsilon} \sum\limits_{m=1}^{k-1} b_{m-1} \Big(\frac{\alpha_s}{\pi}\Big)^m\right) \left(1 + \frac{1}{4\epsilon} \sum\limits_{m=1}^{k} b_{m-1} \Big(\frac{\alpha_s}{\pi}\Big)^m\right)} . \end{aligned} \tag{6.35}$$

Substitution of these two relations into the first term of (6.33) leads to (neglecting terms that contain powers of α_s higher than $k + 1$)

$$\begin{aligned} &\frac{\sum\limits_{m=1}^{k} \widetilde{G}_m \Big(\frac{\alpha_s}{\pi}\Big)^m}{1 + \frac{1}{4\epsilon} \sum\limits_{m=1}^{k-1} b_{m-1} \Big(\frac{\alpha_s}{\pi}\Big)^m} + \frac{\widetilde{G}_{k+1} \Big(\frac{\alpha_s}{\pi}\Big)^{k+1}}{1 + \frac{1}{4\epsilon} \sum\limits_{m=1}^{k-1} b_{m-1} \Big(\frac{\alpha_s}{\pi}\Big)^m} \\ &- \frac{\frac{1}{4\epsilon} b_{k-1} \Big(\frac{\alpha_s}{\pi}\Big)^k \sum\limits_{m=1}^{k} \widetilde{G}_m \Big(\frac{\alpha_s}{\pi}\Big)^m}{\left(1 + \frac{1}{4\epsilon} \sum\limits_{m=1}^{k-1} b_{m-1} \Big(\frac{\alpha_s}{\pi}\Big)^m\right) \left(1 + \frac{1}{4\epsilon} \sum\limits_{m=1}^{k} b_{m-1} \Big(\frac{\alpha_s}{\pi}\Big)^m\right)} \end{aligned} \tag{6.36}$$

and, similarly, the second term of (6.33) turns into

$$\begin{aligned} &\frac{\sum\limits_{m=1}^{k} \sum\limits_{l=0}^{\infty} G_m^l \epsilon^l \Big(\frac{\alpha_s}{\pi}\Big)^m}{1 + \frac{1}{4\epsilon} \sum\limits_{m=1}^{k-1} b_{m-1} \Big(\frac{\alpha_s}{\pi}\Big)^m} + \frac{\sum\limits_{l=0}^{\infty} G_{k+1}^l \epsilon^l \Big(\frac{\alpha_s}{\pi}\Big)^{k+1}}{1 + \frac{1}{4\epsilon} \sum\limits_{m=1}^{k-1} b_{m-1} \Big(\frac{\alpha_s}{\pi}\Big)^m} \\ &- \frac{\frac{1}{4\epsilon} b_{k-1} \Big(\frac{\alpha_s}{\pi}\Big)^k \sum\limits_{m=1}^{k} \sum\limits_{l=0}^{\infty} G_m^l \epsilon^l \Big(\frac{\alpha_s}{\pi}\Big)^m}{\left(1 + \frac{1}{4\epsilon} \sum\limits_{m=1}^{k-1} b_{m-1} \Big(\frac{\alpha_s}{\pi}\Big)^m\right) \left(1 + \frac{1}{4\epsilon} \sum\limits_{m=1}^{k} b_{m-1} \Big(\frac{\alpha_s}{\pi}\Big)^m\right)} . \end{aligned} \tag{6.37}$$

One must now show that terms at order $k + 1$ do not upset the cancellations between (6.36) and (6.37) to lower orders than $k + 1$, and that the cancellation in (6.33) works also at order $k + 1$ by choosing $\widetilde{G}_{k+1}$ appropriately. As a corollary, an explicit expression for $\widetilde{G}_{k+1}$ can be derived that effects this cancellation.

The cancellation to orders lower than $k+1$ still works by invoking the initial hypothesis, since all lower order α_s-dependence is contained entirely in the first terms of (6.36) and (6.37), respectively.

One now considers all $(\alpha_s/\pi)^{k+1}$ terms in the expressions. Note that all terms of (6.36) as well as (6.37) contribute at this order. One first shows that the contribution in (6.36) from

$$\frac{\sum\limits_{m=1}^{k}\widetilde{G}_m\left(\frac{\alpha_s}{\pi}\right)^m}{1+\frac{1}{4\epsilon}\sum\limits_{m=1}^{k-1}b_{m-1}\left(\frac{\alpha_s}{\pi}\right)^m} \tag{6.38}$$

together with its tildeless counterpart from (6.37), namely

$$\frac{\sum\limits_{m=1}^{k}\sum\limits_{l=0}^{\infty}G_m^l\epsilon^l\left(\frac{\alpha_s}{\pi}\right)^m}{1+\frac{1}{4\epsilon}\sum\limits_{m=1}^{k-1}b_{m-1}\left(\frac{\alpha_s}{\pi}\right)^m} \tag{6.39}$$

is at most a constant, but contains no poles in ϵ. Assume there was at order $k+1$ some t-fold pole left uncancelled in the difference. Now multiply this difference by the denominator common to (6.38) and (6.39) to find

$$\begin{aligned}\sum_{m=1}^{k}\widetilde{G}_m\left(\frac{\alpha_s}{\pi}\right)^m &- \sum_{m=1}^{k}\sum_{l=0}^{\infty}G_m^l\epsilon^l\left(\frac{\alpha_s}{\pi}\right)^m \\ &= \left(\sum_{m=1}^{k}\sum_{l=1}^{\infty}c_m^l\epsilon^l\left(\frac{\alpha_s}{\pi}\right)^m + c'\left(\frac{\alpha_s}{\pi}\right)^{k+1}\epsilon^t\right)\left(1-\frac{1}{4\epsilon}\sum_{m=1}^{k-1}b_{m-1}\left(\frac{\alpha_s}{\pi}\right)^m\right)\end{aligned} \tag{6.40}$$

where the values of the coefficients c_m^l are irrelevant and the integer t must be shown to satisfy $t \geq 0$. Note that the sums over powers of ϵ start at different initial values. Now clearly, the *l.h.s.* of this equality contains neither poles in ϵ nor powers of α_s higher than $k+1$. Consequently, such contributions must cancel on the *r.h.s.* However, multiplying out the sums generates no terms to cancel the $c'\left(\alpha_s/\pi\right)^{k+1}\epsilon^t$ for $t \leq -1$, hence one must have $t \geq 0$.

At order $k+1$ one thus obtains no powers of ϵ lower than zero from the difference of (6.38) and (6.39). As a consequence of this all poles in the second and third terms of (6.36) and (6.37), respectively, must cancel among themselves, as is easily checked since $\widetilde{G}_1 = G_1^{(0)}$. So only the constant terms have to be cancelled by choosing $\widetilde{G}_{k+1}$ appropriately. To find explicit expressions one has to consider the coefficient of $(\alpha_s/\pi)^{k+1}$, ϵ^0 in (6.39). It must be equal to $\widetilde{G}_{k+1}+G_{k+1}^{(0)}+1/4b_{k-1}G_1^{(1)}$. Alternatively, one can compute the $(\alpha_s/\pi)^{k+1}$, ϵ^0 coefficient of

$$\frac{\sum\limits_{m=1}^{k+1}\sum\limits_{l=0}^{\infty}G_m^l\epsilon^l\left(\frac{\alpha_s}{\pi}\right)^m}{1+\frac{1}{4\epsilon}\sum\limits_{m=1}^{k}b_{m-1}\left(\frac{\alpha_s}{\pi}\right)^m}\,, \tag{6.41}$$

which is exactly $\widetilde{G}_{k+1}$. It is given explicitly by

$$\widetilde{G}_{k+1} = G_{k+1}^{(0)} - \frac{b_0}{4}G_k^{(1)} - \frac{b_1}{4}G_{k-1}^{(1)} + \frac{b_0^2}{16}G_{k-1}^{(2)} - \frac{b_2}{4}G_{k-2}^{(1)} + \frac{b_0b_1}{8}G_{k-2}^{(2)} - \frac{b_0^3}{64}G_{k-2}^{(3)} + \ldots \tag{6.42}$$

6.3.2 Real emission contributions

The complete expression for the $\overline{\rm MS}$–scheme DY cross section in the present framework is given by

$$\widehat{\omega}_{\overline{\rm MS}}(N) = \left|\frac{\Gamma(Q^2,\epsilon)}{\Gamma(-Q^2,\epsilon)}\right|^2 \cdot \left(\frac{\Gamma(-Q^2,\epsilon)}{\phi_V(\epsilon)}\right)^2 \left[U_R(N,\epsilon)\left(\frac{\psi_R(N,\epsilon)}{\phi_R(N,\epsilon)}\right)^2\right] \ , \tag{6.43}$$

where the factor in square brackets arises from real gluon emission. Each function appearing in the real emission contribution exponentiates: ψ_R and U_R according to (6.5) and (6.6), respectively, while ϕ_R is defined as the ratio of (6.25) to (6.29). Renormalization group arguments can be applied to each function, in $d = 4-2\epsilon$ dimensions, as described in section 6.4. It is interesting to notice that running the coupling in d dimensions generates poles at two loops in the ratio $U_R\psi_R/\phi_R$, although the input at one loop is finite. The ratio must however be finite to all orders, as a consequence of the factorization theorem, together with the finiteness of the virtual contributions demonstrated above. This poses constraints on the two–loop coefficients of the functions involved, as described in more detail in section 6.5, tying together real and virtual contributions to the cross section.

Collecting and organizing the exponential expressions of the real emission functions, one can cast (6.43) in the standard form

$$\begin{aligned}\widehat{\omega}_{\overline{\rm MS}}(N) &= \left|\frac{\Gamma(Q^2,\epsilon)}{\Gamma(-Q^2,\epsilon)}\right|^2 \cdot \left(\frac{\Gamma(-Q^2,\epsilon)}{\phi_V(Q^2,\epsilon)}\right)^2 \cdot \exp\left[F_{\overline{\rm MS}}(\alpha_s)\right] \\ &\times \exp\left[\int_0^1 dz\,\frac{z^{N-1}-1}{1-z}\left\{2\int_{Q^2}^{(1-z)^2Q^2}\frac{d\mu^2}{\mu^2}\,A\left(\alpha_s(\mu^2)\right)\right.\right. \\ &+ \left.\left. D\left(\alpha_s\left((1-z)^2Q^2\right)\right)\right\}\right] + \mathcal{O}(1/N)\ . \end{aligned}\tag{6.44}$$

A one loop calculation, with the inclusion of running coupling effects, yields

$$\begin{aligned}\log\left(\frac{\Gamma(-Q^2,\epsilon)}{\phi_V(Q^2,\epsilon)}\right) &= \frac{\alpha_s}{\pi}C_F\left(\frac{\zeta(2)}{4}-2\right)+\left(\frac{\alpha_s}{\pi}\right)^2\left[C_F b_0\left(1-\frac{3}{32}\zeta(2)-\frac{7}{24}\zeta(3)\right)+\delta R^{(2)}\right]\ , \\ F_{\overline{\rm MS}}(\alpha_s) &= \frac{\alpha_s}{\pi}C_F\left(-\frac{3}{2}\zeta(2)\right)+\left(\frac{\alpha_s}{\pi}\right)^2\left[-\frac{1}{4}b_0 C_F\left(1-\frac{3}{8}\zeta(2)-\frac{7}{4}\zeta(3)\right)+\delta F^{(2)}_{\overline{\rm MS}}\right]\ , \end{aligned}\tag{6.45}$$

where $\delta R^{(2)}$ and $\delta F^{(2)}_{\overline{\rm MS}}$ are genuine two–loop contributions unrelated to running coupling effects. Note that the function D in (6.44) is the same as in (6.15): a non–trivial statement, due to the fact that such a function, summarizing wide angle soft radiation, can be taken to vanish in the threshold–resummed deep–inelastic structure function [105, 112, 113, 114].

6.4 Renormalization group techniques

Before the discussion of the relevance of the exponentiation of constants in the two schemes to be presented in section 6.5, this section briefly discusses the application of renormalization group techniques to unconventional parton distributions such as the functions

$\psi(N,\epsilon)$ and $\chi(N,\epsilon)$ described in the previous sections. It will focus specifically on the contributions involving real gluon emission. The techniques of [26] lead to an expression of the form

$$\psi_R(N,\epsilon) = \exp\left\{\int_0^1 dz\ \frac{z^{N-1}}{1-z}\int_z^1 \frac{dy}{1-y}\ \kappa_\psi\left(\frac{(1-y)Q}{\mu},\alpha_s(\mu^2),\epsilon\right)\right\} + \mathcal{O}\left(1/N\right)\ , \quad (6.46)$$

and similarly for χ. The functions ψ_R and χ_R are both renormalization group invariant (*i.e.* their respective anomalous dimensions vanish) to this accuracy, for slightly different reasons: ψ_R cannot have overall UV divergences because its phase space is restricted to fixed total energy emitted in the final state. This automatically restrict also transverse momentum, so the phase space integration is UV finite. χ_R, on the other hand, has a phase space restricted to fixed total light–cone momentum fraction, so that in principle it may have UV divergences arising from transverse momentum integration. These divergences are in fact present, however it can be shown that, at least at one loop and in the chosen axial gauge, these divergences are suppressed by powers of N. Note that this is not in contradiction with the fact that the divergent terms for any quark distribution must be proportional to the Altarelli–Parisi kernel. It simply means that the corresponding divergences are of IR–collinear origin for the distributions at hand.

The consequence of this statement for the functions κ_ψ and κ_χ is that

$$\left(\mu\frac{\partial}{\partial\mu} + \beta\left(\epsilon,\alpha_s\right)\frac{\partial}{\partial\alpha_s}\right)\kappa_\psi\left(\frac{(1-y)Q}{\mu},\alpha_s(\mu^2),\epsilon\right) = 0\ , \quad (6.47)$$

where $\beta\left(\epsilon,\alpha_s\right)$ is the β function in $d = 4-2\epsilon$. An identical equation is obeyed by κ_χ. Such equations can be solved perturbatively to determine the dependence of the distributions on the momentum scale. Consider again for example κ_ψ, and let $\xi \equiv (1-y)Q/\mu$. Expanding

$$\kappa_\psi\left(\xi,\alpha_s,\epsilon\right) = \sum_{n=1}^{\infty}\left(\frac{\alpha_s}{\pi}\right)\kappa_\psi^{(n)}\left(\xi,\epsilon\right)\ , \quad (6.48)$$

one easily finds that at the two loop level the coefficients must be of the form

$$\begin{aligned}\kappa_\psi^{(1)}\left(\xi,\epsilon\right) &= \kappa_{\psi,0}^{(1)}\left(\epsilon\right)\xi^{-2\epsilon}\ ,\\ \kappa_\psi^{(2)}\left(\xi,\epsilon\right) &= \kappa_{\psi,0}^{(2)}\left(\epsilon\right)\xi^{-4\epsilon} + \frac{b_0}{4\epsilon}\kappa_{\psi,0}^{(1)}\left(\epsilon\right)\xi^{-2\epsilon}\left(\xi^{-2\epsilon}-1\right)\ .\end{aligned} \quad (6.49)$$

explicit evaluation at one loop [26] yields

$$\begin{aligned}\kappa_{\psi,0}^{(1)}\left(\epsilon\right) &= 2C_F\left(4\pi\right)^\epsilon\frac{\Gamma(2-\epsilon)}{\Gamma(2-2\epsilon)}\ ,\\ \kappa_{\chi,0}^{(1)}\left(\epsilon\right) &= 2C_F\left(4\pi\right)^\epsilon\Gamma(2+\epsilon)\cos\left(\pi\epsilon\right)\ .\end{aligned} \quad (6.50)$$

As observed in section 6.2, the finiteness of the ratio ψ_R/χ_R, which is a consequence of factorization, requires that $\kappa_{\psi,0}^{(1)}(\epsilon)-\kappa_{\chi,0}^{(1)}(\epsilon) = \mathcal{O}(\epsilon^2)$, since the double integration in (6.46) generates a double pole. In fact, upon redefining μ according to the $\overline{\rm MS}$ prescription to absorb factors of $\log(4\pi)$ and γ_E,

$$\kappa_{\psi,0}^{(1)}\left(\epsilon\right) - \kappa_{\chi,0}^{(1)}\left(\epsilon\right) = 2C_F\epsilon^2\left[2+\zeta(2)+\epsilon\left(4+\zeta(2)-2\zeta(3)\right)+\mathcal{O}(\epsilon^2)\right]\ . \quad (6.51)$$

One can go slightly further and observe that the finiteness of the ratio ψ_R/χ_R also constrains the form of the pure two–loop contribution to κ_ψ and κ_χ, given by the functions $\kappa^{(2)}_{\psi,0}(\epsilon)$ and $\kappa^{(2)}_{\chi,0}(\epsilon)$. Specifically, inserting (6.48) and (6.49) into (6.46), and doing the same for χ_R, one finds that the ratio ψ_R/χ_R will develop a simple pole in ϵ at two loops, unless

$$\kappa^{(2)}_{\psi,0}(\epsilon) - \kappa^{(2)}_{\chi,0}(\epsilon) = \frac{3}{2} C_F b_0 \epsilon \left(2 + \zeta(2)\right) + \epsilon^2 \delta\kappa^{(2)}_2 + \mathcal{O}\left(\epsilon^3\right) \ , \tag{6.52}$$

in analogy with (6.51), with $\delta\kappa^{(2)}_2$ a constant arising at two loops to be used below. This constraint also fixes the coefficient of a contribution to the ratio proportional to $\log N$ at two loops, *i.e.* at NNL level. To be precise one finds

$$\begin{aligned}\left(\frac{\psi_R(N,\epsilon)}{\chi_R(N,\epsilon)}\right)^2 \ = \ & \exp\left[\frac{\alpha_s}{\pi} C_F \left(2 + \zeta(2)\right) + \left(\frac{\alpha_s}{\pi}\right)^2 \left(\frac{1}{8}\delta\kappa^{(2)}_2 + \frac{1}{2} C_F b_0 \left(2 + \zeta(2)\right)\left(\log N + \gamma_E\right)\right.\right. \\ & \left.\left. - \ \frac{3}{16} C_F b_0 \left(4 + \zeta(2) - 2\zeta(3)\right)\right) + \mathcal{O}\left(\epsilon, \frac{1}{N}, \alpha_s^3\right)\right] \ . \end{aligned} \tag{6.53}$$

Once again, the contributions arising at two loops should be taken with a grain of salt when constructing the full cross section. It is true in fact that in this way the leading logarithmic contribution to this particular ratio has been determined. However, in the full cross section there are competing $\log N$ terms arising at two loops from other functions, and in fact in the present case the logarithmic term in (6.53) goes in the wrong direction to 'predict' NNL logarithms at two loops, as to be discussed in section 6.5. Similarly, there is no guarantee that the uncalculated constant $\delta\kappa^{(2)}_2$ will not overwhelm the running coupling effects explicitly displayed in (6.53).

6.5 Two-loop analysis

It is clear that the results derived on the exponentiation of N–independent terms do not have the predictive strength of the standard resummation of threshold logarithms. In that case, in fact, the pattern of exponentiation is highly nontrivial, and the perturbative coefficients of entire classes of logarithms can be exactly predicted to all perturbative orders performing just a low order calculation. In the present case, even though constant terms exponentiate, the determination of the exact value of the N–independent contribution at, say, g loops, always requires a g–loop calculation, albeit in some cases a simplified one.

It remains true, however, that exponentiation and running coupling effects generate contributions to all orders which originate from low–order calculations. These contributions are an easily computable subset of higher order corrections, and it is reasonable to use them to estimate the full impact of higher orders. Specifically, given a g–loop calculation of one of the cross sections discussed here, one can extract the value of the various functions appearing in the exponent to that order, and then use exponentiation and RG running to estimate the $(g+1)$–loop result. Given the existing results at two loops [115, 116], one could construct an estimate of the three–loop partonic cross section. Before embarking on such a calculation, it is however advisable to test the case $g = 1$, *i.e.* to use the two–loop results to verify the reliability of the method, by comparing the exact results with the estimate obtained by exponentiating the one–loop calculation and letting

the couplings run. To this end, one can expand the partonic cross section in scheme s, $\widehat{\omega}_s(N)$ as

$$\widehat{\omega}_s(N) = \sum_{p=0}^{\infty} \omega_s^{(p)}(N) \left(\frac{\alpha_s}{\pi}\right)^p \ . \tag{6.54}$$

Next, one can identify the coefficients of different powers of $\log N$, by writing

$$\omega_s^{(p)}(N) = \sum_{i=0}^{2p} \omega_{s,i}^{(p)} \left(\log N + \gamma_E\right)^i \ . \tag{6.55}$$

So far the exact cross sections have been dealt with. Let now $\widetilde{\omega}_{s,i}^{(p)}$ be the estimate for $\omega_{s,i}^{(p)}$ obtained by evaluating the exponent exactly at $p-1$ loops, adding running coupling effects, and expanding the result to order p. One can define the deviation

$$\Delta\omega_{s,i}^{(p)} \equiv \frac{\omega_{s,i}^{(p)} - \widetilde{\omega}_{s,i}^{(p)}}{\omega_{s,i}^{(p)}} \ . \tag{6.56}$$

In computing estimates for the DIS scheme, one can employ (6.15), with the one–loop results taken from (6.17), (6.21) and (6.23). Furthermore, since running coupling effects are to be taken into account, terms proportional to b_0 in (6.24) and (6.53) will be included. As far as the $\overline{\rm MS}$ scheme is concerned, (6.44) will be used together with (6.45), with all purely two–loop contributions defined to vanish. Exact results are taken from [115, 116], focusing on "soft and virtual" contributions (all other contributions are suppressed by powers of N at large N. To obtain numerical results one also needs to specify $SU(3)$ and set $n_f = 5$. The results for the deviations $\Delta\omega_{s,i}^{(2)}$ in the two schemes are given in Table 6.1. To gain a little further insight, the contributions proportional to the possible combinations of group invariants arising at two loops (*i.e.* C_F^2, $C_A C_F$ and $n_f C_F$) can be given separately. Table 6.2 displays results for the powers of $\log N$ which do not lead to exact agreement (*i.e.* $i = 0, 1, 2$). Here the coefficients are given separately for $\omega_{s,i}^{(2)}$ and $\widetilde{\omega}_{s,i}^{(2)}$ for each scheme, since some of the exact coefficients vanish so that the corresponding deviations as given in (6.56) are ill–defined.

Several remarks are in order. From Table 6.1 one observes that, as expected, leading and next–to–leading logs are exactly predicted by one–loop results and running coupling effects. Similarly, also as expected, NNL logarithms have a small discrepancy which is entirely traceable to the two–loop cusp anomalous dimension $\gamma_K^{(2)}$. At the level of N–independent terms ($i = 0$), the agreement is quite reasonable, and in fact rather satisfactory in the DIS scheme, where exponentiation accounts for three quarters of the exact answer.

Single results for the logarithms, on the other hand, are much less satisfactory, displaying a discrepancy larger than 100% in both schemes. The reasons for this discrepancy

i	0	1	2	3	4
DIS	0.26	1.17	0.13	0	0
$\overline{\rm MS}$	- 0.69	1.79	0.33	0	0

Table 6.1: The deviations $\Delta\omega_{s,i}^{(2)}$, as defined in the text, for the DIS and $\overline{\rm MS}$ schemes.

	DIS		$\overline{\text{MS}}$	
	estimate	exact	estimate	exact
coefficients of C_F^2				
i = 0	38.06	39.03	3.33	1.79
i = 1	- 13.09	- 14.41	0	0
i = 2	9.85	9.85	5.16	5.16
coefficients of $C_A C_F$				
i = 0	5.63	18.12	13.12	6.82
i = 1	9.83	- 0.25	1.51	- 0.47
i = 2	- 0.69	0.35	0	2.08
coefficients of $n_f C_F$				
i = 0	- 1.02	- 4.40	- 2.38	- 0.80
i = 1	- 1.79	0.35	- 0.27	- 0.52
i = 2	0.12	- 0.15	0	- 0.56

Table 6.2: Comparison between estimates from exponentiation and exact results at two loops, presented separately for different colour structures, both in the DIS and $\overline{\text{MS}}$ schemes.

are slightly different in the two schemes, but they highlight the same generic problem. In the DIS scheme, as discussed in section 6.4, running coupling effects in the ratio of parton distributions ψ/χ generate a single log term with the wrong sign with respect to the exact result. This term must then be compensated by contributions which could be called 'genuine two–loop', which as a result display a rough proportionality to b_0.

This phenomenon could be described as an 'excess of factorization', in the following sense: to achieve the accuracy and generality of (6.15) it is necessary to introduce several functions, depending on different scales. Not all of these dependencies, however, are physical, and there may be (in fact there are) large cancellations in the scale dependence between different functions. This fact has been observed in the past [117, 114]. As a consequence, approximate coefficients dominated by running coupling effects, but not completely determined, may turn out to be quite inaccurate.

In the $\overline{\text{MS}}$ scheme, the same kind of cancellation is displayed in a different way: there, as described in more detail below, one may use the constraint imposed by the finiteness of the real emission contributions to reexpress the single log coefficient in terms of purely virtual functions. In the process, the weight of running coupling effects changes considerably. Again, this indicates that computed running coupling effects may easily be compensated by unevaluated two–loop contributions.

Finally, observe in Table 6.2 that abelian (C_F^2) contributions exponentiate with impressive accuracy, particularly in the DIS scheme. The slight superiority of the DIS scheme in this regard appears to be a fairly generic feature in Tables 6.1 and 6.2, perhaps to be ascribed to the more direct physical interpretation of the subtractions, as compared to the $\overline{\text{MS}}$ scheme. On the other hand, if one departs from the strict limitation to one loop terms plus running coupling effects and incorporates also two loop information in the form of $\gamma_K^{(2)}$ as well as in the Sudakov form factor $\Gamma(Q^2, \epsilon)$ (cf. (6.19)) and consequently in $G_1^{(2)}$, the picture changes slightly, as can be seen from Table 6.3. The zero entries in the DIS

	DIS		$\overline{\text{MS}}$	
	estimate	exact	estimate	exact
coefficients of $n_f C_F$				
const	0	-4.2	25.2	21.2
ζ_2	-25.3	-37.8	-20.2	-12.4
ζ_3	0	5.3	0.44	8
coefficients of $C_A C_F$				
c	0	23.9	-157.9	-127.9
ζ_2	155.3	233.1	117.9	65.8
ζ_2^2	-24	-30.8	-6.4	-2.4
ζ_3	0	-65.3	69.6	28
coefficients of C_F^2				
c	34	0	127.8	127.8
ζ_2	14	-3	-70	-70
ζ_2^2	124.8	109.6	1.6	1.6
ζ_3	48	120	-60	-60

Table 6.3: Comparison of resummation estimates with exact results for the order α_s^2 constant contributions, presented separately for different colour structures, both in the DIS and $\overline{\text{MS}}$ schemes, using two loop on $\Gamma(Q^2, \epsilon)$ and in the form of $\gamma_K^{(2)}$.

scheme estimates in Table 6.3 can be traced directly to the structure of the constants in (6.15), and in particular (6.21). In the $\overline{\text{MS}}$ scheme the ratio (6.30) does generate entries for these cases. However, these results will not be discussed any further.

The methods of exponentiation outlined here may be used not only for numerical estimates, but also to obtain, or test, analytical results. Specifically, since all functions employed have precise diagrammatic definitions, the computation of certain coefficients at two loops may be simplified using this approach, as compared to a full calculation of the cross section. Further, the factorization into separately finite real and virtual contributions leads to constraints connecting different coefficients, so that different two–loop results can be nontrivially connected. To give an example, consider (6.43). There, the finiteness of the ratio $U_R \psi_R / \phi_R$ at two loops imposes constraints tying together real and virtual contributions to the cross section (recall that ϕ_R is defined as $\phi_{\overline{\text{MS}}}/\phi_V$). Using the methods outlined in section 6.4 and imposing the cancellation of double poles in the ratio of real functions, one may verify that the two–loop coefficient of $\log^2 N$ in $\widehat{\omega}_{\overline{\text{MS}}}(N)$ must equal the two–loop cusp anomalous dimension $\gamma_K^{(2)}$, as is well known. Further, imposing the cancellation of single poles in the same ratio, one finds that the value of the function D at two loops is completely determined by purely virtual diagrams. One finds

$$D_2 = \frac{3}{4}\zeta_2 b_0 C_F + 4B_2^\delta - 2\widetilde{G}_2 \ , \tag{6.57}$$

where B_2^δ, the two–loop virtual part of the non–singlet quark–quark splitting function is given by [118, 119]

$$B_2^\delta = \frac{3}{2}C_F^2\left(\frac{1}{16} - \frac{1}{2}\zeta_2 + \zeta_3\right) + \frac{C_A C_F}{4}\left(\frac{17}{24} + \frac{11}{3}\zeta_2 - 3\zeta_3\right) - \frac{n_f C_F}{6}\left(\frac{1}{8} + \zeta_2\right) \ , \tag{6.58}$$

while the second order contribution to the function $\widetilde{G}$ can be determined via (6.42) and (6.19), by matching the resummed expression for $\Gamma(Q^2,\epsilon)$ to the explicit results for the dimensionally regularized one– and two–loop Sudakov form factors, as given for example in [101, 120, 121]. One obtains

$$\begin{aligned}
\widetilde{G}_2 &= G_2^{(0)} - \frac{b_0}{4} G_1^{(1)} \\
G_2^{(0)} &= 3C_F^2 \left(\frac{1}{16} - \frac{1}{2}\zeta_2 + \zeta_3\right) - \frac{C_A C_F}{4}\left(13 - \frac{11}{3}\zeta_2 - \frac{2545}{108}\zeta_3\right) - \frac{n_f C_F}{6}\left(\frac{209}{36} + \zeta_2\right) \\
G_1^{(1)} &= C_F\left(4 - \frac{1}{2}\zeta_2\right) \ . \qquad (6.59)
\end{aligned}$$

The coefficient D_2, obtained earlier [35, 104] through matching to the two-loop cross sections [115, 116], has thus been rederived by using only information from purely virtual contributions.

6.6 Conclusions

It has been shown how to organize *all* constants in the N–th moment of the Drell-Yan cross section in the DIS and $\overline{\rm MS}$ schemes into exponential forms. The $\overline{\rm MS}$–scheme result presented has the special feature that real and virtual contributions are separately finite. This organization rests crucially upon the refactorization properties of the unsubtracted Drell–Yan cross section and, for the DIS scheme, of the non–singlet deep–inelastic structure function near threshold [26]. For the $\overline{\rm MS}$ scheme the organization involves the construction of an exponential series of pure counterterms that cancels all divergences in the spacelike Sudakov form factor. This cancellation has been proven to all orders. It should be emphasized that the arguments imply exponentiation to the same degree of accuracy for the $\overline{\rm MS}$–scheme DIS cross section $\widehat{F}_2(N)$, although a detailed evaluation has not been given in that case.

Although exponentiation of N–independent terms does not have the same degree of predictive power as the resummation of threshold logarithms, it can be used with some degree of confidence to gauge the impact of higher order corrections to fixed order cross sections. N–independent contributions at two loops are reasonably well approximated by the exponentiation of one–loop results. The refactorization approach also leads to nontrivial connections between real and virtual contributions to the cross section, which can be used to test or in some cases simplify finite order calculations. On the negative side, one cannot in general trust running coupling effects to give by themselves a good approximation of two–loop results, unless the various scales at which the couplings are evaluated are tied to the physical scales of the full cross section.

It might be interesting to make full use of the available two–loop information for the Drell–Yan and DIS cross sections to provide an estimate of three–loop effects, along the lines of section 6.5. In any case, the techniques presented here, which extend threshold resummations to a new class of terms, are a step towards the analysis of yet other classes of perturbative corrections which might be expected to exponentiate. A natural example is given by threshold logarithms suppressed by an extra power of the Mellin variable N, which have recently been analized in the case of longitudinal DIS structure function

[122, 123], and were shown to be phenomenologically important [124]. Another possible extension of this work is the study of N–independent contributions to more complicated hard cross sections, involving more coloured particles, along the lines of [28]: this would be an ingredient towards a precise resummed determination of such cross sections, which would be of considerable phenomenological interest for present and future hadron colliders.

Chapter 7

IR divergences and numerical integration

Numerical phase space integrations constitute important tools in high energy phenomenology. Not only do they hold out where analytical integration methods fail (e.g. for processes with many final state particles), but upon including appropriate binning routines they easily acquire the extra flexibility of generating besides inclusive also fully differential QCD cross sections. These in turn are important observables for studies at high-energy colliders. By allowing detector-specific acceptance cuts on phase space variables they obviate the need for extrapolation into unmeasured, and often also poorly calculable regions, and thereby improve theory-experiment comparisons.

Reliable theoretical predictions for such differential cross sections require the inclusion of at least next-to-leading order (NLO) QCD corrections. NLO calculations combine virtual one-loop corrections with the real emission contributions from unresolved partons. These two parts are usually computed separately and each is infrared divergent, only their sum is infrared finite. This has already been discussed in section 1.3 for the case of inclusive deep inelastic scattering, where the cancellation of divergences took place only after analytical integration over phase space. NLO Monte Carlo programs evaluate both real emission and virtual diagrammes and allow the simultaneous computation of many differential cross sections for the particular reaction considered. However, these programs require that infrared singularities be eliminated before any numerical integration can be done. In this chapter two such methods, namely the phase space slicing (PSS) and the dipole subtraction methods, will be discussed, emphasizing the first of the two. So far, these two methods have mostly been applied extensively to massless partons (for a recent application to Higgs radiation in $t\bar{t}$ production cf. [125, 126, 127]). Here, their performances are studied and compared for the process of virtual photon decay into two heavy quarks $\gamma^* \to Q\bar{Q}$. For the dipole method, the results are a first check of a counterterm derived in [128]. The mass of the heavy partons on the one hand prevents the occurrence of collinear divergences, but on the other hand complicates for both methods the analytical integrals required to cancel soft divergences. Furthermore, they introduce besides the overall energy a second scale into the process, namely the heavy quark mass. Consequently, the allowed range for the regularization parameter required in the phase space slicing approach and the importance of correction terms have to be reconsidered, as to be discussed below. It will be shown in this chapter that, by including improvement

terms in the phase space slicing method, restrictions on the regularization parameter can be removed. This is true also for quantities differential in variables like rapidity or transverse momentum, in numerical integrations realized in a very flexible way by the inclusion of binning routines. In this sense the process under consideration captures the generic hurdles to be taken in the numerical computation of higher order QCD cross sections involving heavy partons.

The chapter is structured as follows. Section 7.1 introduces and compares the concepts of dipole subtraction and phase space slicing, highlighting in particular the regularization parameter dependence of the latter. Section 7.2 applies the phase space slicing method to the particular process under consideration, and contains some numerical results. Section 7.3 describes in more detail the dipole method, followed by a comparison of the numerical performance of the two methods in section 7.4. Section 7.5 contains some concluding remarks.

7.1 Phase space slicing vs. dipole subtraction

The phase space slicing (PSS) method [129, 130, 131, 132] approximates the matrix elements and the phase space integration measure in boundary regions of phase space so integration may be carried out analytically. The subtraction method [133, 134, 135] is based on adding and subtracting counter terms designed to on the one hand render finite the integrand in phase space boundary regions of real emission, and on the other hand be integrable with respect to the momentum of an unresolved parton. For massless partons both methods are well-developed and have been widely used.

The two concepts are best illustrated by means of a simple one dimensional example due to Kunszt [136]. Consider an quantity I which is expressed as the sum of real emission and a virtual contributions, the former of which still needs to be integrated over phase space before cancelling the pole from the latter,

$$I = \int_0^1 \frac{dx}{x^{1+\epsilon}} F(x) + \frac{1}{\epsilon} F(0) \ . \tag{7.1}$$

In the PSS approach the toy matrix element $F(x)$ is approximated as $F(0)$ in the problematic boundary region $0 < x < \delta$, with δ small. This allows one to write

$$I = \int_\delta^1 \frac{dx}{x^{1+\epsilon}} F(x) + \int_0^\delta \frac{dx}{x^{1+\epsilon}} F(0) + \frac{1}{\epsilon} F(0) \ .$$

In the first term of this expression the limit $\epsilon \to 0$ can safely be taken, and the last two terms combine to give

$$\int_\delta^1 \frac{dx}{x} F(x) + F(0) \ln \delta + \mathcal{O}(\delta) \ , \tag{7.2}$$

where the pole has cancelled. The regularization parameter δ must be chosen small, reflecting the approximative character of the PSS approach. In the next section, where $s_{\min}$ takes the role of the regularization parameter, this restriction will be relaxed.

In the subtraction method the term $F(0)/x^{1+\epsilon}$ is added to and subtracted from the integrand to yield

$$I = \int_0^1 \frac{dx}{x^{1+\epsilon}} \left(F(x) - F(0)\right) + \int_0^1 \frac{dx}{x^{1+\epsilon}} F(0) + \frac{1}{\epsilon} F(0) \ .$$

It should be noted that, in contrast to the PSS approach, this rewriting contains no approximation. Taking the limit $\epsilon \to 0$ one finally finds for the subtraction method

$$\int_0^1 \frac{dx}{x} \left(F(x) - F(0)\right) \ . \tag{7.3}$$

Unlike the subtraction method the PSS result thus contains a small parameter δ (in subsequent sections identified as the product of two final state four-momenta and called $s_{\min}$ then), independence of which is not clear a priori but must be explicitly demonstrated.

A quite general formulation of phase space slicing has been given in [137, 138]. It was extended to include massive quarks and identified hadrons in [139]. Of the subtraction method there exist two general formulations. One is the residue approach [140], the other the dipole formalism [141]. Both can handle massless partons and identified hadrons in the final and/or initial state. The extension of the dipole method to massive quarks, using dimensional regularization, has been given in [128], and recently been confirmed by [142]. An extension to photon radiation off massive fermions, using small masses for infrared regularization, was developed by Dittmaier in [143]. There are also hybrid methods [144] that combine elements of the slicing and subtraction methods such that both the resolved and unresolved contributions are numerically small and can be reliably integrated.

With general formulations of the phase space slicing and dipole methods for massless and massive quarks now available, it is interesting to compare their efficiency and accuracy. In the case of the NLO cross section for $t\bar{t}H$ production [125, 126, 127] it was recently verified [127] that the slicing method and a somewhat differently phrased dipole method [142] agreed.

In this chapter the (differential) "cross section" is considered for heavy quark production in the process

$$\gamma^*(q) \to Q(p_1) + \bar{Q}(p_2) \,, \tag{7.4}$$

with $p_1^2 = p_2^2 = m^2$. This case is of course quite simple in minimizing the number of particles involved but nevertheless generic for more complicated processes containing parton masses. The NLO corrections involve virtual corrections to (7.4) and the gluon bremsstrahlung reaction

$$\gamma^*(q) \to Q(p_1) + \bar{Q}(p_2) + g(p_3) \,, \tag{7.5}$$

with $p_3^2 = 0$. Since the final state quarks are massive there occur no collinear singularities, but $p_3^\mu \longrightarrow 0$ produces a soft divergence. It is customary to define the invariants

$$s_{ij} \equiv 2 p_i \cdot p_j \,, \qquad \tilde{s}_{ij} \equiv \left(p_i + p_j\right)^2 \ . \tag{7.6}$$

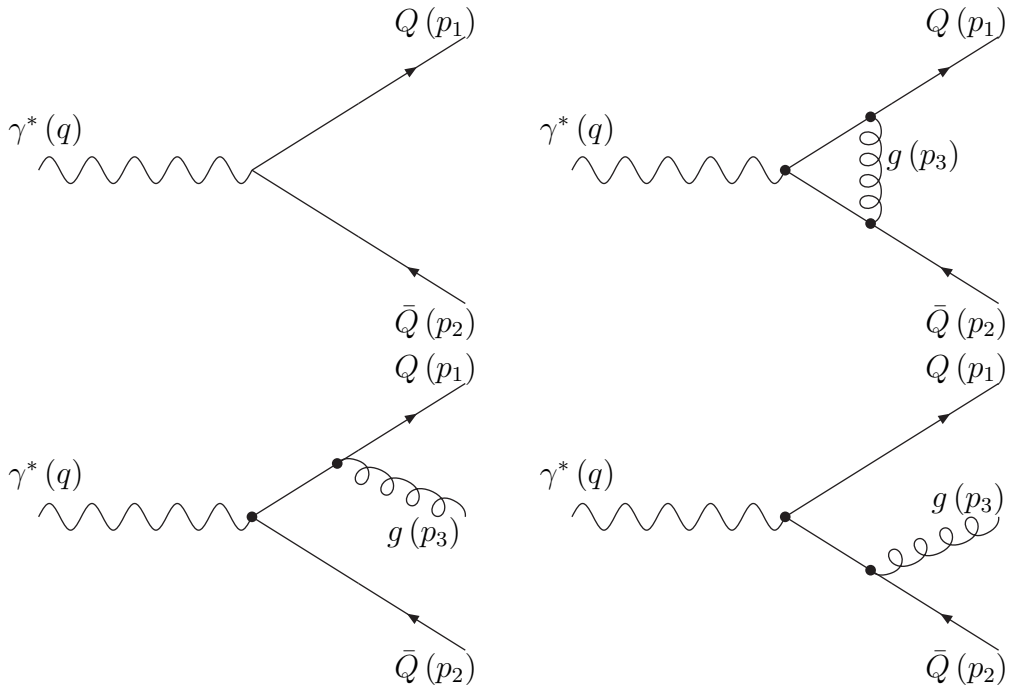

Figure 7.1: *Decay of a virtual photon into two massive quarks at LO as well as virtual and real NLO corrections.*

7.2 Phase Space Slicing

The final state phase space for the 3 parton contribution (7.5) is divided into *hard* and *soft* regions. The hard region, in which all 3 final state particles in (7.4) are resolved, is defined such that $s_{13} > s_{\min}$ or $s_{23} > s_{\min}$, i.e. at least one of the soft invariants exceeds the regulator. The complementary region is soft. The division is relatively simple in this case, but for more complicated configurations extra care must be taken to avoid cutting out non-singular regions. The PSS method thus requires the introduction of a regulator $s_{\min}$ usually required to be quite small, the concrete realization of the δ in (7.2). This $s_{\min}$ can be interpreted as a theoretical resolution parameter describing the acceptance of a fictitious parton detector. It should be carefully distinguished from and be much smaller than final state resolution limits imposed on any experiment by the finite acceptance of actual particle detectors.

To remove restrictions on the size of the phase space slicing cutoff improvement terms can be included in the PSS method [145]. This becomes especially important for cross sections involving heavy quark production, and allows for a free choice of slicing parameter without reference to the heavy quark mass, a prerequisite for considering the high-energy or zero-mass limits. The possibility of removing restrictions on the size of the phase space slicing cutoff will be studied numerically for the case at hand. Including the appropriate improvement terms, the 3 parton contribution to the fully differential decay can be written schematically as [1]

$$\begin{aligned} d\,\Gamma_3 &= |\mathcal{M}_3|^2 \times d\,\mathrm{PS}_3 \\ &= \Big(|\mathcal{M}_3|^2 \times (1-\theta_s) + |\mathcal{M}_3|^2 \times \theta_s\Big) \times d\,\mathrm{PS}_3 \end{aligned}$$

[1] Considering instead of a full cross section the decay width for the virtual photon only seems justified here since the discussion is anyhow focussed on the final state infrared divergences and their cancellation.

$$= |\mathcal{M}_3|^2 \times (1-\theta_s) d\,\mathrm{PS}_3 + \theta_s \times (T_1(\theta_s) + T_2(\theta_s) + T_3(\theta_s)) \ , \tag{7.7}$$

where $|\mathcal{M}_3|^2$ is the exact matrix element squared, and $d\,\mathrm{PS}_3$ denotes the exact 3 particle phase space measure. Note that the effect of jet-algorithms is not considered here (they would be included in the definition of the phase space). The slicing of phase space is indicated by the symbol θ_s, which is 0 in the hard phase space region and 1 in the soft region. T_1 is given by

$$\begin{aligned} T_1(\theta_s) &= S\,|\mathcal{M}_2|^2 \times d\,\mathrm{PS}_{\mathrm{soft}}\ d\,\mathrm{PS}_2 \\ &= |\mathcal{M}|^2_{\mathrm{soft}} \times d\,\mathrm{PS}_2 \ , \end{aligned} \tag{7.8}$$

and represents the integral of the approximate matrix element $|\mathcal{M}_3|^2 \to S\,|\mathcal{M}_2|^2$ over the approximate phase space $d\,\mathrm{PS}_3 \to d\,\mathrm{PS}_{\mathrm{soft}}\ d\,\mathrm{PS}_2$. As indicated on the second line of (7.8) the approximate matrix element can be analytically integrated over $d\,\mathrm{PS}_{\mathrm{soft}}$ to derive a soft matrix element $|\mathcal{M}|^2_{\mathrm{soft}}$. Such calculations can be carried out for a wide range of multiparton processes [137, 138, 139]. They rest on a factorization of soft (eikonal) gluons from colourless ordered subamplitudes. Such amplitudes containing besides a heavy quark anti-quark pair also $n+1$ gluons factorize, in the limit of one gluon going soft, into lower order amplitudes times eikonal factors according to

$$\begin{aligned} S(P;1,\ldots,n,s;\bar{P}) &\longrightarrow e^{\lambda}(n;s;\bar{P}) S(P;1,\ldots,n;\bar{K}) \\ S(P;1,\ldots,m,s,m+1,\ldots,n;\bar{P}) &\longrightarrow e^{\lambda}(m;s;m+1) S(P;1,\ldots,n;\bar{K}) \\ S(P;s,1,\ldots,n;\bar{P}) &\longrightarrow e^{\lambda}(P;s;1) S(P;1,\ldots,n;\bar{K}) \ , \end{aligned} \tag{7.9}$$

with the eikonal factor

$$e^{\lambda}(a;s;b) = \left(\frac{\epsilon^{\lambda}(s)\cdot p_a}{p_a \cdot p_s} - \frac{\epsilon^{\lambda}(s)\cdot p_b}{p_b \cdot p_s} \right) \ . \tag{7.10}$$

Squaring, summing over the helicities λ of the soft gluon and integrating the result over the soft phase space $d\,\mathrm{PS}_{\mathrm{soft}}$ gives the soft matrix element $|\mathcal{M}|^2_{\mathrm{soft}}$. It will be seen in section 7.2.1 to contain the same divergences as the virtual matrix element, but with opposite sign. Explicit expressions for the 3-particle exact phase space as well as its eikonal approximation will be given in section 7.2.2.

The second and third terms in the soft region of (7.7) reverse the approximations initially made on matrix element and phase space, respectively. T_2 is given by

$$T_2(\theta_s) = \left(|\mathcal{M}_3|^2 - S\,|\mathcal{M}_2|^2 \right) \times d\,\mathrm{PS}_3 \ , \tag{7.11}$$

and represents the integral over the exact 3-particle phase space phase space of the difference between the true matrix element and the approximate matrix element. T_3 is given by

$$T_3(\theta_s) = S\,|\mathcal{M}_2|^2 \left(d\,\mathrm{PS}_3 - d\,\mathrm{PS}_2\, d\,\mathrm{PS}_{\mathrm{soft}} \right) \ , \tag{7.12}$$

and represents the difference between the integrals of the approximate matrix element over the true and approximate unresolved phase space. Note that unlike T_1, which contains the soft divergences needed to cancel the singularities of the virtual term, T_2 and T_3 are both finite and vanish as the domain of support for θ_s is taken to zero.

7.2.1 Matrix element

At lowest order the process is described by

$$\begin{aligned} d\Gamma_2 &= \frac{1}{3}\frac{1}{2\sqrt{s}} N e_q^2 e^2 \left(8m^2 + 4s\right) d\mathrm{PS}_2 \\ &= \frac{1}{3}\frac{1}{2\sqrt{s}} \left|\mathcal{M}_{\mathrm{Born}}\right|^2 d\mathrm{PS}_2 \end{aligned} \tag{7.13}$$

where N is the number of colours, e_q the fraction of the elementary charge e of the heavy quark, m its mass, $s = q^2$ and the 2-particle phase space is given by

$$d\mathrm{PS}_2 = \frac{1}{(2\pi)^2}\frac{d^3p_1}{2E_1}\frac{d^3p_2}{2E_2}\delta^{(4)}(q - p_1 - p_2)\,. \tag{7.14}$$

At $\mathcal{O}(\alpha_s)$ there are virtual and real emission contributions. The PSS method separates the latter into hard and soft contributions. The (spin and colour-summed) matrix element for the real emission process (7.5) is

$$\left|\mathcal{M}_3\right|^2 = 16\, e_q^2 e^2 g_s^2 N C_F\, I_R \tag{7.15}$$

with g_s the strong coupling, $C_F = (N^2-1)/2N$ and

$$\begin{aligned} I_R &= -\frac{m^2 s_{23}}{s_{13}^2} - \frac{m^2 s_{12}}{s_{13}^2} - \frac{4m^4}{s_{13}^2} + \frac{4m^2 s_{12}}{s_{13}s_{23}} + \frac{s_{12}^2}{s_{13}s_{23}} + \frac{s_{23}}{2s_{13}} + \frac{s_{12}}{s_{13}} \\ &\quad -\frac{m^2}{s_{13}} - \frac{m^2 s_{13}}{s_{23}^2} + \frac{s_{13}}{2s_{23}} - \frac{m^2 s_{12}}{s_{23}^2} - \frac{4m^4}{s_{23}^2} + \frac{s_{12}}{s_{23}} - \frac{m^2}{s_{23}} \end{aligned} \tag{7.16}$$

In the T_1 term (7.8) the eikonal approximation of the exact matrix element is used. The integral over $d\mathrm{PS}_{\mathrm{soft}}$ is then performed analytically and added to the virtual corrections. The approximated matrix element in the soft region (7.8) is

$$S\ \left|\mathcal{M}_2\right|^2 = 16\, e_q^2 e^2 g_s^2 N C_F\, I_S\ , \tag{7.17}$$

where

$$I_S = -\frac{m^2 s_{12}}{s_{13}^2} + \frac{4m^2 s_{12}}{s_{13}s_{23}} - \frac{m^2 s_{12}}{s_{23}^2} - \frac{4m^4}{s_{13}^2} - \frac{4m^4}{s_{23}^2} + \frac{s_{12}^2}{s_{13}s_{23}}\ . \tag{7.18}$$

This follows from particularizing (7.10) to the case at hand where only one gluon is present. Making the replacement $\sum\limits_\lambda \epsilon_\mu^\lambda \epsilon_\nu^{*\lambda} \longrightarrow -g_{\mu\nu}$ it follows that

$$\sum_\lambda \left|\frac{\epsilon^\lambda \cdot p_1}{p_1 \cdot p_3} - \frac{\epsilon^\lambda \cdot p_2}{p_2 \cdot p_3}\right| = 4\left(\frac{s_{12}}{s_{13}s_{23}} - \frac{m^2}{s_{13}^2} - \frac{m^2}{s_{23}^2}\right)\ . \tag{7.19}$$

This is to be multiplied by the Born contribution to derive (7.18). Note that the difference of (7.16) and (7.18) entering the T_2 term (7.11) contains only terms less singular than $1/s_{\mathrm{soft}}^2$, where s_{soft} stands collectively for any of the soft invariants s_{13} or s_{23}. When integrated over the phase space $d\mathrm{PS}_3 \sim ds_{13}\, ds_{23}$ this difference does not contribute in the limit $s_{\mathrm{soft}} \to 0$.

The result of integrating (7.17) over $d\mathrm{PS}_{\mathrm{soft}}$ is given in [139], and when added to the virtual contributions, yields the following finite expression for the 2 particle $\mathcal{O}(\alpha_s)$ differential cross section for process (7.4)

$$d\Gamma_2 = \frac{1}{3}\frac{1}{2\sqrt{s}}\left(|\mathcal{M}|^2_{\mathrm{soft}} + |\mathcal{M}|^2_{\mathrm{virt}}\right) d\mathrm{PS}_2\,, \tag{7.20}$$

with

$$\begin{aligned}
|\mathcal{M}|^2_{\mathrm{soft}} &= \frac{\alpha_s C_F}{\pi}\left[\frac{1}{\epsilon}\left(1+\left(1-\frac{2m^2}{s}\right)\frac{\ln x}{\beta}\right)\right] C_\epsilon\, |\mathcal{M}_{\mathrm{Born}}|^2 \\
&\quad + \frac{\alpha_s C_F}{\pi}\Bigg[-2\left(1+\left(1-\frac{2m^2}{s}\right)\frac{\ln x}{\beta}\right)\left(\ln x - \ln\left(\frac{s}{s_{\min}}\right) - \ln\beta\right) \\
&\quad -2\left(\ln(1-x)+\ln(1+x)-\ln x\right) \\
&\quad +1 - \frac{\ln x}{\beta}\left(1-\frac{2m^2}{s}\right)\left(1+2\ln\frac{(1-x)(1+x)}{x}\right) \\
&\quad +\frac{1}{2\beta}\left(1-\frac{2m^2}{s}\right)\left(\mathrm{Li}_2\left(1-\frac{1}{x^2}\right)-\mathrm{Li}_2\left(1-x^2\right)\right) - \beta \\
&\quad +\frac{m^2}{s\beta}\ln x\left(\frac{1-x^2}{x}+\frac{s}{m^2}\left(1-\frac{2m^2}{s}\right)\ln x\right) + \frac{\ln^2 x}{2\beta}\left(1-\frac{2m^2}{s}\right)\Bigg.\Bigg] |\mathcal{M}_{\mathrm{Born}}|^2 \\
&\quad + \frac{\alpha_s C_F}{\pi} N e_q^2 e^2\left[\left(1+\left(1-\frac{2m^2}{s}\right)\frac{\ln x}{\beta}\right)(-4s)\right]
\end{aligned} \tag{7.21}$$

and

$$\begin{aligned}
|\mathcal{M}|^2_{\mathrm{virt}} &= -\frac{\alpha_s C_F}{\pi}\left[\frac{1}{\epsilon}\left(1+\left(1-\frac{2m^2}{s}\right)\frac{\ln x}{\beta}\right)\right] C_\epsilon\, |\mathcal{M}_{\mathrm{Born}}|^2 \\
&\quad + \frac{\alpha_s C_F}{\pi} N e_q^2 e^2\Bigg[-4s - 16m^2 - \frac{m^4}{s\beta}\left(32\mathrm{Li}_2(x) + 64\zeta_2\right) \\
&\quad +\frac{s}{\beta}\left(8\mathrm{Li}_2(x)+16\zeta_2\right) + \frac{1}{\beta}\ln^2(x)\left(8\frac{m^4}{s}-2s\right) \\
&\quad -\beta\ln x\left(6s+8m^2\right) + \frac{\ln x}{\beta}\left(-32\frac{m^4}{s}\ln(1-x) + 8s\ln(1-x) + 4s - 8m^2\right)\Bigg]
\end{aligned} \tag{7.22}$$

Here $C_\epsilon = (4\pi\mu^2/m^2)^\epsilon/\Gamma(1-\epsilon)$, $\beta = \sqrt{1-4m^2/s}$ and $x = (1-\beta)/(1+\beta)$. The divergent terms are explicitly included, even though they cancel between the soft and virtual contributions, so that the method independent (virtual) and method dependent (soft) terms can be easily read off. In particular, one can obtain the results within the dipole method by replacing the soft contribution with the integrated dipole terms. Note the logarithmic dependence on the slicing parameter $s_{\min}$ in the finite soft contribution. [2]

[2] For a triangular slicing, in which the sum of the soft invariants is required to exceed the soft regulator in the hard part of phase space, this logarithmic $s_{\min}$-dependence as well as the poles in (7.21) remain unchanged, but finite terms can be redistributed between (7.21) and (7.22). The same statement holds if one requires *all* invariants to exceed $s_{\min}$ in the hard region.

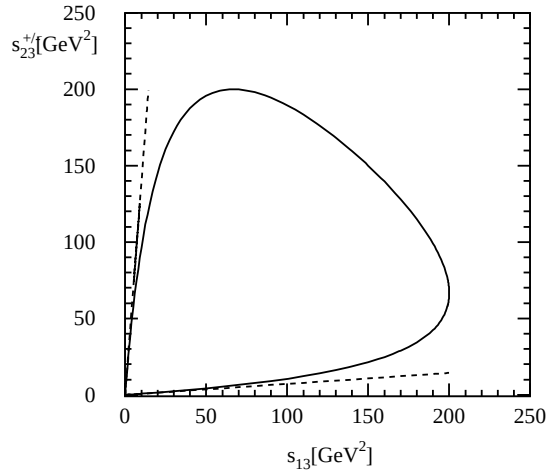

Figure 7.2: *Dalitz plot for $s_{23}^{\pm}$ as a function of s_{13} for exact (cf. (7.25), solid) and eikonal (cf. (7.27), dashed) phase space boundaries at $m = 5$ GeV and $s = 400$ GeV^2.*

7.2.2 Phase space

The spin-summed squared matrix elements of the previous section are functions of the final state momenta only via the invariants s_{12}, s_{13}, s_{23}. The exact 3 particle phase space

$$d\mathrm{PS}_3 = \frac{1}{(2\pi)^5}\frac{d^3p_1}{2E_1}\frac{d^3p_2}{2E_2}\frac{d^3p_3}{2E_3}\delta^{(4)}(q - p_1 - p_2 - p_3) \tag{7.23}$$

may be parametrized in terms of these invariants (after integrating over all remaining variables)

$$d\mathrm{PS}_3 = \frac{1}{4s}\frac{1}{32\pi^3} ds_{12}\, ds_{13}\, ds_{23}\, \delta(s - s_{12} - s_{13} - s_{23} - 2m^2)\,. \tag{7.24}$$

The integration limits of s_{23} at fixed s_{13} are

$$s_{23}^{\pm} = \frac{1}{2\,(s_{13} + m^2)}\left(-s_{13}\left(s_{13} - s + 2m^2\right) \pm s_{13}\sqrt{s_{13}^2 - 2s_{13}s - 4sm^2 + s^2}\right)\,. \tag{7.25}$$

The limits of s_{13} at fixed s_{23} are found by exchanging the indices 13 and 23. Setting $s_{23}^{+} = s_{23}^{-}$ one finds the maxima of these two invariants

$$s_{13}^{\max} = s_{23}^{\max} = s - 2m\sqrt{s}\,. \tag{7.26}$$

In the soft (eikonal) approximation, the limits for s_{23} simplify to

$$\begin{aligned} s_{23}^{\pm,\mathrm{eik}} &= \frac{1}{2m^2}\left(-s_{13}\left(2m^2 - s\right) \pm s_{13}\sqrt{s^2 - 4sm^2}\right) \\ &= s_{13}\left(\frac{s - 2m^2}{2m^2} \pm \frac{s}{2m^2}\beta\right)\,. \end{aligned} \tag{7.27}$$

The phase space boundaries for the exact and approximate cases are given by the Dalitz plot in Fig. 7.2. The random phase space points needed for numerical integration can most easily be generated based on these Lorentz invariants; this method was used to compute the results to be presented in the next section. However, they are independent of the particular generator employed, only the implementation of the phase space boundaries (7.25) and (7.27) can be more tedious to implement in e.g. a cascade type of algorithm.

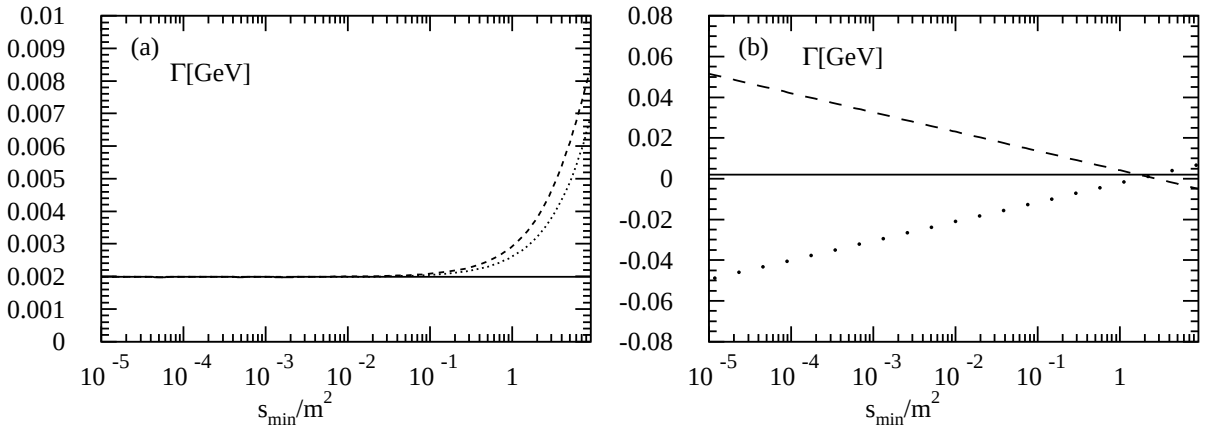

Figure 7.3: *(a) The $s_{\min}/m^2$ dependence of the one-loop corrections to $\Gamma(s, m^2)$, when including the T_1 (dotted), T_1+T_2 (dashed), and $T_1+T_2+T_3$ (solid) contributions. (b) The $s_{\min}/m^2$ dependence of the one-loop corrections to $\Gamma(s, m^2)$ for the soft+virtual (spaced dotted) and the real emission (spaced dashed) final state contributions as well as their sum (solid) in the $T_1 + T_2 + T_3$ approximation.*

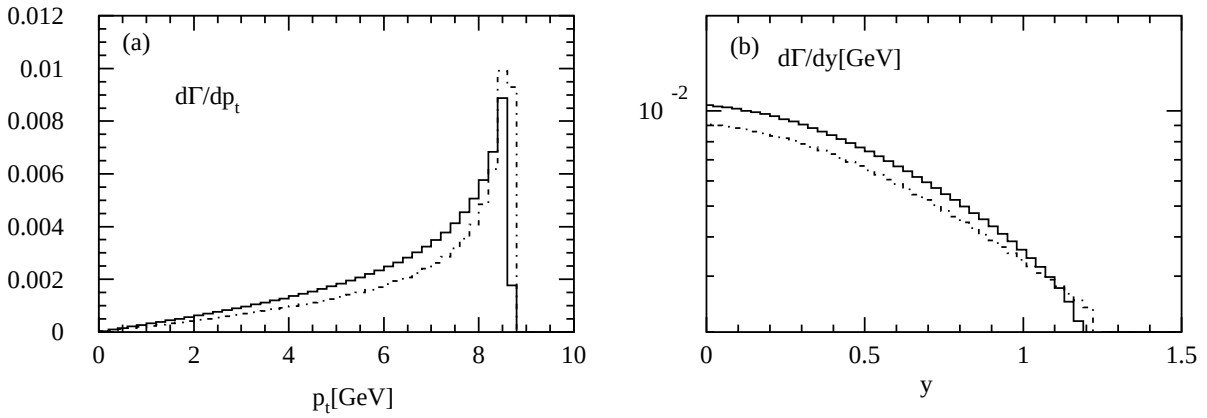

Figure 7.4: *Differential decay widths at Born (dotted-dashed) and NLO (solid) levels, with parameters $s = 400$ GeV^2, $m = 5$ GeV, and $s_{\min} = 0.001$ GeV^2 for differential variables (a) transverse momentum $d\Gamma/dp_T$, (b) rapidity $d\Gamma/dy$ [GeV].*

7.2.3 Numerical results for phase space slicing

In this section some results for the fully inclusive cross section, as well as some differential distributions for process (7.4) will be presented. The effect of the T_i contributions on the $s_{\min}$ dependence of the results will be studied quantitatively. Indeed, as was to be expected, including all T_i will be shown to effect $s_{\min}$-independence. Default values for the analysis will be $s = 400$ GeV^2, and $m = 5$ GeV. Figure 7.3a shows that, for the inclusive cross section, omitting any T_i leads to $s_{\min}$ dependence (in fact the T_2 worsens the $s_{\min}$ dependence slightly here), but including T_2 and T_3 relaxes all constraints on the slicing parameter. This, however, comes at the expense of potentially lower numerical accuracy, particularly for the differential distributions to be considered below. Especially the inclusion of the T_3 term requires, to achieve a given accuracy, a larger number of

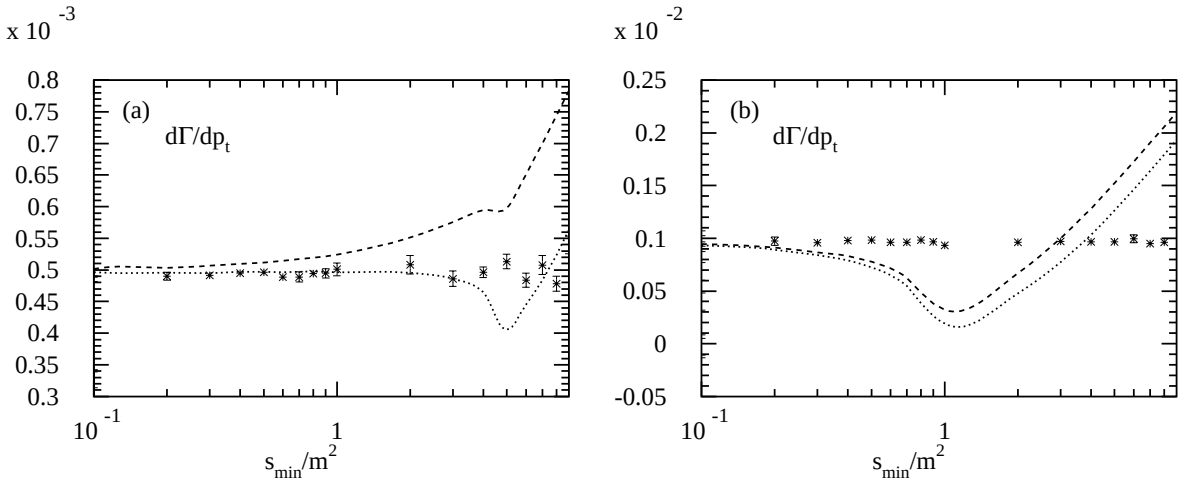

Figure 7.5: *a) The $s_{\min}$-dependence of the one-loop contributions to $d\Gamma/p_T$ for $p_T = 5$ GeV, including the T_1 (dotted), T_1+T_2 (dashed) and $T_1+T_2+T_3$ (individual points with error bars) terms. b) The $s_{\min}$-dependence of the one-loop contributions to $d\Gamma/p_T$ for $p_T = 8$ GeV. Labels as in (a).*

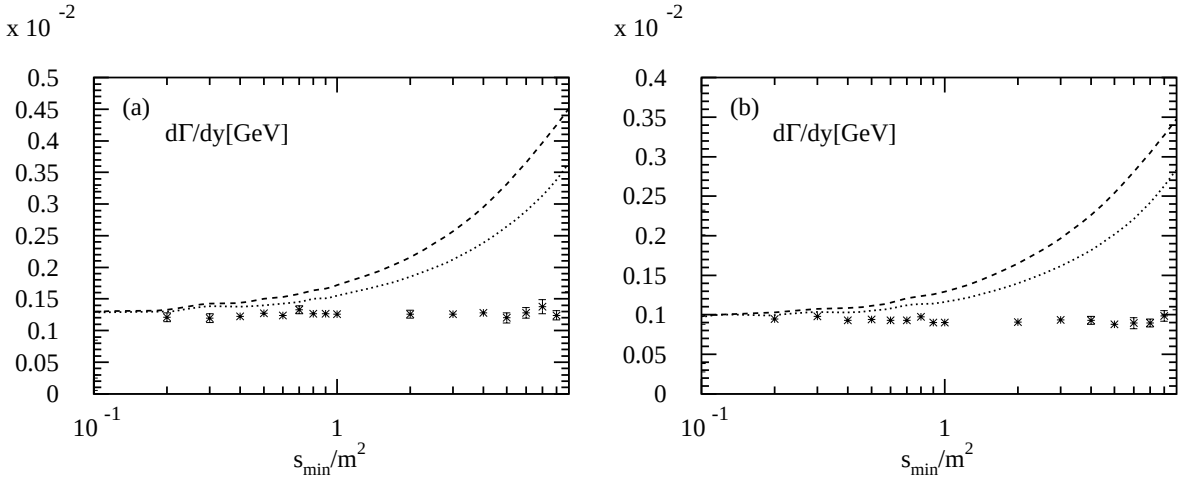

Figure 7.6: *a) The $s_{\min}$-dependence of of the one-loop contributions to $d\Gamma/dy$ at $y = 0.3$. Labels as in Fig. 7.5. b) The $s_{\min}$-dependence of the one-loop contributions to $d\Gamma/dy$ at $y = 0.6$. Labels as in Fig. 7.5.*

points in the Monte Carlo integration than using T_1 alone. In practice, therefore, it is common to use only the T_1 in a PSS calculation, with an $s_{\min}$ value small enough for the combined T_2+T_3 contribution to be negligible. One must however be careful not to choose $s_{\min}$ too small in order to avoid numerical inaccuracies resulting from large opposite sign soft+virtual and real emission contributions, as illustrated by Figure 7.3b.

Turning to distributions, shown in Fig. 7.4 are the single heavy quark transverse momentum and rapidity distributions at a small value of $s_{\min} = 0.001\text{GeV}^2$, computed with T_1 only. Note the usual Jacobian peak near the kinematic maximum of the p_T spectrum. Plotted in Fig. 7.5 is the $s_{\min}$ dependence of the one-loop contributions to $d\Gamma/p_T$ at two fixed values of p_T, one halfway and the other close to the kinematic maximum. The dip in the curves is an artefact which arises because at that $s_{\min}$ and for the p_T given, it is no longer kinematically possible for the full phase space in Fig. 7.2 to contribute. Note that the dip disappears for the exact $T_1+T_2+T_3$ case. Similar results are shown for

the heavy quark rapidity distributions in Fig. 7.6 (only the positive-rapidity part of the symmetric distribution is plotted). These figures make clear that the freedom to choose $s_{\min}$ when including all T_i persists for distributions.

7.3 Dipole Subtraction

The following sketch of the dipole subtraction method will be somewhat briefer than the PSS section. In the dipole formalism one subtracts a suitable term from the real emission part and adds it again to the virtual correction after having performed one phase-space integration, i.e. one writes the NLO cross section as

$$\sigma^{\mathrm{NLO}} = \int\limits_{n+1} d\sigma^R + \int\limits_{n} d\sigma^V = \int\limits_{n+1} \left(d\sigma^R - d\sigma^A \right) + \int\limits_{n} \left(d\sigma^V + \int\limits_{1} d\sigma^A \right) \ . \tag{7.28}$$

The approximation term $d\sigma^A$ should have the same singular behaviour as the real emission term $d\sigma^R$ and hence serve as a local counterterm. Furthermore, it should be analytically integrable with respect to the one-parton subspace simply denoted by 1 in (7.28) in order to cancel the divergences of $d\sigma^V$. The subtraction term can now be constructed starting from the observation that leading contributions are independent of the detailed structure of the scattering amplitude for $m+1$ final state partons $\mathcal{M}_{m+1}$, but arise only from real emission soft gluons attaching to final state particles. From this universality if follows that in the singular regions $|\mathcal{M}_{m+1}|^2$ can be obtained from $|\mathcal{M}_m|^2$ by inserting partons in between all external particles. This is shown graphically in Fig.7.7 and leads to the factorized expression

$$|\mathcal{M}_{m+1}|^2 \to \sum_{i,j,k\neq i,j} |\mathcal{M}_m|^2 \otimes D_{ij,k} = \sum_{i,j,k\neq i,j} \mathcal{D}_{ij,k} \ . \tag{7.29}$$

The $\mathcal{D}_{ij,k}$ are referred to as dipoles, since they are analogous to a coloured antenna radiating a soft particle from the emitter (partons i, j in Fig.7.7) to the spectator (partons k). The dipoles respect conservation of all quantum numbers carried by the final state particles and therefore must incorporate colour correlations between the pair (ij) and the spectator k. In the soft limit the dipoles reduce to eikonal current insertions, and in the collinear limit they reproduce the splitting functions appropriate for the participating partons, but do not introduce any spurious extra divergences. The full subtraction term is then obtained as a sum over all possible attachments of the soft parton, or in other words a sum over all dipoles.

The subtraction terms required to describe heavy quarks were computed in [128], generalizing the approach of [141]. These results have recently been confirmed by [142]. In the case at hand, there are only two dipoles. In one of these the heavy quark constitutes the emitter with the antiquark being the spectator. The second dipole has the roles of the quark and antiquark exchanged. The resulting matrix element, corresponding to the $d\sigma^A$ in (7.28), displays the same soft singularities as the real emission part it is to be subtracted from. It is given by

$$|\mathcal{M}_{\mathrm{A}}|^2 = 2C_F g_s^2 \ |\mathcal{M}_{\mathrm{Born}}|^2 \ \frac{1}{r_0 r \sqrt{(1-r)(1-r_0 r)}} \tag{7.30}$$

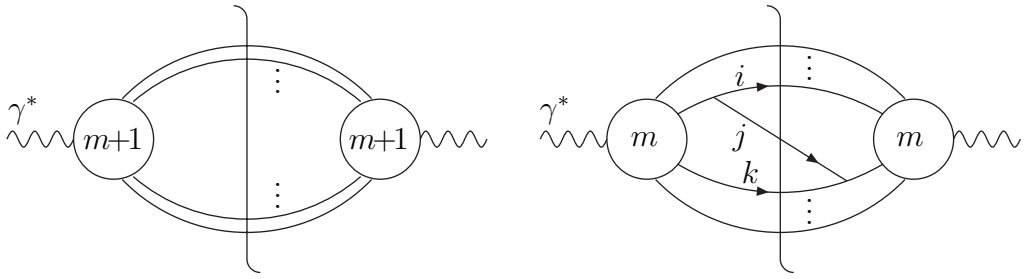

Figure 7.7: *The singular regions of* $|\mathcal{M}_{m+1}|^2$ *can be obtained by inserting dipoles between final state partons in* $|\mathcal{M}_m|^2$ *and summing over all possible insertions* $\{ijk\}$.

$$\times \left\{ \frac{1}{s_{13}} \left[2(1-r_0 r) - (1-r_0) - \frac{1-r_0}{1-u_0 u} \right] + \frac{1}{s_{23}} \left[2(1-r_0 r) - (1-r_0) - \frac{1-r_0}{1+u_0 u} \right] \right\},$$

where

$$r_0 = \beta^2,\ r = \frac{s_{13}+s_{23}}{s-4m^2},\ u_0 = \sqrt{\frac{r_0(1-r)}{1-r_0 r}},\ u = -\frac{1}{u_0}\frac{s_{13}-s_{23}}{s_{13}+s_{23}}. \tag{7.31}$$

This contribution is then integrated over the dipole phase space and added to the virtual corrections. Note that r goes to zero in the soft limit. From a factorization of the full phase-space [128] it follows that

$$\int d\,\mathrm{PS}_{\mathrm{dipole}} = \frac{(4\pi)^{\epsilon-2}}{\Gamma(1-\epsilon)} s^{1-\epsilon} r_0^{2-2\epsilon} 2^{2\epsilon-1} \int_0^1 dr r^{1-2\epsilon} (1-r)^{-\epsilon+1/2} (1-r_0 r)^{-1/2} \int_{-1}^1 du \left(1-u^2\right)^{-\epsilon}. \tag{7.32}$$

The integrated version of (7.31) over the soft phase space can be found in [2]. Its poles in ϵ cancel against those of the virtual corrections. It should be stressed again that the dipole method is exact and independent of any theoretical cut-off parameter. Numerical results for the dipole method will not be displayed separately here, but a comparison to the PSS method can be found in the next section.

7.4 PSS vs. Dipoles revisited

In this section some numerical comparisons between the two methods will be performed for the process at hand. Expression (7.24) will be used as phase space measure. The integrations over its variables are performed using the well-known Monte Carlo iterative integration routine VEGAS [146]. Similar results are found when using (7.23), i.e. when generating the 4-vectors via a cascade algorithm. This method, however, requires more random number points in order to achieve the same accuracy as the invariants-based approach.

The PSS method is relatively easy to implement, with little analytical calculation, at the expense of requiring cancellations between large numbers (for small $s_{\min}$) or having multiple negative contributions (for large $s_{\min}$ when including T_1, T_2 and T_3). Since the dipole method requires more analytical preparation work to be implemented, one

$s = 400$ GeV^2		
points	DIP	PSS
1000	0.04%	1%
10000	0.009%	0.3%
100000	0.003%	0.1%

Table 7.1: Accuracy $\delta r/r$ of the inclusive cross section attained for a given number of points per iteration in the two methods. The same phase space and random number generators are employed. The PSS results use the T_1 contribution only, with $s_{\min} = 0.001\text{GeV}^2$.

iteration	DIP	PSS
1	0.1%	100%
2	0.09%	70%
3	0.06%	10%

Table 7.2: Comparison of the two methods as to the approximate relative deviations of their first three (grid-setting) iterations from the final mean (computed starting from the fifth iteration), for the case of the inclusive cross section. The same phase space and random number generators are employed, at $s = 400$ GeV^2. The PSS results use the T_1 contribution only, with $s_{\min} = 0.001\text{GeV}^2$.

would expect it to show better numerical integration in the Monte Carlo program. This expectation is borne out by numerical results.

The first comparison addresses the relative accuracy achieved in the computation of the inclusive cross section as a function of the number of points, for 20 iterations, of which the first five do not make it into the final average but are used solely to set the VEGAS grid [146], leaving a sample of $N = 15$ results. For each method, separate runs are performed for the $O(\alpha_s)$ 2-particle and $O(\alpha_s)$ 3-particle contributions, and then combined for each iteration, leading to 15 results r_i. The mean result r and its error δr are then computed as

$$r = \frac{1}{N}\sum_{i=1}^{N} r_i, \qquad \delta r = \sqrt{\frac{1}{N}\frac{\sum_{i=1}^{N}(r_i - r)^2}{N-1}}\,. \tag{7.33}$$

The results for this comparison are given in Table 7.1. Note that the PSS method suffers further penalties in accuracy and efficiency if the value of $s_{\min}$ is chosen so large that the T_2 and T_3 become necessary; in particular the T_3 contribution requires generating the soft phase space measure, and involves the difference of two phase space measures which are very similar in magnitude for small values of the soft invariants, cf. (7.12).

The second comparison addresses the efficiency in the computation of the inclusive cross section as a function of the number of iterations, for 10^4 random number points. Clearly, the dipole method reaches a given accuracy with less iterations.

The efficiency of these methods to compute transverse momentum and rapidity distributions will be compared next. As before, the first 5 of 20 iterations are used solely for grid-setting, with 10^4 points per iteration. The values and their errors for each bin are computed according to (7.33). The dipole methods thus produces somewhat smaller

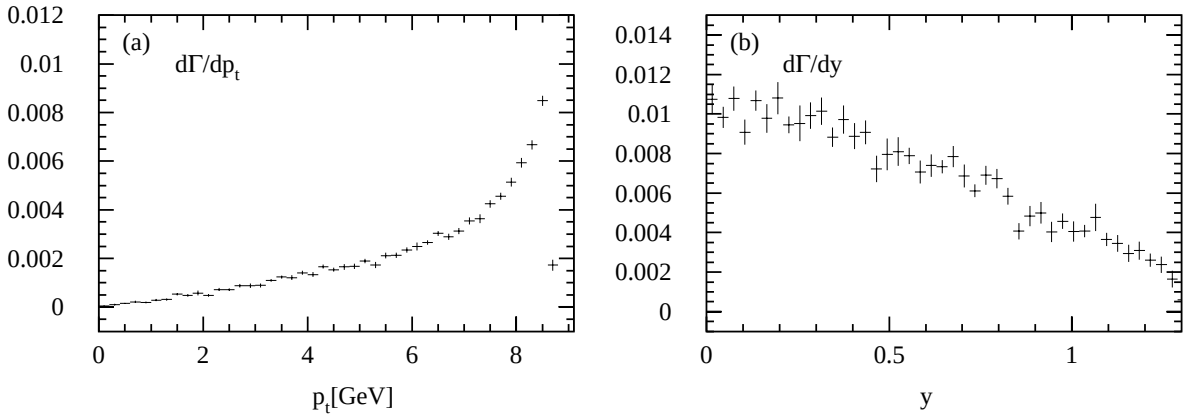

Figure 7.8: *Differential decay widths at NLO level, with parameters* $s = 400$ *GeV*^{2}, $m = 5$ *GeV, for the phase space slicing method (at* $s_{\min} = 0.001\text{GeV}^2$*) for differential variables (a) transverse momentum* $d\Gamma/dp_T$ *(b) rapidity* $d\Gamma/dy$ *[GeV]*

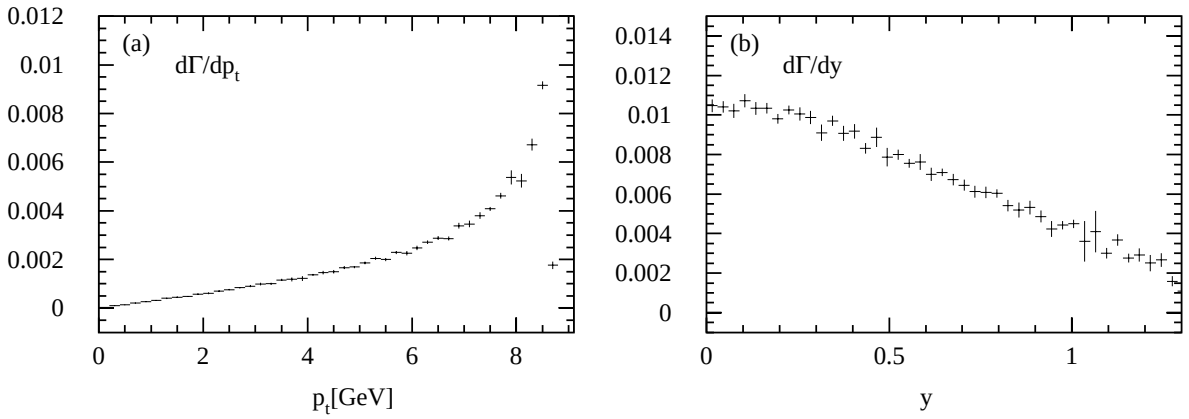

Figure 7.9: *Differential decay widths at NLO level, with parameters* $s = 400$ *GeV*^{2}, $m = 5$ *GeV, for the dipole method for differential variables (a) transverse momentum* $d\Gamma/dp_T$ *(b) rapidity* $d\Gamma/dy$ *[GeV]*

errors, with slightly less bin to bin variations. With an increased number of points, both methods perform not too differently, the loss of superiority being progressive with the number of bins. This suggests that parts of the positive and negative contributions end up in different bins. To test this idea, one can apply a simple smearing where each event with weight w that would normally end up in bin i is distributed in bins $i-1, i, i+1$, each with weight $w/3$. Such a smearing is indeed found to reduce the errors somewhat, but in about equal measure for both methods.

Finally, the accuracies of the methods will be compared in the large s limit for the inclusive cross section, where the heavy quarks become effectively massless. It is of interest to investigate how to choose $s_{\min}$ for the PSS method in order to minimize the calculation error. It turns out that $s_{\min}$ is best chosen not too small (which would lead to large numerical cancellations), and as a fraction of s between 0.01 and 0.1. For large $s_{\min}$ this may require the inclusion of the T_2 and T_3 terms, which contribute about 10% to the cross section for $s_{\min} = 0.1\,s$ at $s = 250000$ GeV^2. For $s = 250000$ GeV^2 and $s_{\min} = 0.01\,s$

their contribution is only 2%, with a slightly larger total error for the same number of points. Similar results are found keeping s fixed and letting m become smaller. For the dipole method an accuracy consistently better than in the PSS method is obtained in these limits. In general, in the high-energy limit, both these methods lead to cancellations between contributions with $+\ln(s/m^2)$ and $-\ln(s/m^2)$ terms, which is not advantageous numerically. Therefore a method which avoids such logarithms is desirable [142].

7.5 Concluding remarks

When numerically computing NLO QCD cross sections a method must be chosen to handle infrared divergences. In this chapter the accuracy and efficiency of two such general-purpose methods to compute NLO heavy quark production cross sections have been compared. The dipole method [141, 128], while involving additional analytical work, has in efficiency and accuracy been found superior to the phase space slicing approach. A similar conclusion was reached by Dittmaier [143] who compared his method with a slicing calculation for a number of electroweak cross sections.

The phase space slicing method [137, 138, 139], which is easy to use and minimizes analytical work, has been extended [145, 2] to become fully independent of the slicing parameter, which has been demonstrated in this chapter for heavy quark production. Although the present case-study involves only the simplest of heavy quark production processes, it provides a useful first step toward gaining numerical experience with general methods for constructing NLO Monte Carlo programs for heavy quark production. Moreover, such experience gained at NLO is likely to be very valuable when these methods are generalized for NNLO cross sections.

Chapter 8

Conclusions

In this thesis resummation and numerical phase space integration have been studied, two important perturbative methods in QCD phenomenology. After a review of the QCD factorization proofs and the general framework of resummation, these techniques were applied to (polarized) heavy quark electroproduction. The resummed exponent, the result of this computation, was utilized as a generating functional to obtain near-threshold estimates for higher order contributions so far not known exactly. Furthermore, the full resummed exponent was investigated numerically. Whereas in the discussion of heavy quark electroproduction only logarithmic terms dominating near threshold were considered, the subsequent treatment of the Drell Yan process included also constant terms. Besides resummation also numerical phase space integrations have been applied in this work to the production of heavy quarks. Numerical integrations are of great phenomenological relevance since they allow to incorporate experiment-specific kinematics cuts and provide easy access to differential observables via appropriate binning.

The resummation and numerical integration techniques dealt with in this thesis are applicable also in other processes of phenomenological interest. They help to understand better the higher order behaviour of perturbative QCD and constitute important steps towards more and more accurate QCD precision physics. Consequently, they are important for QCD *per se* but also as background for possible new physics discoveries.

Appendix A

Mellin and Laplace transforms

The Mellin transforms

$$I_n(N) = \int_0^1 dz z^{N-1} \left[\frac{\ln^n(1-z)}{1-z}\right]_+ \tag{A.1}$$

for $n = 0$ up to $n = 7$ are up to $\mathcal{O}(\tilde{N}^0)$ given by

$$\begin{aligned}
I_0(N) &= -\ln \tilde{N} \\
I_1(N) &= \frac{1}{2}\ln^2 \tilde{N} + \frac{\zeta_2}{2} \\
I_2(N) &= -\frac{1}{3}\ln^3 \tilde{N} - \zeta_2 \ln \tilde{N} - \frac{2}{3}\zeta_3 \\
I_3(N) &= \frac{1}{4}\ln^4 \tilde{N} + \frac{3}{2}\zeta_2 \ln^2 \tilde{N} + 2\zeta_3 \ln \tilde{N} + \frac{3}{2}\zeta_4 + \frac{3}{4}\zeta_2^2 \\
I_4(N) &= -\frac{1}{5}\ln^5 \tilde{N} - 2\zeta_2 \ln^3 \tilde{N} - 4\zeta_3 \ln^2 \tilde{N} - 3(\zeta_2^2 + 2\zeta_4)\ln \tilde{N} - 4(\zeta_2\zeta_3 + \frac{6}{5}\zeta_5) \\
I_5(N) &= \frac{1}{6}\ln^6 \tilde{N} + \frac{5}{2}\zeta_2 \ln^4 \tilde{N} + \frac{20}{3}\zeta_3 \ln^3 \tilde{N} + \frac{15}{2}(\zeta_2^2 + 2\zeta_4)\ln^2 \tilde{N} \\
&\quad +4(5\zeta_2\zeta_3 + 6\zeta_5)\ln \tilde{N} + 5\left(\frac{\zeta_2^3}{2} + \frac{4}{3}\zeta_2^3 + 3\zeta_2\zeta_4 + 4\zeta_6\right) \\
I_6(N) &= -\frac{1}{7}\ln^7 \tilde{N} - 3\zeta_2 \ln^5 \tilde{N} - 10\zeta_3 \ln^4 \tilde{N} - 15(\zeta_2^2 + 2\zeta_4)\ln^3 \tilde{N} \\
&\quad -12(6\zeta_5 + 5\zeta_2\zeta_3)\ln^2 \tilde{N} - 15\left(8\zeta_6 + \zeta_2^3 + \frac{8}{3}\zeta_3^2 + 6\zeta_2\zeta_4\right)\ln \tilde{N} \\
&\quad -60\zeta_3\zeta_4 - \frac{720}{7}\zeta_7 - 72\zeta_2\zeta_5 - 30\zeta_2^2\zeta_3 \\
I_7(N) &= \frac{1}{8}\ln^8 \tilde{N} + \frac{7}{2}\zeta_2 \ln^6 \tilde{N} + 14\zeta_3 \ln^5 \tilde{N} + \frac{105}{4}(\zeta_2^2 + 2\zeta_4)\ln^4 \tilde{N} \\
&\quad +4(42\zeta_5 + 35\zeta_2\zeta_3)\ln^3 \tilde{N} + \frac{105}{2}\left(\zeta_2^3 + 8\zeta_6 + \frac{8}{3}\zeta_3^2 + 6\zeta_2\zeta_4\right)\ln^2 \tilde{N} \\
&\quad +4\left(126\zeta_2\zeta_5 + 105\zeta_3\zeta_4 + 180\zeta_7 + \frac{105}{2}\zeta_2^3\zeta_3\right)\ln \tilde{N} \\
&\quad +\frac{105}{8}\zeta_2^4 + 336\zeta_3\zeta_5 + \frac{315}{2}\zeta_4\left(\zeta_2^2 + \zeta_4\right) + 420\zeta_2\zeta_6 + 630\zeta_8 + 140\zeta_2\zeta_3^2 \ ,
\end{aligned} \tag{A.2}$$

where $\tilde{N} = Ne^{\gamma_E}$ with γ_E the Euler constant. The Riemann ζ functions are given by $\zeta_2 = \pi^2/6$, $\zeta_3 = 1.2020569$, $\zeta_4 = \pi^4/90$, $\zeta_5 = 1.0369278$, $\zeta_6 = \pi^6/945$, $\zeta_7 = 1.0083493$, and $\zeta_8 = \pi^8/9450$.

Note that the results in (A.2) are identical to those for the Laplace transformation

$$I_n(N) = \int_0^\infty dx e^{-Nx} \left[\frac{\ln^n(x)}{x}\right]_+ . \tag{A.3}$$

List of Figures

Bibliography

[1] T. O. Eynck and S.-O. Moch, Phys. Lett. **B495**, 87 (2000), hep-ph/0008108.

[2] T. O. Eynck, E. Laenen, L. Phaf, and S. Weinzierl, Eur. Phys. J. **C23**, 259 (2002), hep-ph/0109246.

[3] T. O. Eynck, E. Laenen, and L. Magnea, JHEP **06**, 057 (2003), hep-ph/0305179.

[4] T. O. Eynck, E. Laenen, S.-O. Moch, and A. Vogt, in preparation.

[5] G. Sterman, Cambridge, Univ. Pr. (1993).

[6] G. Sterman, (1995), hep-ph/9606312, TASI lecture 1995.

[7] J. Kubar-Andre and F. E. Paige, Phys. Rev. **D19**, 221 (1979).

[8] G. Altarelli, R. K. Ellis, and G. Martinelli, Nucl. Phys. **B157**, 461 (1979).

[9] B. Humpert and W. L. van Neerven, Nucl. Phys. **B184**, 225 (1981).

[10] G. Parisi, Phys. Lett. **B90**, 295 (1980).

[11] T. Gehrmann and W. J. Stirling, Phys. Rev. **D53**, 6100 (1996), hep-ph/9512406.

[12] M. Gluck, E. Reya, M. Stratmann, and W. Vogelsang, Phys. Rev. **D53**, 4775 (1996), hep-ph/9508347.

[13] L. D. Landau, Nucl. Phys. **13**, 181 (1959).

[14] S. Coleman and R. E. Norton, Nuovo Cim. **38**, 438 (1965).

[15] J. C. Collins, D. E. Soper, and G. Sterman, in *Perturbative Quantum Chromodynamics*, A.H. Mueller ed., (World Scientific, Singapore (1989)).

[16] G. Sterman, Phys. Rev. **D17**, 2773 (1978).

[17] J. C. Collins, D. E. Soper, and G. Sterman, Nucl. Phys. **B261**, 104 (1985).

[18] J. C. Collins, D. E. Soper, and G. Sterman, Nucl. Phys. **B308**, 833 (1988).

[19] J. C. Collins, D. E. Soper, and G. Sterman, Phys. Lett. **B438**, 184 (1998), hep-ph/9806234.

[20] M. E. Peskin and D. V. Schroeder, Reading, Addison-Wesley (1995).

[21] L. H. Ryder, Cambridge, Univ. Pr. (1985).

[22] G. Sterman, In *Tallahassee 1981, Proceedings, Perturbative Quantum Chromodynamics*, 22-40.

[23] G. T. Bodwin, S. J. Brodsky, and G. P. Lepage, Phys. Rev. Lett. **47**, 1799 (1981).

[24] J. C. Collins and D. E. Soper, Nucl. Phys. **B193**, 381 (1981).

[25] J. C. Collins and G. Sterman, Nucl. Phys. **B185**, 172 (1981).

[26] G. Sterman, Nucl. Phys. **B281**, 310 (1987).

[27] N. Kidonakis, G. Oderda, and G. Sterman, Nucl. Phys. **B525**, 299 (1998), hep-ph/9801268.

[28] N. Kidonakis and G. Sterman, Nucl. Phys. **B505**, 321 (1997), hep-ph/9705234.

[29] N. Kidonakis and G. Sterman, Phys. Lett. **B387**, 867 (1996).

[30] N. Kidonakis, (1998), hep-ph/9904507, to be published in the proceedings of 6th Hellenic School and Workshop on Elementary Particle Physics.

[31] N. Kidonakis, E. Laenen, S. Moch, and R. Vogt, Phys. Rev. **D64**, 114001 (2001), hep-ph/0105041.

[32] N. Kidonakis, J. Smith, and R. Vogt, Phys. Rev. **D56**, 1553 (1997), hep-ph/9608343.

[33] E. Laenen, G. Oderda, and G. Sterman, Phys. Lett. **B438**, 173 (1998), hep-ph/9806467.

[34] E. Laenen, G. Sterman, and W. Vogelsang, Phys. Rev. **D63**, 114018 (2001), hep-ph/0010080.

[35] H. Contopanagos, E. Laenen, and G. Sterman, Nucl. Phys. **B484**, 303 (1997), hep-ph/9604313.

[36] C. F. Berger, Phys. Rev. **D66**, 116002 (2002), hep-ph/0209107.

[37] S. Catani and L. Trentadue, Nucl. Phys. **B327**, 323 (1989).

[38] J. G. M. Gatheral, Phys. Lett. **B133**, 90 (1983).

[39] J. Frenkel and J. C. Taylor, Nucl. Phys. **B246**, 231 (1984).

[40] N. Kidonakis, G. Oderda, and G. Sterman, Nucl. Phys. **B531**, 365 (1998), hep-ph/9803241.

[41] N. Kidonakis, G. Oderda, and G. Sterman, (1998), hep-ph/9805279, in Brussels 1998, Deep inelastic scattering and QCD, 579-583.

[42] European Muon, J. J. Aubert *et al.*, Nucl. Phys. **B213**, 31 (1983).

[43] ZEUS, J. Breitweg *et al.*, Phys. Lett. **B407**, 402 (1997), hep-ex/9706009.

[44] H1, C. Adloff *et al.*, Z. Phys. **C72**, 593 (1996), hep-ex/9607012.

[45] E. Laenen, S. Riemersma, J. Smith, and W. L. van Neerven, Nucl. Phys. **B392**, 229 (1993).

[46] G. Ingelman and G. A. Schuler, Z. Phys. **C40**, 299 (1988).

[47] B. W. Harris and J. Smith, Nucl. Phys. **B452**, 109 (1995), hep-ph/9503484.

[48] B. W. Harris and J. Smith, Phys. Rev. **D57**, 2806 (1998), hep-ph/9706334.

[49] E. Laenen and S.-O. Moch, Phys. Rev. **D59**, 034027 (1999), hep-ph/9809550.

[50] M. Anselmino, A. Efremov, and E. Leader, Phys. Rept. **261**, 1 (1995), hep-ph/9501369.

[51] H.-Y. Cheng, Int. J. Mod. Phys. **A11**, 5109 (1996), hep-ph/9607254.

[52] H.-Y. Cheng, Chin. J. Phys. **38**, 753 (2000), hep-ph/0002157.

[53] B. Lampe and E. Reya, Phys. Rept. **332**, 1 (2000), hep-ph/9810270.

[54] J. R. Ellis and R. L. Jaffe, Phys. Rev. **D9**, 1444 (1974).

[55] J. R. Ellis and R. L. Jaffe, Phys. Rev. **D10**, 1669 (1974).

[56] HERMES, K. Ackerstaff *et al.*, Phys. Lett. **B404**, 383 (1997), hep-ex/9703005.

[57] HERMES, M. Amarian *et al.*, DESY-HERMES-97-04.

[58] E. Volk, DESY-THESIS-2001-002.

[59] D. Heesbeen, PhD thesis Rijksuniversiteit Groningen 2003.

[60] COMPASS, G. Baum *et al.*, CERN-SPSLC-96-14.

[61] A. Weber, Nucl. Phys. **B382**, 63 (1992).

[62] I. Bojak and M. Stratmann, Nucl. Phys. **B540**, 345 (1999), hep-ph/9807405.

[63] I. Bojak and M. Stratmann, Phys. Lett. **B433**, 411 (1998), hep-ph/9804353.

[64] I. Schienbein, Phys. Rev. **D59**, 013001 (1999), hep-ph/9711507.

[65] J. Smith, Nucl. Phys. Proc. Suppl. **79**, 602 (1999).

[66] J. Smith and W. van Neerven, in preparation.

[67] E. B. Zijlstra and W. L. van Neerven, Nucl. Phys. **B417**, 61 (1994).

[68] E. B. Zijlstra and W. L. van Neerven, Nucl. Phys. **B426**, 245 (1994).

[69] M. Buza, Y. Matiounine, J. Smith, and W. L. van Neerven, Nucl. Phys. **B485**, 420 (1997), hep-ph/9608342.

[70] E. Leader, Cambridge Monogr. Part. Phys. Nucl. Phys. Cosmol. **15**, 1 (2001).

[71] S. D. Bass, Eur. Phys. J. **A5**, 17 (1999), hep-ph/9902280.

[72] European Muon, J. Ashman *et al.*, Phys. Lett. **B206**, 364 (1988).

[73] R. D. Carlitz, J. C. Collins, and A. H. Mueller, Phys. Lett. **B214**, 229 (1988).

[74] G. Altarelli and G. G. Ross, Phys. Lett. **B212**, 391 (1988).

[75] K. Sasaki, Prog. Theor. Phys. **54**, 1816 (1975).

[76] M. A. Ahmed and G. G. Ross, Nucl. Phys. **B111**, 441 (1976).

[77] G. Altarelli and G. Parisi, Nucl. Phys. **B126**, 298 (1977).

[78] J. Feltesse, F. Kunne, and E. Mirkes, Phys. Lett. **B388**, 832 (1996), hep-ph/9607336.

[79] A. Bravar, D. von Harrach, and A. Kotzinian, Phys. Lett. **B421**, 349 (1998), hep-ph/9710266.

[80] HERMES, M. G. Vincter, RIKEN Rev. **28**, 70 (2000).

[81] J. A. M. Vermaseren, (2000), math-ph/0010025.

[82] R. Mertig and W. L. van Neerven, Z. Phys. **C70**, 637 (1996), hep-ph/9506451.

[83] W. Vogelsang, Nucl. Phys. **B475**, 47 (1996), hep-ph/9603366.

[84] J. Kodaira and L. Trentadue, Phys. Lett. **112B**, 66 (1982).

[85] A. P. Contogouris, Z. Merebashvili, and G. Grispos, Phys. Lett. **B482**, 93 (2000), hep-ph/0003204.

[86] Z. Merebashvili, A. P. Contogouris, and G. Grispos, Phys. Rev. **D62**, 114509 (2000), hep-ph/0007050.

[87] A. D. Watson, Zeit. Phys. **C12**, 123 (1982).

[88] M. Gluck, E. Reya, and W. Vogelsang, Nucl. Phys. **B351**, 579 (1991).

[89] E. Laenen, S. Riemersma, J. Smith, and W. L. van Neerven, Nucl. Phys. **B392**, 162 (1993).

[90] HERMES, A. Airapetian *et al.*, Phys. Rev. Lett. **84**, 2584 (2000), hep-ex/9907020.

[91] M. Stratmann and W. Vogelsang, Z. Phys. **C74**, 641 (1997), hep-ph/9605330.

[92] G. Sterman and W. Vogelsang, (2000), hep-ph/0002132, to be published in the proceedings of Physics at Run II: QCD and Weak Boson Physics Workshop: Final General Meeting, Batavia, Illinois, 4-6 Nov 1999.

[93] G. Sterman and W. Vogelsang, JHEP **02**, 016 (2001), hep-ph/0011289.

[94] J. Blumlein and S. Kurth, Phys. Rev. **D60**, 014018 (1999), hep-ph/9810241.

[95] S. Catani, M. L. Mangano, P. Nason, and L. Trentadue, Nucl. Phys. **B478**, 273 (1996), hep-ph/9604351.

[96] D. Graudenz, M. Hampel, A. Vogt, and C. Berger, Z. Phys. **C70**, 77 (1996), hep-ph/9506333.

[97] A. Vogt, Phys. Lett. **B471**, 97 (1999), hep-ph/9910545.

[98] G. Oderda, N. Kidonakis, and G. Sterman, (1999), hep-ph/9906338, in Bloomington 1999, Physics with a high luminosity polarized electron ion collider 377-388.

[99] J. C. Collins, in *Perturbative Quantum Chromodynamics*, A.H. Mueller ed., (World Scientific, Singapore (1989)).

[100] L. Magnea and G. Sterman, Phys. Rev. **D42**, 4222 (1990).

[101] T. Matsuura, S. C. van der Marck, and W. L. van Neerven, Nucl. Phys. **B319**, 570 (1989).

[102] L. Magnea, Nucl. Phys. **B349**, 703 (1991).

[103] L. Magnea and G. Sterman, in Batavia 1990, Hadron structure functions and parton distributions.

[104] A. Vogt, Phys. Lett. **B497**, 228 (2001), hep-ph/0010146.

[105] S. Moch, J. A. M. Vermaseren, and A. Vogt, (2002), hep-ph/0209100.

[106] W. L. van Neerven and A. Vogt, Phys. Lett. **B490**, 111 (2000), hep-ph/0007362.

[107] A. Sen, Phys. Rev. **D24**, 3281 (1981).

[108] A. H. Mueller, Phys. Rev. **D20**, 2037 (1979).

[109] J. C. Collins, Phys. Rev. **D22**, 1478 (1980).

[110] G. P. Korchemsky and G. Marchesini, Nucl. Phys. **B406**, 225 (1993), hep-ph/9210281.

[111] G. P. Korchemsky and A. V. Radyushkin, Phys. Lett. **B279**, 359 (1992), hep-ph/9203222.

[112] S. Forte and G. Ridolfi, Nucl. Phys. **B650**, 229 (2003), hep-ph/0209154.

[113] E. Gardi, G. P. Korchemsky, D. A. Ross, and S. Tafat, Nucl. Phys. **B636**, 385 (2002), hep-ph/0203161.

[114] E. Gardi and R. G. Roberts, Nucl. Phys. **B653**, 227 (2003), hep-ph/0210429.

[115] R. Hamberg, W. L. van Neerven, and T. Matsuura, Nucl. Phys. **B359**, 343 (1991).

[116] W. L. van Neerven and E. B. Zijlstra, Nucl. Phys. **B382**, 11 (1992).

[117] S. Catani and L. Trentadue, Nucl. Phys. **B353**, 183 (1991).

[118] R. T. Herrod and S. Wada, Phys. Lett. **B96**, 195 (1980).

[119] G. Curci, W. Furmanski, and R. Petronzio, Nucl. Phys. **B175**, 27 (1980).

[120] G. Kramer and B. Lampe, Z. Phys. **C34**, 497 (1987).

[121] R. J. Gonsalves, Phys. Rev. **D28**, 1542 (1983).

[122] R. Akhoury, M. G. Sotiropoulos, and G. Sterman, Phys. Rev. Lett. **81**, 3819 (1998), hep-ph/9807330.

[123] R. Akhoury and M. G. Sotiropoulos, (2003), hep-ph/0304131.

[124] M. Kramer, E. Laenen, and M. Spira, Nucl. Phys. **B511**, 523 (1998), hep-ph/9611272.

[125] L. Reina and S. Dawson, Phys. Rev. Lett. **87**, 201804 (2001), hep-ph/0107101.

[126] L. Reina, S. Dawson, and D. Wackeroth, Phys. Rev. **D65**, 053017 (2002), hep-ph/0109066.

[127] W. Beenakker *et al.*, Phys. Rev. Lett. **87**, 201805 (2001), hep-ph/0107081.

[128] L. Phaf and S. Weinzierl, JHEP **04**, 006 (2001), hep-ph/0102207.

[129] K. Fabricius, I. Schmitt, G. Kramer, and G. Schierholz, Zeit. Phys. **C11**, 315 (1981).

[130] G. Kramer and B. Lampe, Fortschr. Phys. **37**, 161 (1989).

[131] H. Baer, J. Ohnemus, and J. F. Owens, Phys. Rev. **D40**, 2844 (1989).

[132] B. W. Harris and J. F. Owens, Phys. Rev. **D65**, 094032 (2002), hep-ph/0102128.

[133] R. K. Ellis, D. A. Ross, and A. E. Terrano, Nucl. Phys. **B178**, 421 (1981).

[134] Z. Kunszt, P. Nason, G. Marchesini, and B. R. Webber, Proceedings of the 1989 LEP Physics Workshop, Geneva, edited by G. Altarelli, R. Kleiss and C. Verzegnassi, vol.1, p. 373.

[135] M. L. Mangano, P. Nason, and G. Ridolfi, Nucl. Phys. **B373**, 295 (1992).

[136] Z. Kunszt, (1996), hep-ph/9603235, Boulder TASI 95:515-538.

[137] W. T. Giele and E. W. N. Glover, Phys. Rev. **D46**, 1980 (1992).

[138] W. T. Giele, E. W. N. Glover, and D. A. Kosower, Nucl. Phys. **B403**, 633 (1993), hep-ph/9302225.

[139] S. Keller and E. Laenen, Phys. Rev. **D59**, 114004 (1999), hep-ph/9812415.

[140] S. Frixione, Z. Kunszt, and A. Signer, Nucl. Phys. **B467**, 399 (1996), hep-ph/9512328.

[141] S. Catani and M. H. Seymour, Nucl. Phys. **B485**, 291 (1997), hep-ph/9605323.

[142] S. Catani, S. Dittmaier, M. H. Seymour, and Z. Trocsanyi, Nucl. Phys. **B627**, 189 (2002), hep-ph/0201036.

[143] S. Dittmaier, Nucl. Phys. **B565**, 69 (2000), arXiv:hep-ph/9904440.

[144] J. M. Campbell, M. A. Cullen, and E. W. N. Glover, Eur. Phys. J. **C9**, 245 (1999), hep-ph/9809429.

[145] W. B. Kilgore and W. T. Giele, Phys. Rev. **D55**, 7183 (1997), hep-ph/9610433.

[146] G. P. Lepage, J. Comput. Phys. **27**, 192 (1978).

Samenvatting

(Dutch summary)

In het kader van het Standard Model van de elementaire deeltjesfysica wordt de sterke wisselwerking tussen quarks en gluonen beschreven door de Quantum Chromodynamica (QCD). De fundamentele QCD bouwstenen, de quarks en gluonen, ofwel partonen, komen echter niet als vrije deeltjes in de natuur voor, maar vormen gebonden toestanden, de hadronen. Dit gedrag is een rechtstreeks gevolg van de energieafhankelijke koppelingssterkte α_s. Bij hoge energien neemt α_s kleine waarden aan, zodat de wisselwerking tussen de partonen in sterkte afneemt. In dit domein kunnen experimenteel waarneembare grootheden (zoals werkzame doorsnedes) worden berekend als storingsreeksen in α_s. Zulke storingstheoretische methodes zijn echter niet geschikt voor toepassing in het lage energie gebied corresponderend met grote α_s.

Ter beschrijving van hadronische verstrooiingen moeten storingstheoretische en niet-storingstheoretische bijdrages eerst worden gefactorizeerd. De tot nu toe alleen experimenteel toegankelijke distributies van partonen in hadronen kunnen dan met storingstheoretische partonische grootheden worden gecombineerd. Maar ook bij puur partonische berekeningen stoot men op verschillende problemen. In hogere orde diagrammen leiden parallel bewegende partonen en partonen van lage energie tot oneindigheden, ofwel infrarood divergenties. Deze divergenties vallen pas weg na sommatie over alle aan een bepaald proces bijdragende diagrammen. In sommige experimenteel relevante gebieden van de fase ruimte laten deze cancellaties logarithmische en/of constante termen achter, die numeriek groot kunnen zijn en dus de betrouwbaarheid van de partonische storingsreeks twijfelachtig maken.

Dit proefschrift begint met een discussie van het QCD factorizatie concept. Het vormt de fundering voor elke storingstheoretische beschrijving van hadronische verstrooiingen.

Een generalisatie van het factorizatie concept leidt tot een hersommatie van de storingsreeks. Hersommatie is een methode om logarithmische en bijbehorende constante termen, de overblijfsels van de divergenties, te hergroeperen in termen van analytische functies en daarmee de betrouwbaarheid van de storingsreeks te herstellen. De gehersommeerde termen komen te staan in een exponent, die het resterende resultaat, een zich nu goed gedragende storingsreeks, vermenigvuldigt. Dankzij het feit dat deze exponent veldentheoretische informatie tot oneindige orde in α_s bevat, kan hij ook worden beschouwd als een genererende functionaal, waaruit door herexpansie eindige orde benaderingen afleidbaar zijn.

In dit proefschrift wordt hersommatie toegepast op de gepolarizeerde productie van charm quarks in diep-inelastische vertrooiing van electronen en protonen. De gehersommeerde exponent wordt niet alleen als genererende functionaal gebruikt om eindige orde correcties af te leiden, maar vervolgens ook als geheel vooral numeriek geanalyseerd. Bovendien wordt de methode op het Drell-Yan proces toegepast om niet alleen logarithmische maar ook constante bijdragen aan de werkzame doorsnede te hersommeren.

In bovengenoemde voorbeelden gebeurde de cancellatie van infrarood divergenties altijd in een analytische stap van de berekeningen. In veel gevallen is het echter noodzakelijk

om de fase ruimte volledig numeriek te integreren (in reacties met een groot aantal deeltjes in de eindtoestand, of voor een flexibele aanpassing aan de specifieke geometrie van een experiment). In het laatste hoofdstuk van dit proefschrift worden twee manieren om zulke integraties door te voeren voorgesteld en met elkaar vergeleken.

Acknowledgements

The research described in this thesis was carried out at the National Institute for Nuclear and High Energy Physics (NIKHEF) in Amsterdam. During the years I have spent at NIKHEF I have much enjoyed the stimulating scientific and international environment it provides. Contrary to what the uninitiated may believe, theoretical physics does not require (voluntary) solitary confinement but instead a lot of intense discussions with and advice from colleagues.

First of all I would like to thank my supervisor Eric Laenen for his readiness to tutor and advice, to discuss and cross-check. He even managed to read my two least legible outputs (handwriting and source code). We had rather few fixed appointments during those years, but instead made ample use of our almost continuous *inloopspreekuur*.

This policy of open doors brings me naturally to the NIKHEF theory group, where I have much appreciated the informal and semi-institutionalized exchanges (e.g. Jan-Willem van Holten's SDC). Some people I would like to thank in particular: Sven Moch, who much helped me get started with QCD and resummation in the initial phase of my PhD, Lukas Phaf, who rarely lost patience with me when it came to programming, Stefan Weinzierl for sharing his knowledge on numerical integration, and Andreas Vogt, who has taught me a good many logarithmic tricks. Also thanks to Jos Vermaseren for helping with FORM, to Justus Koch for his careful reading of the manuscript, and to all the fellow theory PhD students, especially my office companions Jan, Tim, Andrea, and Hylke.

There have been many guests to the NIKHEF theory group I have had the chance to discuss with. Jack Smith has kindly provided us with preliminary results from a paper draft of his. Probably the most lasting impression has been left by Lorenzo Magnea and his highly entertaining combination of spotless physics with colourful language.

Besides the theorists there is a much larger group of experimental physicists at NIKHEF, which facilitates a continuous exchange both groups profit from. Gerard van der Steenhoven from the NIKHEF HERMES group was a very attentive reader and came up with quite a few suggestions. There is a scientific world not only outside the theory group, but also beyond the NIKHEF fence. My local walkabouts have repeatedly led me to the Vrije Universiteit, where I have benefited not only from private discussions with Alessandro Bacchetta, but also from the student seminars he organized.

My teaching duties at the Universiteit van Amsterdam and at the summer school in Monschau have been a rewarding experience. I thank Justus Koch and Thorsten Feldmann for the good teamwork. I have also had the opportunity to attend quite a few schools in the role of participant. The subatomic physics research winter schools in Nijmegen, Maria Laach, the CTEQ school on QCD analysis and phenomenology in St. Andrews, and Erice all provided stimulating input. The same is true for the ICHEP conference in Amsterdam.

To some people the word interdisciplinary may sound like just another threat from the funding authorities. I am glad to have found in Holger Lyre a teacher and friend who thinks otherwise.

No, physicists do not always talk physics. Cheers to all the running couplings who showed their field strength representing the theory group at the FOM sportdagen. For

some reason my social contacts with the NIKHEF experimentalists were very much focussed on the HERMES group. Thank you for all those enjoyable barbecues and dinners (and Jan's filling Italian dishes). Thanks to Chiara, who shares my passions for all four combinations of the adjectives classical or modern with the nouns physics or ballet (and to her parents for allowing us to turn their front yard into a campground). Also, Amsterdam would have been a lot less fun without the following: Bettina & Simon, Sandra & Jord, Lucia & Alessandro, Joana & Daniel, Martijn, Andrea & Alejandro & Tristan, Johanna & Lukas, Jan, Mina, Johan, Freya, Silke, Bram, and Gabriel.

It has been a special pleasure to share our house with Tino, who has so many stories to tell.

For obvious reasons, special thanks go to Vanessa, my favourite experimental physicist ♡.

Curriculum Vitae

The author of this dissertation was born on 18 October 1971 in Düsseldorf. He attended the grammar school *Freiherr-vom-Stein-Gymasium* in Lünen and was awarded the *Abitur* in 1991. After a year of compulsory alternative service at the German Red Cross he enrolled at the Universität Dortmund in 1992 to study physics. In 1994 he moved to King's College London, where he graduated in 1996 as Master in Science, Theoretical Physics. He then returned to the Universität Dortmund where he wrote a diploma thesis on path-integral quantization of non-abelian gauge theories on two-dimensional manifolds, for which he was awarded the *Diplom der Physik* in 1998. Also in 1998 he attended a summer school organized jointly by the Universität Jena and the Heraeus-Stiftung. From 1998 until 2003 he worked as junior researcher (*onderzoeker in opleiding*) at the National Institute for Nuclear and High Energy Physics (NIKHEF) in Amsterdam, where the research described in this thesis was carried out. While employed at NIKHEF, the author had the opportunity to attend schools and conferences in Nijmegen, Maria Laach, St. Andrews, Erice, and Amsterdam. He was also involved in undergraduate as well as postgraduate teaching at the Universiteit van Amsterdam and at the joint Belgian-Dutch-German summer school for experimental particle physics in Monschau.